

UNCLASSIFIED

AD NUMBER: AD0831922

LIMITATION CHANGES

TO:

Approved for public release; distribution is unlimited.

FROM:

Distribution authorized to U.S. Defense agencies;  
Administrative/Operational Use; 1 DEC 1967. Other requests shall be  
referred to the Army Chief of Engineers, Military Construction,  
Washington, D. C. 20315

AUTHORITY

OCE, D/A LTR, 23 JAN 1981

[REDACTED]

1

100



11

100

AD

AD831922  
AD-831922

**OCE NEMP PROGRAM**  
**Development of Criteria**  
**for**  
**Protection of NIKE-X Power Plant and Facilities**  
**Electrical Systems Against**  
**Nuclear Electromagnetic Pulse Effects**  
**TECHNICAL AND SUMMARY REPORT**

**1 December 1967**

**Submitted by:**  
**E. R. UHLIG**

**Placed by:**  
**Military Construction**  
**Office of the Chief of Engineers**  
**Department of the Army**  
**Washington, D.C. 20315**

The findings in this report are not to be construed as an official Department of the Army position unless so designated by other authorized documents.

**CONTRACT NUMBER DA - 49 - 129 - ENG - 543**

**GENERAL ELECTRIC COMPANY**  
**PITTSFIELD, MASS.**

Each transmittal of this document outside the Department of Defense must have prior approval of Military Construction, Office of the Chief of Engineers, Department of the Army, Washington, D.C. 20315.

Unclassified  
Security Classification

| DOCUMENT CONTROL DATA - R&D  |   |  |
|--|---|--|
| (Security classification of title, body of abstract and indexing annotation must be entered when the overall report is classified)   |   |  |
| 1. ORIGINATING ACTIVITY (Corporate author)<br>General Electric Company<br>100 Woodlawn Avenue<br>Pittsfield, Massachusetts 01201   |   | 2a. REPORT SECURITY CLASSIFICATION<br>Unclassified |
|  |   | 2b. GROUP<br>None                                  |
| 3. REPORT TITLE<br>OCE NEMP Program, Development of Criteria for Protection of NIKE-X Power Plant and Facilities Electrical Systems Against Nuclear Electromagnetic Pulse Effects, Technical and Summary Report, 1 December 1967   |   |  |
| 4. DESCRIPTIVE NOTES (Type of report and inclusive dates)<br>Technical Data  |   |  |
| 5. AUTHOR(S) (Last name, first name, initial)<br>Uhlig, E. R.<br>Caverly, D. W.<br>Ricci, R.   |   |  |
| 6. REPORT DATE<br>1 December 1967  | 7a. TOTAL NO. OF PAGES<br>139   | 7b. NO. OF REFS                                    |
| 8a. CONTRACT OR GRANT NO.<br>DA-49-129-ENG-543   | 8b. ORIGINATOR'S REPORT NUMBER(S)<br>67U15  |  |
| a. PROJECT NO.   |   |  |
| c.   | 9a. OTHER REPORT NO(S) (Any other numbers that may be assigned this report)   |  |
| d.   | None  |  |
| 10. AVAILABILITY/LIMITATION NOTICES<br>Each transmittal of this document outside the Department of Defense must have prior approval of Military Construction, Office of the Chief of Engineers, Department of the Army, Washington, D. C. 20315  |   |  |
| 11. SUPPLEMENTARY NOTES<br>None  | 12. SPONSORING MILITARY ACTIVITY<br>Military Construction, OCE<br>Department of the Army<br>Washington, D. C. 20315 |  |
| 13. ABSTRACT<br><p>This document is comprised of reports on experiments performed during the period from 1 April 1967 to 1 December 1967. This data covers two technical areas; testing techniques for shielded enclosures and conduit and H-field induced current in buried conduit. Abstracts of reports, issued under separate covers during this time period, documenting other areas of investigation are contained at the end of this report.</p> <p>This information expands the technical "backup" material for the "OCE NEMP PROGRAM, Development of Criteria for Protection of NIKE-X Power Plant and Facilities Electrical Systems Against Nuclear Electromagnetic Pulse Effects, PROTECTIVE MEASURES".</p> |   |  |

DD FORM 1473

Unclassified  
Security Classification

| 14. KEY WORDS                | LINK A |    | LINK B |    | LINK C |    |
|------------------------------|--------|----|--------|----|--------|----|
|                              | ROLE   | WT | ROLE   | WT | ROLE   | WT |
| EMP Effects<br>Power Systems |        |    |        |    |        |    |

#### INSTRUCTIONS

1. **ORIGINATING ACTIVITY:** Enter the name and address of the contractor, subcontractor, grantee, Department of Defense activity or other organization (corporate author) issuing the report.
- 2a. **REPORT SECURITY CLASSIFICATION:** Enter the overall security classification of the report. Indicate whether "Restricted Data" is included. Marking is to be in accordance with appropriate security regulations.
- 2b. **GROUP:** Automatic downgrading is specified in DoD Directive 5200.10 and Armed Forces Industrial Manual. Enter the group number. Also, when applicable, show that optional markings have been used for Group 3 and Group 4 as authorized.
3. **REPORT TITLE:** Enter the complete report title in all capital letters. Titles in all cases should be unclassified. If a meaningful title cannot be selected without classification, show title classification in all capitals in parenthesis immediately following the title.
4. **DESCRIPTIVE NOTES:** If appropriate, enter the type of report, e.g., interim, progress, summary, annual, or final. Give the inclusive dates when a specific reporting period is covered.
5. **AUTHOR(S):** Enter the name(s) of author(s) as shown on or in the report. Enter last name, first name, middle initial. If military, show rank and branch of service. The name of the principal author is an absolute minimum requirement.
6. **REPORT DATE:** Enter the date of the report as day, month, year, or month, year. If more than one date appears on the report, use date of publication.
- 7a. **TOTAL NUMBER OF PAGES:** The total page count should follow normal pagination procedures, i.e., enter the number of pages containing information.
- 7b. **NUMBER OF REFERENCES:** Enter the total number of references cited in the report.
- 8a. **CONTRACT OR GRANT NUMBER:** If appropriate, enter the applicable number of the contract or grant under which the report was written.
- 8b, 8c, & 8d. **PROJECT NUMBER:** Enter the appropriate military department identification, such as project number, subproject number, system numbers, task number, etc.
- 9a. **ORIGINATOR'S REPORT NUMBER(S):** Enter the official report number by which the document will be identified and controlled by the originating activity. This number must be unique to this report.
- 9b. **OTHER REPORT NUMBER(S):** If the report has been assigned any other report numbers (either by the originator or by the sponsor), also enter this number(s).

10. **AVAILABILITY/LIMITATION NOTICES:** Enter any limitations on further dissemination of the report, other than those imposed by security classification, using standard statements such as:

- (1) "Qualified requesters may obtain copies of this report from DDC."
- (2) "Foreign announcement and dissemination of this report by DDC is not authorized."
- (3) "U. S. Government agencies may obtain copies of this report directly from DDC. Other qualified DDC users shall request through \_\_\_\_\_."
- (4) "U. S. military agencies may obtain copies of this report directly from DDC. Other qualified users shall request through \_\_\_\_\_."
- (5) "All distribution of this report is controlled. Qualified DDC users shall request through \_\_\_\_\_."

If the report has been furnished to the Office of Technical Services, Department of Commerce, for sale to the public, indicate this fact and enter the price, if known.

11. **SUPPLEMENTARY NOTES:** Use for additional explanatory notes.

12. **SPONSORING MILITARY ACTIVITY:** Enter the name of the departmental project office or laboratory sponsoring (paying for) the research and development. Include address.

13. **ABSTRACT:** Enter an abstract giving a brief and factual summary of the document indicative of the report, even though it may also appear elsewhere in the body of the technical report. If additional space is required, a continuation sheet shall be attached.

It is highly desirable that the abstract of classified reports be unclassified. Each paragraph of the abstract shall end with an indication of the military security classification of the information in the paragraph, represented as (TS), (S), (C), or (U).

There is no limitation on the length of the abstract. However, the suggested length is from 150 to 225 words.

14. **KEY WORDS:** Key words are technically meaningful terms or short phrases that characterize a report and may be used as index entries for cataloging the report. Key words must be selected so that no security classification is required. Identifiers, such as equipment model designation, trade name, military project code name, geographic location, may be used as key words but will be followed by an indication of technical content. The assignment of links, rules, and weights is optional.

END 6-68

**OCE NEMP PROGRAM**  
**Development of Criteria**  
**for**  
**Protection of NIKE-X Power Plant and Facilities**  
**Electrical Systems Against**  
**Nuclear Electromagnetic Pulse Effects**  
**TECHNICAL AND SUMMARY REPORT**

**1 December 1967**

**Report by:**  
**D. W. CAVERLY**  
**GENERAL ELECTRIC COMPANY**

**AND**

**R. J. RICCI**  
**PROCEDYNE CORPORATION**  
**(SECTION 5.0)**

**Placed by:**  
**Military Construction**  
**Office of the Chief of Engineers**  
**Department of the Army**  
**Washington, D. C. 20315**

The findings in this report are not to be construed as an official Department of the Army position unless so designated by other authorized documents.

**CONTRACT NUMBER DA - 49 - 129 - ENG - 543**

**GENERAL ELECTRIC COMPANY**  
**PITTSFIELD, MASS.**

Each transmittal of this document outside the Department of Defense must have prior approval of Military Construction, Office of the Chief of Engineers, Department of the Army, Washington, D. C. 20315.

## **Table of Contents**

## TABLE OF CONTENTS

|  | <u>Page</u> |
|--|-------------|
| 1.0 SUMMARY . . . . .  | 1 - 1       |
| 2.0 INTRODUCTION . . . . .   | 2 - 1       |
| 3.0 HIGH FREQUENCY TESTING TECHNIQUES FOR DETERMINATION OF<br>SHIELDING DISCONTINUITIES IN CONDUIT . . . . .   | 3 - 1       |
| 3.1 Introduction . . . . .   | 3 - 1       |
| 3.2 Objectives . . . . .   | 3 - 1       |
| 3.3 Approaches to the Problem . . . . .  | 3 - 2       |
| 3.4 Feasibility Evaluation and Application of Conduit<br>Discontinuity Test Techniques . . . . .   | 3 - 4       |
| 3.4.1 Preliminary Tests . . . . .  | 3 - 4       |
| 3.4.2 Circulating Current in an Extended Piping System . . . . .   | 3 - 6       |
| 3.4.3 Loose Joints - Accessible Conduit . . . . .  | 3 - 6       |
| 3.4.4 Loose Joints - Inaccessible Conduit . . . . .  | 3 - 8       |
| 3.4.5 Pinpointing Loose Joints . . . . .   | 3 - 11      |
| 3.4.6 Internal Magnetic Field Source . . . . .   | 3 - 12      |
| 3.5 Conclusions . . . . .  | 3 - 14      |
| 4.0 MEASUREMENT OF SHIELDING EFFECTIVENESS OF SHIELDING ENCLOSURES<br>BY CONTINUOUS SINUSOIDAL WAVE ATTENUATION AS COMPARED TO<br>IMPULSE WAVE ATTENUATION . . . . . | 4 - 1       |
| 4.1 Introduction . . . . .   | 4 - 1       |
| 4.2 Objectives . . . . .   | 4 - 1       |
| 4.3 Test Setup and Procedure . . . . .   | 4 - 3       |
| 4.4 Test Results . . . . .   | 4 - 3       |
| 4.5 Conclusions . . . . .  | 4 - 9       |
| References . . . . .   | 4 - 10      |
| 5.0 GEOMETRIC MODELS FOR THE INVESTIGATION OF NEMP INDUCED<br>CURRENTS IN BURIED CONDUITS . . . . .  | 5 - 1       |
| 5.1 Introduction . . . . .   | 5 - 1       |
| 5.2 Geometric Models . . . . .   | 5 - 1       |
| 5.2.1 Models in General . . . . .  | 5 - 1       |
| 5.2.2 Modeling for the Buried Conduit Problem . . . . .  | 5 - 2       |

# Table of Contents

- 2 -

|  | <u>Page</u> |
|--|-------------|
| 5.3 Modeling Facility . . . . .  | 5 - 2       |
| 5.3.1 Experimental Tank . . . . .  | 5 - 2       |
| 5.3.2 Conductivity Measurement Apparatus . . . . .   | 5 - 4       |
| 5.3.3 Magnetic Field Generator . . . . .   | 5 - 4       |
| 5.3.4 Instrumentation . . . . .  | 5 - 4       |
| 5.4 Experiments Performed . . . . .  | 5 - 7       |
| 5.4.1 Objective . . . . .  | 5 - 7       |
| 5.4.2 Procedure . . . . .  | 5 - 8       |
| 5.4.3 Results . . . . .  | 5 - 10      |
| 5.5 Analysis of Results . . . . .  | 5 - 18      |
| 5.5.1 Resistance Measurements . . . . .  | 5 - 18      |
| 5.5.2 Circuit Parameters . . . . .   | 5 - 18      |
| 5.5.3 Induced Currents . . . . .   | 5 - 19      |
| 5.6 Conclusions . . . . .  | 5 - 25      |
| Appendix 5 A   |             |
| Appendix 5 B   |             |
| References   |             |
| 6.0 EXPERIMENTAL MEASUREMENT OF CURRENT ON BURIED CONDUIT<br>RESULTING FROM ELECTRIC AND MAGNETIC FIELDS - Part II . . . . . | 6 - 1       |
| 6.1 Introduction . . . . .   | 6 - 1       |
| 6.2 Objective . . . . .  | 6 - 1       |
| 6.3 Test Facility and Setup . . . . .  | 6 - 1       |
| 6.3.1 Experimental Setup . . . . .   | 6 - 1       |
| 6.3.2 Generator Voltage and Current . . . . .  | 6 - 2       |
| 6.3.3 Measurements . . . . .   | 6 - 6       |
| 6.4 Tests . . . . .  | 6 - 6       |
| 6.4.1 Buried Conduit - 100, 200, and 400 Feet . . . . .  | 6 - 6       |
| 6.4.2 Buried Conduit, Isolated from Direct Contact with<br>Ground, Tied to Ground Rod Beds at Each End . . . . .             | 6 - 14      |
| 6.4.3 Guard Wire and Screening Investigation - Buried<br>Conduit . . . . .   | 6 - 20      |

Table of Contents  
- 3 -

|  | <u>Page</u> |
|--|-------------|
| 6.4.4 Current Shunt Plates - Buried Conduit . . . . .        | 6 - 31      |
| 6.4.5 Ambient H-Field Distortion with 400 Foot Conduit . . . | 6 - 42      |
| 6.5 Conclusions . . . . .                                    | 6 - 42      |
| References   |             |
| 7.0 ABSTRACTS . . . . .                                      | 7 - 1       |
| APPENDIX   |             |

## **List of Illustrations**

# LIST OF ILLUSTRATIONS

| <u>Figure</u> |   | <u>Page</u> |
|---------------|---|-------------|
| 3.1           | Typical Arrangement of Conduit Runs Showing Undefinable Current Paths . . . . .   | 3 - 3       |
| 3.2           | Preliminary Setup for RF Current Measurement Through an Empty Conduit Loop . . . . .  | 3 - 5       |
| 3.3           | Test Circuit for Calibrating Wound Core, Multiturn Current Transformer for Measurement of High-Frequency Current through a Conduit or Piping System . . . . . | 3 - 7       |
| 3.4           | Variation-of-Impedance Drop Technique of Detecting Defective Joints in an Accessible Conduit Loop . . . . .   | 3 - 9       |
| 3.5           | "Sensing Loop" Technique of Detecting Discontinuities or Unshielded Wiring in an Inaccessible Conduit Run . . . . .   | 3 - 10      |
| 3.6           | "Inducing Loop" Technique of Detecting Discontinuities or Unshielded Wiring in an Inaccessible Conduit Run . . . . .  | 3 - 13      |
| 4.1           | Pulsed Magnetic Field Testing Setup . . . . .   | 4 - 2       |
| 4.2           | Test Setup . . . . .  | 4 - 4       |
| 4.3           | Wiring Diagram of Continuous Wave Attenuation Measuring Circuit . . . . .   | 4 - 5       |
| 4.4           | Continuous Wave Attenuation vs. Frequency for Various Methods of Sealing Enclosure Door . . . . .   | 4 - 7       |
| 4.5           | Comparison of Impulse Tests to Sine Wave Tests vs. Time and Frequency . . . . .   | 4 - 8       |
| 5.1           | Experimental Tank Details . . . . .   | 5 - 3       |
| 5.2a          | Box for Measurement of Sand Resistivity . . . . .   | 5 - 5       |
| 5.2b          | Wenner Array . . . . .  | 5 - 5       |
| 5.3           | Wave Forms of the Current and Derivative of the Magnetic Field . . . . .  | 5 - 6       |
| 5.4a          | Typical Arrangement for Frequency-Response Measurement . . . . .  | 5 - 9       |
| 5.4b          | Equivalent Circuit for (a) Based on an Assumed R-L Model for the Underground Loop . . . . .   | 5 - 9       |
| 5.5           | Frequency Response for Parallel Rods, 2' Apart . . . . .  | 5 - 12      |
| 5.6           | Frequency Response for Two Spheres, 2' Apart . . . . .  | 5 - 13      |
| 5.7           | Induced Current in Underground Conductor and B at Surface for Parallel Rod Grounds at Ends of Conductor . . . . .   | 5 - 14      |

# List of Illustrations

- 2 -

| <u>Figure</u> |  | <u>Page</u> |
|---------------|--|-------------|
| 5.8a          | Parallel Rods . . . . .  | 5 - 15      |
| 5.8b          | Parallel Rods, Conductor Above Surface . . . . .   | 5 - 15      |
| 5.8c          | Flat Plates . . . . .  | 5 - 15      |
| 5.9           | Effective Area and Induced Current at $T = 25$ s for<br>Parallel Rods Separated by d Feet . . . . .                    | 5 - 21      |
| 5.10          | Effective Area and Induced Current for Flat Plates<br>h Feet Long . . . . .  | 5 - 23      |
| 6.1           | Test Facility Setup . . . . .  | 6 - 3       |
| 6.2           | 400' Buried Conduit Setup . . . . .  | 6 - 4       |
| 6.3           | 100' Buried Conduit (isolated) Setup . . . . .   | 6 - 4       |
| 6.4           | Buried Conduit Test Pit . . . . .  | 6 - 5       |
| 6.5           | 400' Conduit Test - Middle Test Pit . . . . .  | 6 - 5       |
| 6.6           | Generator Voltage and Current . . . . .  | 6 - 7       |
| 6.7           | Average Soil Resistivity over a Hemispherical Volume of<br>Diameter, D, Measured Using the Four Probe Method . . . . . | 6 - 8       |
| 6.8           | Conduit Current - 200' Buried with Ground Rod<br>Termination . . . . .   | 6 - 10      |
| 6.9           | Conduit Current - 200' Buried Ground Termination at<br>Each End. Measurement at Center . . . . .                       | 6 - 11      |
| 6.10          | Conduit Current. 400' Buried, Ground Termination at<br>Each End. Measurement at Center . . . . .                       | 6 - 12      |
| 6.11          | Peak Conduit Current for the First and Second Crests.<br>Calculated and Measured Values . . . . .                      | 6 - 13      |
| 6.12          | Conduit Current (center). 200' Conduit with and<br>without Ground Rod Termination . . . . .                            | 6 - 15      |
| 6.13          | Conduit Current (center). 400' Conduit with and<br>without Ground Rod Termination . . . . .                            | 6 - 16      |
| 6.14          | Conduit Current. 200' Conduit with Ground Rods at<br>Ends. Measurement at Ends and Center . . . . .                    | 6 - 17      |
| 6.15          | Conduit Current. 400' Conduit with Ground Rods at<br>Ends. Measurements at Ends and Center . . . . .                   | 6 - 18      |
| 6.16          | 100' Conduit - Above Ground, Below Ground, and Below<br>Ground Isolated . . . . .                                      | 6 - 21      |

# List of Illustrations

- 3 -

| <u>Figure</u> |  | <u>Page</u> |
|---------------|--|-------------|
| 6.17          | Buried Conduit, Contained in Duct, Galvanized Screen Guard . . . . .   | 6 - 22      |
| 6.18          | Measured Conduit Current, Isolated Conduit, Buried . . . .   | 6 - 23      |
| 6.19          | Conduit Current Reduction . . . . .  | 6 - 24      |
| 6.20          | Top Conduit Current, Measured and Calculated . . . . .   | 6 - 27      |
| 6.21          | Bottom Conduit Current, Measured and Calculated . . . . .  | 6 - 28      |
| 6.22          | Center Conduit Current with and without Screening, Near Field . . . . .  | 6 - 29      |
| 6.23          | End Conduit Current with and without Screening, Near Field . . . . .   | 6 - 30      |
| 6.24          | Grounding System Arrangement in Excavation at Center of Conduit Run . . . . .  | 6 - 32      |
| 6.25          | Conduit Current, Shunting Plates and 200' of Conduit . . .   | 6 - 33      |
| 6.26          | Conduit Current, Center Measurement with and without Aluminum Ground Sheet . . . . .   | 6 - 34      |
| 6.27          | Conduit Current, Shunt Plates, 400' of Conduit . . . . .   | 6 - 36      |
| 6.28          | Conduit Current, Shunt Plates, 400' of Conduit . . . . .   | 6 - 37      |
| 6.29          | Conduit Current, Shunt Plates, with and without Aluminum Ground Strip, 400' of Conduit . . . . .                                 | 6 - 38      |
| 6.30          | Conduit and Shunt Plate Currents, 400' of Conduit . . . .  | 6 - 39      |
| 6.31          | 400' Conduit Grounded, Wire Mesh Added to Conduit Outside Box . . . . .  | 6 - 40      |
| 6.32          | 400' Conduit Grounded, Wire Mesh Added to Conduit Inside Box . . . . .   | 6 - 41      |
| 6.33          | 400' Conduit Grounded and Ungrounded, H-field Measurement in 200' Hole, Probe Halfway between Conduit and Ground Plane . . . . . | 6 - 43      |
| 6.34          | 400' Conduit Grounded and Ungrounded, H-field Measurement in 200' Hole, Probe Halfway between Conduit and Ground Plane . . . . . | 6 - 44      |
| 6.35          | 400' Conduit Grounded, H-field Measurement in 200' Hole, Probe Halfway between Conduit and Ground Plane . . . .                  | 6 - 45      |
| 6.36          | Measurement Setup of the Ambient H-field with and without Conduit Current . . . . .  | 6 - 46      |

# List of Illustrations

- 4 -

| <u>Figure</u> |  | <u>Page</u> |
|---------------|--|-------------|
| 6.37          | H-field 12 Feet from Center Hole, 400' Conduit, with<br>and without Conduit Connected and Grounded . . . . . | 6 - 47      |
| 6.38          | Conduit Current, Calculated and Test Results . . . . .   | 6 - 48      |
| 6.39          | Conduit Current, Buried in Contact with Earth, with<br>and without Ground Rods at the Ends . . . . .         | 6 - 50      |
| APPENDIX      |  |             |
| A.1           | Conduit-Ground Rod Shielding Mat Below Ground . . . . .  | A 2         |
| A.2           | 100' x 15' x 120' Shielding Volume of 2-Inch Steel<br>Conduit . . . . .                                      | A 3         |
| A.3           | Conduit Test Loop with Measured and Calculated<br>Parameters . . . . .                                       | A 4         |
| A.4           | Conduit Loop with Calculated Parameters . . . . .  | A 4         |
| A.5           | Grounding Mat Showing Shielding Volume and Calculated<br>Effective Area . . . . .                            | A 8         |
| A.6           | Conduit Mat-Shielded Volume for a Value of Attenuation<br>of 8 dB . . . . .                                  | A 9         |

**List of Tables**

# LIST OF TABLES

| <u>Table</u> |  | <u>Page</u> |
|--------------|--|-------------|
| 4.1          | Sine Wave and Impulse Wave Attenuation Values . . . . .                                | 4 - 6       |
| 5.1          | Calculated and Measured Resistance between Two<br>Cylinders 12" Apart . . . . .        | 5 - 11      |
| 5.2          | Calculated and Measured Resistance between Two Spheres<br>3" Deep . . . . .            | 5 - 11      |
| 5.3          | Calculated and Measured Resistance between Two<br>Hemispheres on the Surface . . . . . | 5 - 11      |
| 5.4          | Correlate with Figure 5.8a . . . . .   | 5 - 16      |
| 5.5          | Correlate with Figure 5.8c . . . . .   | 5 - 16      |
| 5.6          | Correlate with Figure 5.8b . . . . .   | 5 - 16      |
| 5.7          | Parallel Rods . . . . .  | 5 - 17      |
| 6.1          | Previous Conduit Tests . . . . .   | 6 - 19      |
| 6.2          | Previous Conduit Tests . . . . .   | 6 - 26      |

## **Section 1.0**

### **Summary**

1.0 SUMMARY

This document is comprised of reports on experiments performed during the period from 1 April 1967 to 1 December 1967. This data covers two technical areas, testing techniques for shielded enclosures and conduit and H-field induced current in buried conduit. Abstracts of reports, issued under separate cover during this time period, documenting other areas of investigation are contained at the end of this report.

This information expands the technical "backup" material for the "OCE NEMP PROGRAM, Development of Criteria for Protection of NIKE-X Power Plant and Facilities Electrical Systems Against Nuclear Electromagnetic Pulse Effects, PROTECTIVE MEASURES".

## **Section 2.0**

### **Introduction**

## 2.0 INTRODUCTION

The experimental results contained within this document supplement the previous written technical material and provides the latest reference data. Two previous reports, "Technical Data for General NEMP Criteria for NIKE-X Power Systems" dated 5 August 1966 and revised 1 December 1966 and "OCE NEMP PROGRAM, Development of Criteria for Protection of NIKE-X Power Plant and Facilities Electrical Systems Against Nuclear Electromagnetic Pulse Effects, TECHNICAL DATA" issued 31 March 1967, were comprised of four main categories as follows:

1. Environment
2. Power system responses to NEMP and other surges
3. Component responses and susceptibility
4. Shielding

This document, containing four experimental reports, will be an addendum to Item 4, Shielding.

## **Section 3.0**

### **High Frequency Testing Techniques for Determination of Shielding discontinuities in Conduit**

### 3.0 HIGH FREQUENCY TESTING TECHNIQUES FOR DETERMINATION OF SHIELDING DISCONTINUITIES IN CONDUIT

#### 3.1 Introduction

An important requirement for the suppression of EMP effects on NIKE-X electrical systems is that "all conduit runs shall be continuous so that conductors are never directly exposed to an EMP field". This criteria evolved from tests which indicated that the effectiveness of conduits as a means of shielding contained conductors from spurious voltages produced by EMP and similar transients is seriously degraded by loose couplings, defective welds, poorly constructed joints, or any other conduit discontinuities.

Concern about the seriousness of conduit shielding leaks has prompted an experimental investigation of measurement and test techniques applicable for monitoring the shielding quality of conduit at the time of installation and maintaining its shielding effectiveness during the lifetime of the system.

The experiments reported in this section cover high frequency testing techniques for determination of shielding discontinuities in conduits.

#### 3.2 Objectives

Objectives of this group of experiments included the following:

1. Development of techniques capable of detecting the existence of flaws or discontinuities in conduits that would result in loss of attenuation or degradation of shielding in high intensity ambient electromagnetic fields.
2. Establishment of requirements for detection equipment, featuring availability, simplicity, ease of operation, and portability.
3. Comparison of a number of discontinuity detection methods utilizing high frequency currents to select their most advantageous features.
4. Determination by actual tests of the relative detection ability of such equipment under parametric variations of test frequency, condition of conduit joints, and with different conduit configurations.

5. Evaluation of the reliability and repeatability of the various techniques.

### 3.3 Approaches to the Problem

Tests have shown that even a single discontinuity in a conduit run may seriously degrade its shielding effectiveness. It is necessary, therefore, that the detection equipment be sufficiently responsive to such flaws. The problem is further complicated by the fact that many individual conduit runs are buried so that fittings or sections that may develop shielding leaks are relatively inaccessible.

Several testing schemes depending directly upon the injection of currents and measurement of voltage drops across individual conduit sections were considered, but rejected as impracticable because of the difficulty of electrically isolating a conduit run for testing from the rest of the system, inaccessibility to buried portions of a run, and the length of testing cables required on long runs. It became apparent early in the investigation that although conduction/voltage drop methods are entirely feasible on bench tests under laboratory conditions, they could not be considered as reliable under field testing conditions.

As an example, consider the difficulties involved in using a conduction method for detecting discontinuities by circulating a current in the conduit run designed as Conduit "A" between junction boxes #2 and #3 in Figure 3.1. (It will be assumed that electrical isolation of a conduit run from its termini is impracticable after installation.) Note that Conduit "A" is also shunted by undefinable paths between these junction boxes whose conductivity may change because of other conduit run modifications. Thus, the shunting resistance would affect the amount of test current circulated.

Accordingly, several entirely different approaches were taken in an effort to solve the problem, including:

1. Circulating high frequency currents of the order of 20 kHz to 1000 kHz through conduit systems in a controlled manner and utilizing a

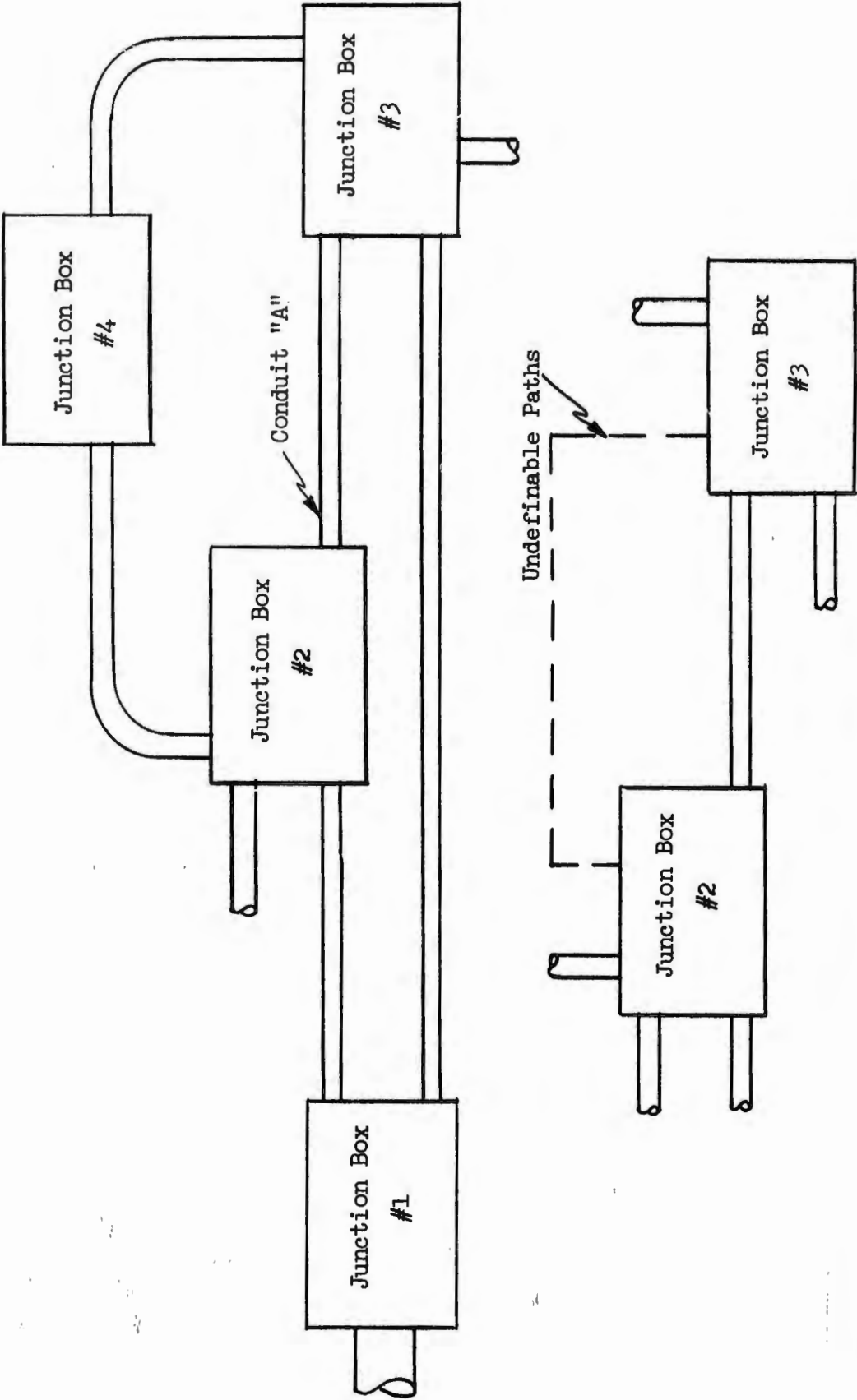


FIGURE 3.1 Typical Arrangement of Conduit Runs, Showing Undefinable Current Paths

permanently installed "sensing" circuit inside each conduit for discontinuity detection. This technique employs a high frequency source energizing a toroidal winding on a split magnetic core which can be clamped over existing conduits. Induced currents are circulated through the conduit run which acts as a secondary winding. High frequency energy, coupled into the "sensing" circuit and measured by a sensitive detector, will depend upon a number of controllable parameters, but also upon the shielding continuity of the conduit. By predetermining the controlled parameters and adjusting the exciting current accordingly, the shielding effectiveness of the conduit can be evaluated.

2. Producing locally-generated, high frequency magnetic fields and utilizing internal "sensing" circuits to search out defective joints, sections and/or connections. This technique could be applied most advantageously to accessible conduits as an adjunct to the method described above to locate conduit discontinuities.
3. Establishing an internal magnetic field within a conduit run on test by circulating currents through specially installed circuits within conduits and detecting conduit shielding discontinuities by means of external search coils.

#### 3.4 Feasibility Evaluation and Application of Conduit Discontinuity Test Techniques

To evaluate the feasibility of using high frequency energy as a means of detecting conduit discontinuities a number of tests which are described below were performed.

##### 3.4.1 Preliminary Tests

Preliminary tests were made with an empty, rectangular loop of 1/2-inch rigid steel conduit having a perimeter of about twenty feet and energized at frequencies up to 10 kHz. Using the setup of Figure 3.2, the practicability of circulating high frequency currents in a conduit system was confirmed.

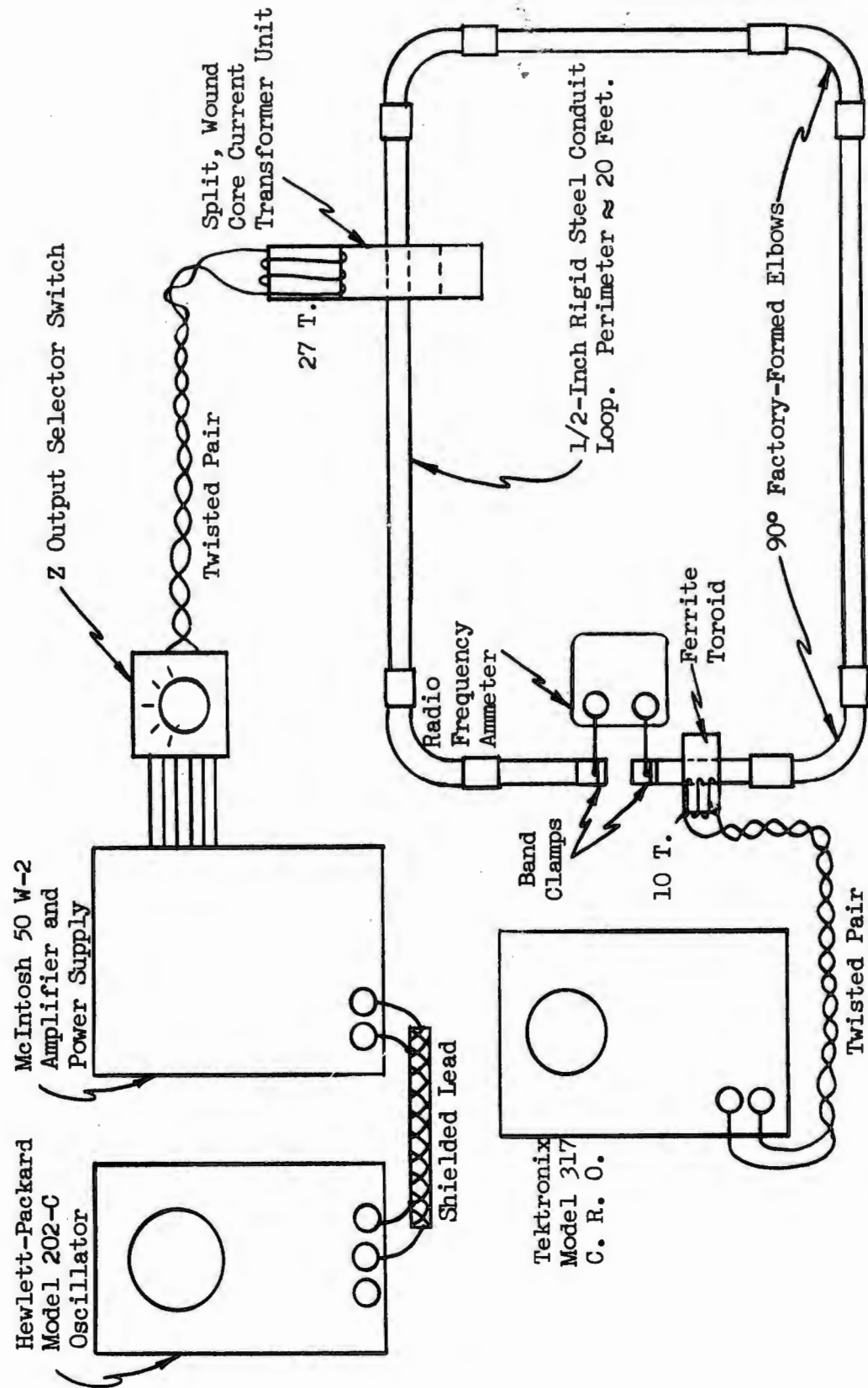


FIGURE 3.2 Preliminary Setup for RF Current Measurement Through an Empty Conduit Loop

In this test arrangement a split, wound core current transformer unit clamped around the conduit loop served as the high frequency current inducer. The high frequency current was generated by a Hewlett-Packard Model 202-C oscillator driving a McIntosh 50 W-2 amplifier. The output was matched at the various test frequencies to the primary impedance of the current transformer by means of an output impedance selector switch. A 0-5 ampere radio-frequency ammeter in series with the conduit loop was used to directly monitor the test current; its frequency and wave form were monitored by displaying on a Tektronix 317 oscilloscope the voltage developed across a sampling winding on a ferrite toroid slipped over the conduit.

The test setup described above required opening the conduit loop in order to insert the ammeter for monitoring the current. This would not be feasible in a practical application.

To overcome this objection another split, wound core, multiturn current transformer was used as a current monitor instead of the RF ammeter. Using the circuit of Figure 3.3 voltages across the multiturn winding of this unit were carefully correlated with conduit loop currents measured by means of a Tektronix 131 current probe used in conjunction with the Tektronix 317 oscilloscope. Calibration tests conducted at test frequencies of 10, 20, 30, 50, and 100 kHz over a wide range of conduit currents indicated that all responses were essentially linear.

#### 3.4.2 Circulating Current in an Extended Piping System

In order to test the practicality of circulating and measuring high frequency currents on an extensive piping system, the split core inducer and split core current transformer were then installed around an overhead sprinkler system supported by grounded hanger clamps. Measurements of the test current circulating through branching paths indicated that the technique is applicable to large, extended systems.

#### 3.4.3 Loose Joints - Accessible Conduit

To investigate the feasibility of detecting the presence of loose

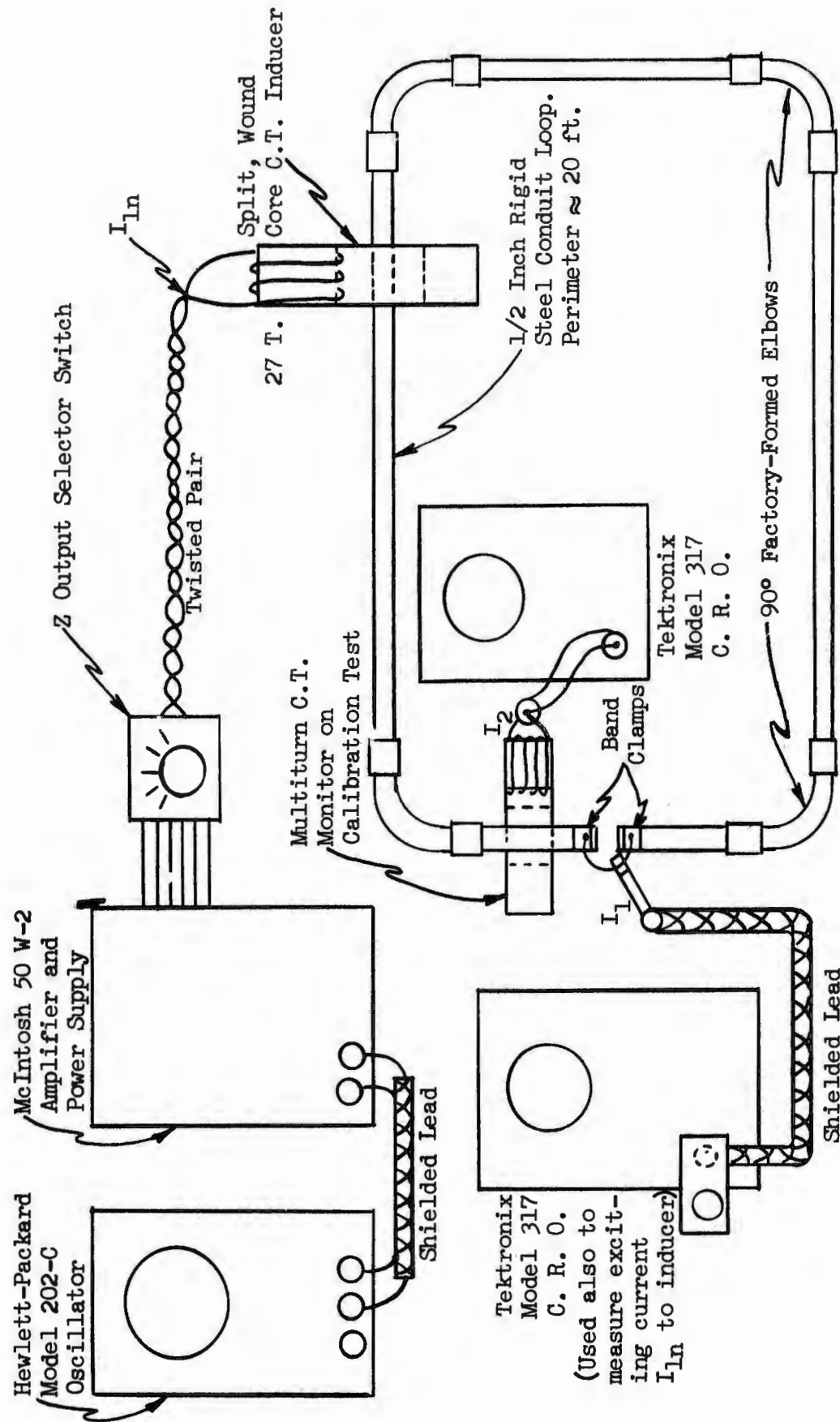


FIGURE 3.3 Test Circuit for Calibrating Wound Core, Multiturn Current Transformer for Measurement of High-Frequency Current through a Conduit or Piping System

couplings or rusted joints in accessible conduit sections, a test was next made on an empty conduit loop containing known joint defects when carrying high frequency currents. This test was set up as shown in Figure 3.4 and utilizes the principle of oscilloscopic display of the variations in voltage drop across a defective joint carrying high frequency current when it is tapped with a hammer or set into mechanical vibration by a similar means.

The same basic test arrangement was used. This consisted of a high frequency oscillator, an amplifier with a matched impedance output feeding a split, wound core current transformer clamped around the conduit. Test currents up to four amperes peak-to-peak at frequencies up to 20 kHz were used, these currents being monitored by a Tektronix Model 131 Current Probe coupled to a Tektronic Model 317 oscilloscope. Each coupling in the conduit loop was tested by securely clamping test leads adjacent to the coupling and displaying the voltage drop developed on a Tektronix Model 317 oscilloscope.

This testing technique, of course, would be feasible only for detection of conduit joint discontinuities in accessible runs, but it offers a valuable supplement to visual inspection of conduits that are accessible.

#### 3.4.4 Loose Joints - Inaccessible Conduit

Attention was next given to the development of a conduit discontinuity detection technique that would be applicable to inaccessible conduit runs. An exploration was made of a technique employing the principle that an insulated "sensing" wire contained in a conduit run would pick up a larger high frequency signal by stray-field inductive coupling with some shielding discontinuity than if the conduit were intact.

To test the feasibility of this technique, equipment was set up as shown in Figure 3.5. The test specimen was a closed rectangular loop of 1/2 inch rigid steel conduit having a perimeter of about 15 feet, assembled with a pipe-union and a pipe-tee in one short side and another pipe-tee in the

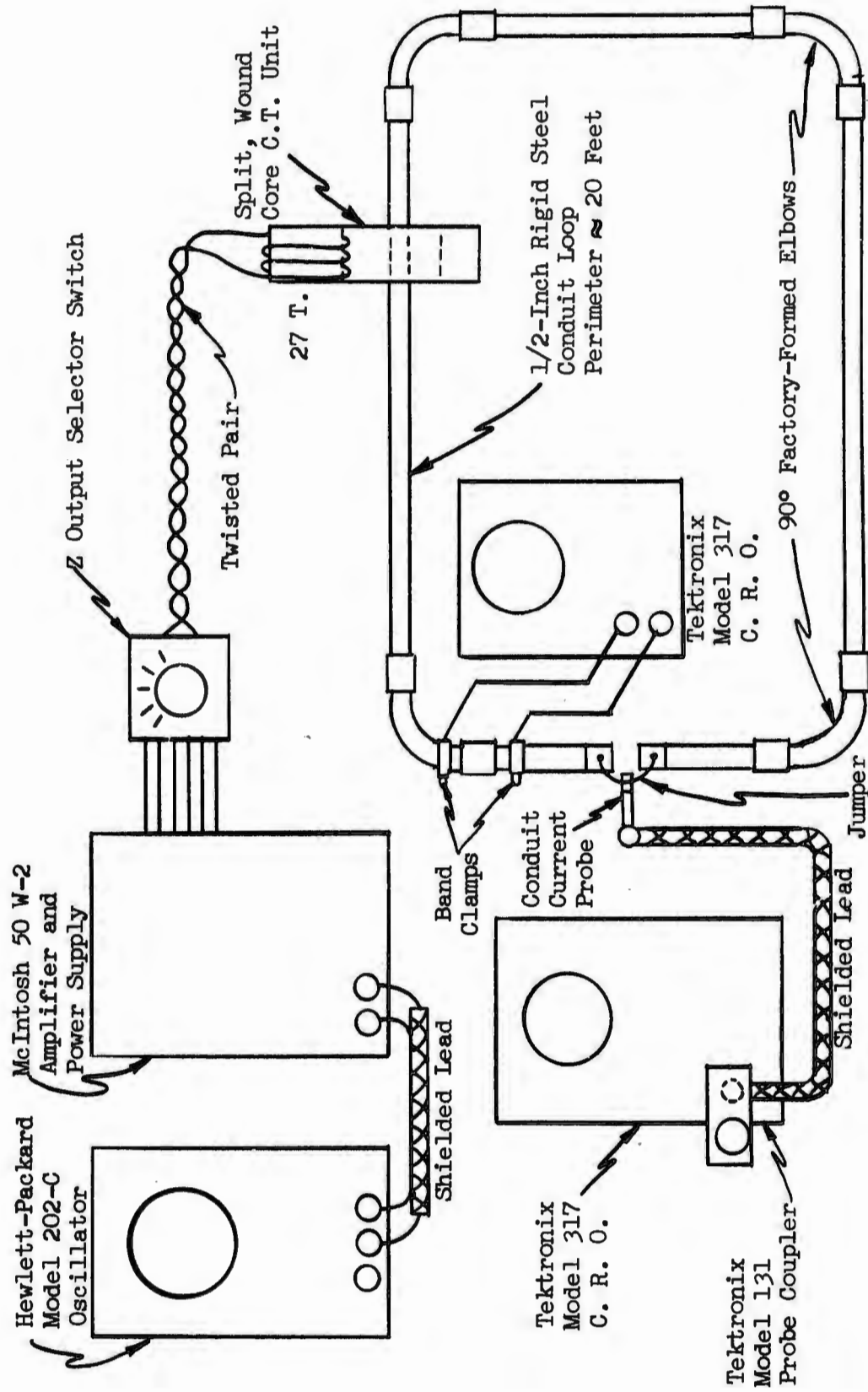
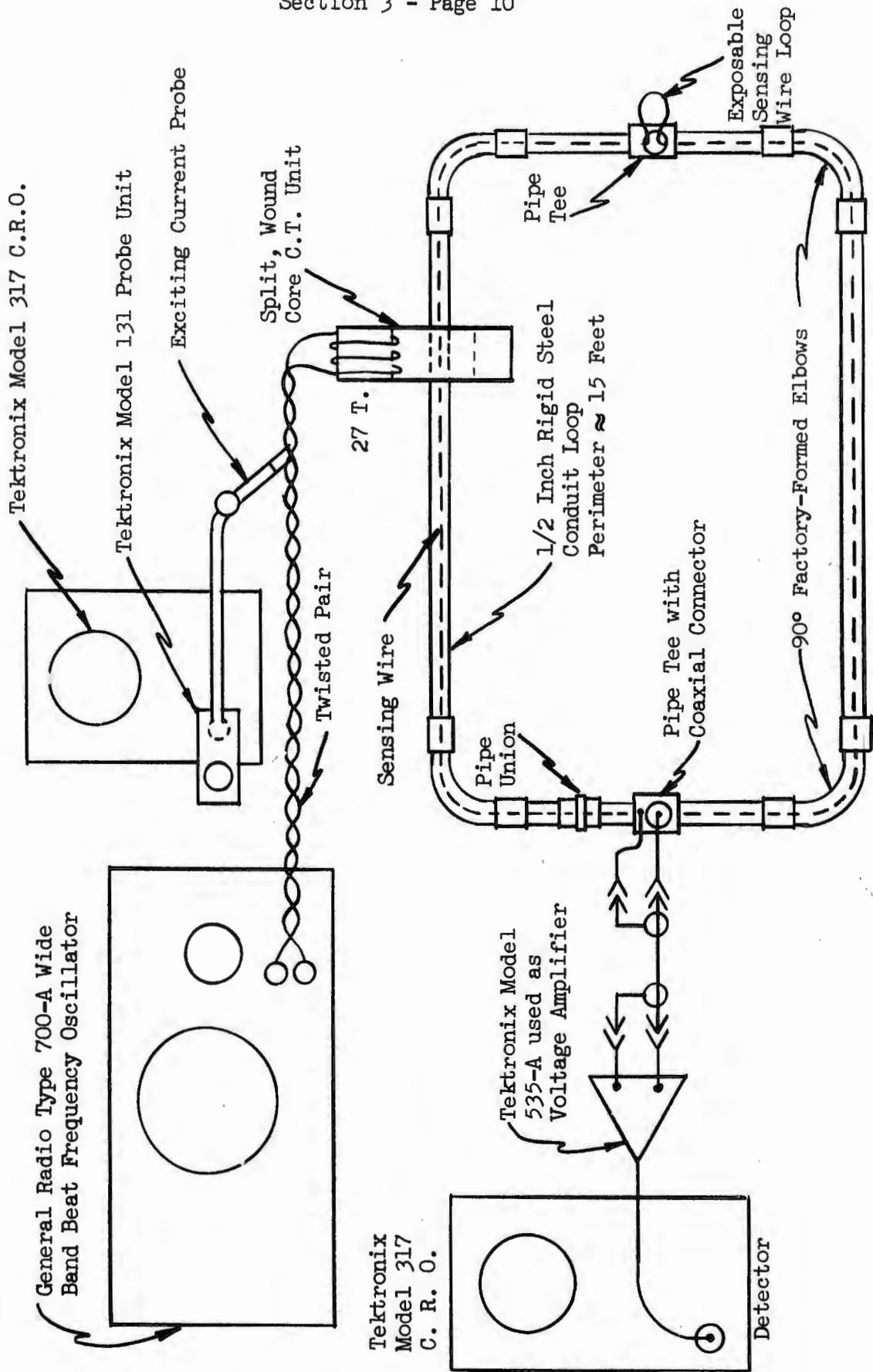


FIGURE 3.4 Variation-of-Impedance Drop Technique of Detecting Defective Joints in an Accessible Conduit Loop

FIGURE 3.5 "Sensing Loop" Technique of Detecting Discontinuities or Unshielded Wiring in an Inaccessible Conduit Run



other short side. Inside the conduit was threaded a single insulated conductor "sensing" loop terminated at a coaxial connector with one side of the connector connected electrically with the conduit. Enough slack wiring was provided to form a 4-inch loop in the pipe-tee at midrun. Here, a threaded pipe plug was used to control the degree of sealing of the pipe-tee.

It was anticipated that test frequencies somewhat higher than those used in the other experiments already described would be desirable. Accordingly, a General Radio Type 700-A wide band beat frequency oscillator capable of providing sinusoidal signals up to 5 MHz was used as the high-frequency source. At test frequencies in the range between 100 kHz and 1000 kHz it was found experimentally that this oscillator could be coupled directly to the primary winding of the split, wound core current transformer inducer for optimum power transfer. (The McIntosh amplifier was not used at these frequencies because of its limited gain, wave form distortion, and the difficulty of matching its output impedance with that of the inducer.)

The discontinuity detection circuit consisted of the sensing loop which fed an amplifier having a voltage gain of approximately 500 and a Tektronix oscilloscope which displayed the amplified signals picked up by the sensing loop. In operation detection of shielding anomalies in the conduit loop was accomplished by comparing the strength of the signal obtained when there was a defective joint or exposed wiring with the signal strength developed with good conduit connections between sections. This test technique could, therefore, be considered feasible for gross detection of defects in an entire conduit run, but not as a means of locating individual defects.

#### 3.4.5 "Pinpointing" Loose Joints

As a variation of this "gross" detection technique, it was then proposed that strong, localized high-frequency fields might be effective in "pinpointing" individual defects in a conduit run provided that portions of the run were accessible.

Generation of a strong localized field was accomplished using the equipment arrangement of Figure 3.5 by physically moving the inducing current transformer while fitted around the conduit, scanning all sections and suspected joints.

Variations of the signal voltage induced across the ends of the sensing loop were noted at the detector whenever the inducing coil was placed in proximity to conduit sections with shielding defects and peak signal voltages were observed when the inducing coil was immediately over the defect.

This localized detection technique was thus found to be feasible and it could be applied as the means of finding defective conduit sections between manholes in a buried run. However, the exact location of a shielding defect could not be found unless the suspected section was accessible.

The final detection technique investigated was one employing the same basic principles as that just described, but with the inducer and detector elements interchanged.

#### 3.4.6 Internal Magnetic Field Source

This test was set up as shown in Figure 3.6. In this arrangement the insulated wire loop threaded through the conduit served as the high-frequency magnetic field source (inducer) and the split, wound core current transformer was used as a "search coil" to pick up any high-frequency signals escaping through discontinuities in the conduit assembly.

The output of the oscillator was coupled directly into the single turn inducing wire loop by a shielded coaxial cable and the loop exciting current was measured by a Tektronic 131 current probe.

The amount of high frequency flux induced in the conduit was somewhat limited with this arrangement because of mismatch between the inductive reactance of the one-turn loop and the output impedance of the oscillator unit. Consequently, voltages induced in the winding of the "search coil" had to be amplified to a higher degree than before, so that they could be displayed on the detector oscilloscope. Nevertheless, results indicated

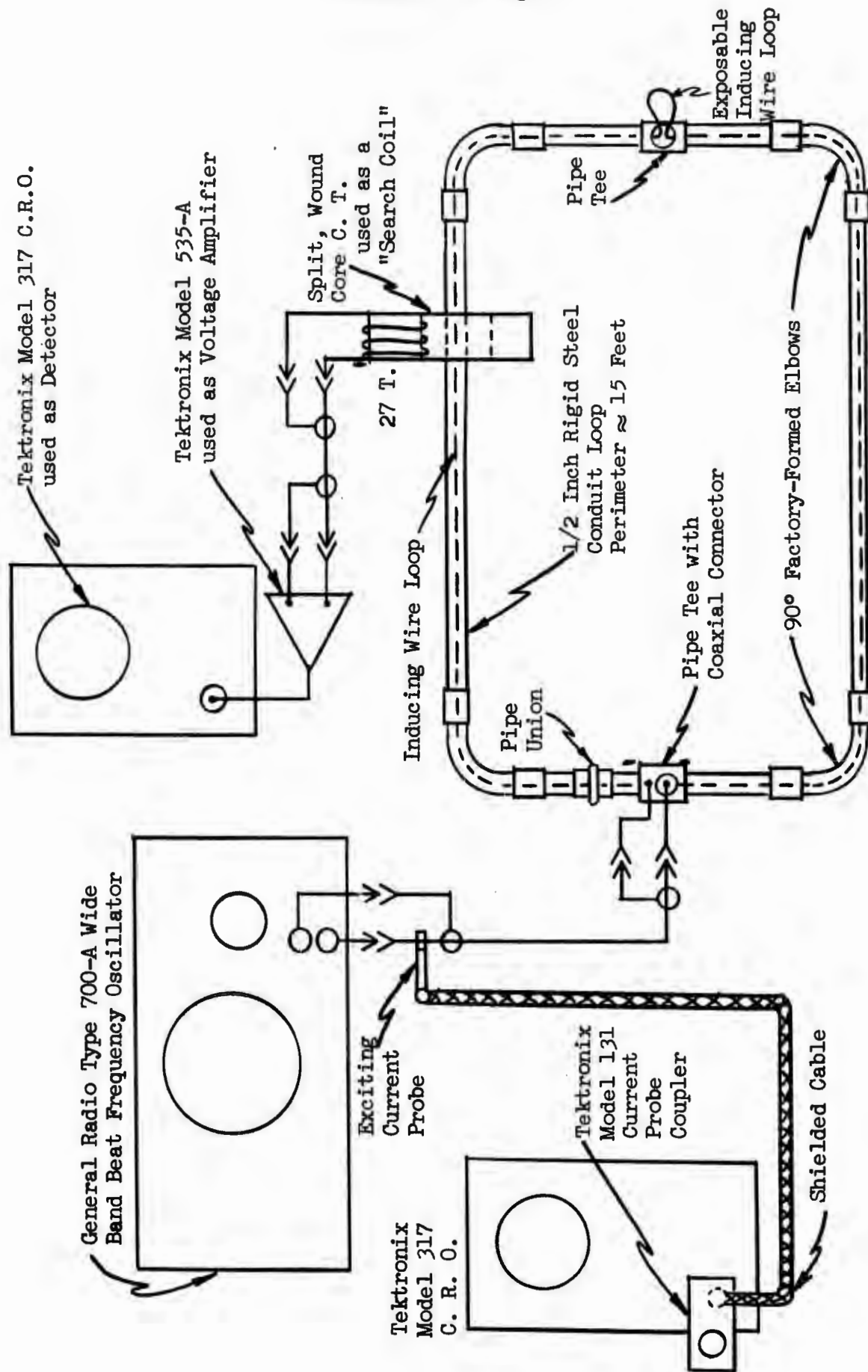


FIGURE 3.6 "Inducing Loop" Technique of Detecting Discontinuities or Unshielded Wiring in an Inaccessible Conduit Run

that this technique could be considered feasible for both the overall (fixed search coil) and the localized (moving search coil) methods of discontinuity detection.

### 3.5 Conclusions

Discontinuity detection techniques utilizing high-frequency currents are feasible for both accessible and inaccessible conduit runs. By properly applying these techniques it will be possible to distinguish between intact and defective sections of buried conduit while in place and, after exposing bad sections, to accurately locate the shielding defects in them.

The most successful detection technique developed by this investigation consists of inducing high-frequency current in the conduit run under test and to measure the relative magnitudes of voltage induced by flux leakage coupling a sensing wire that has been permanently installed in the conduit along with other wiring. Marked changes in induced voltages appear when there is a shielding defect in a bad section in the run. An extension of this technique, using a movable inducer applied in close proximity to the suspected section, is then able to precisely locate serious shielding discontinuities.

Equipment requirements that must be considered are:

1. To achieve the necessary detection sensitivity, either a relatively high power input (order of hundreds of watts) may be used with moderate gain defect display equipment or relatively low power input (less than 10 watts) may be used with high gain defect display equipment. Alternatively, it is possible to select an appropriate compromise between these design limits.
2. The defect detection equipment should be rugged (shock-mounted) and portable (compact and lightweight) enough for field use.
3. If used in remote locations beyond commercial frequency supply lines, auxiliary engine/generators with carefully filtered outputs should be used.

4. For efficient operation care should be exercised in matching the impedances of the high-frequency supply sources with those of the inducer coil.

Additional knowledge is needed about the detection capabilities of this technique with such parametric variations as larger conduits, longer runs, different conduit materials, and wall thicknesses. Another factor that might influence detector sensitivity is the presence of a number of shielded cables in the same conduit with the sensing wire.

A decision as to the merits of a single test frequency or a frequency best suited to the particular characteristics of the section of conduit on test would best be held in abeyance until more is known about these parametric effects.

## **Section 4.0**

**Measurement of Shielding Effectiveness of Shielding  
Enclosures by Continuous Sinusoidal Wave  
Attenuation as Compared to Impulse  
Wave Attenuation**

#### 4.0 MEASUREMENT OF SHIELDING EFFECTIVENESS OF SHIELDING ENCLOSURES BY CONTINUOUS SINUSOIDAL WAVE ATTENUATION AS COMPARED TO IMPULSE WAVE ATTENUATION

##### 4.1 Introduction

Various tests have been made on shielded enclosures involving the use of an impulse generator to create a pulsed magnetic field. Such a setup is shown in Figure 4.1. The generator passes a current through an overhead line down to a ground plane. This current creates a magnetic field (H-field) in the area encompassed by the overhead line and the ground plane. It is within this area that the enclosure is tested. A small H-field pickup loop is placed inside the enclosure and the reduced magnetic field intensity is monitored on equipment outside the immediate test area. The ambient field intensity, with the enclosure removed, but with the pickup loop in the same position, is also recorded. From these two values the amount of electromagnetic field attenuation provided by the shielded enclosure is calculated by using the equation

$$\text{Attenuation} = 20 \log_{10} \frac{H_1}{H_2}$$

where  $H_1$  is the instantaneous ambient magnetic field and  $H_2$  is the instantaneous attenuated magnetic field taken at the same time as  $H_1$ .

Subsequent study of the data collected from these electromagnetic pulse tests have adequately given the shielding properties of various types of enclosures<sup>1,2</sup>.

##### 4.2 Objectives

The object of this series of tests was to compare values of continuous wave attenuation made by an IEEE proposed method with electromagnetic pulse attenuation data that was obtained in previous tests<sup>3</sup>.

Impulse testing requires an elaborate test setup and procedure. Therefore, the idea of continuous wave, or sine wave, attenuation was explored,

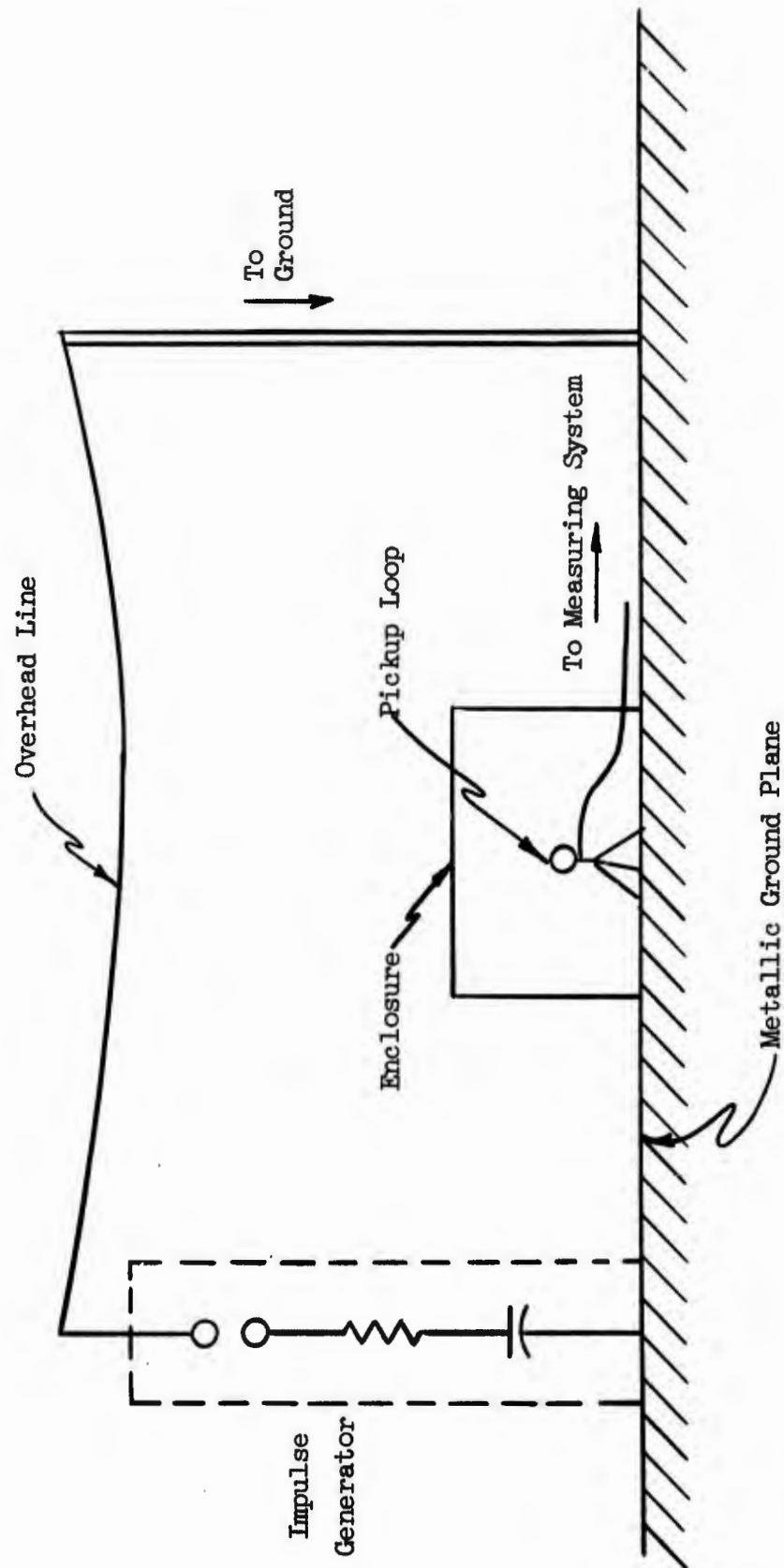


FIGURE 4.1 Pulsed Magnetic Field Testing Setup

for it is possible that this type of testing can require only a small setup area which would include the enclosure and the immediate area next to the enclosure for monitoring equipment. Also, it is possible that all measuring equipment used in continuous wave testing can be hand-carried to the location of the enclosure to be tested.

#### 4.3 Test Setup and Procedure

A series of continuous wave attenuation tests were performed on a simulated switchgear enclosure shown in Figure 4.2. A current signal of known frequency and amplitude is passed through a loop of wire of known physical dimensions. This current immerses the enclosure in a magnetic field oriented to induce appreciable components of current throughout the shield. A significant portion of the seams are subjected to shielding currents by encircling the enclosure with the transmitting loop so as to obtain a gross measure of performance. The field set up by this transmitting loop is sensed by a loop antenna (30" diameter Stoddart 90117-2) and is read on a Stoddart radio interference field intensity meter (RI-FI NM-10A). Readings on the field intensity meter are normally given in terms of an equivalent electric field E. The corresponding magnetic field H is then obtained from the expression

$$H = \frac{E}{12 \pi} = \frac{E}{377}$$

where

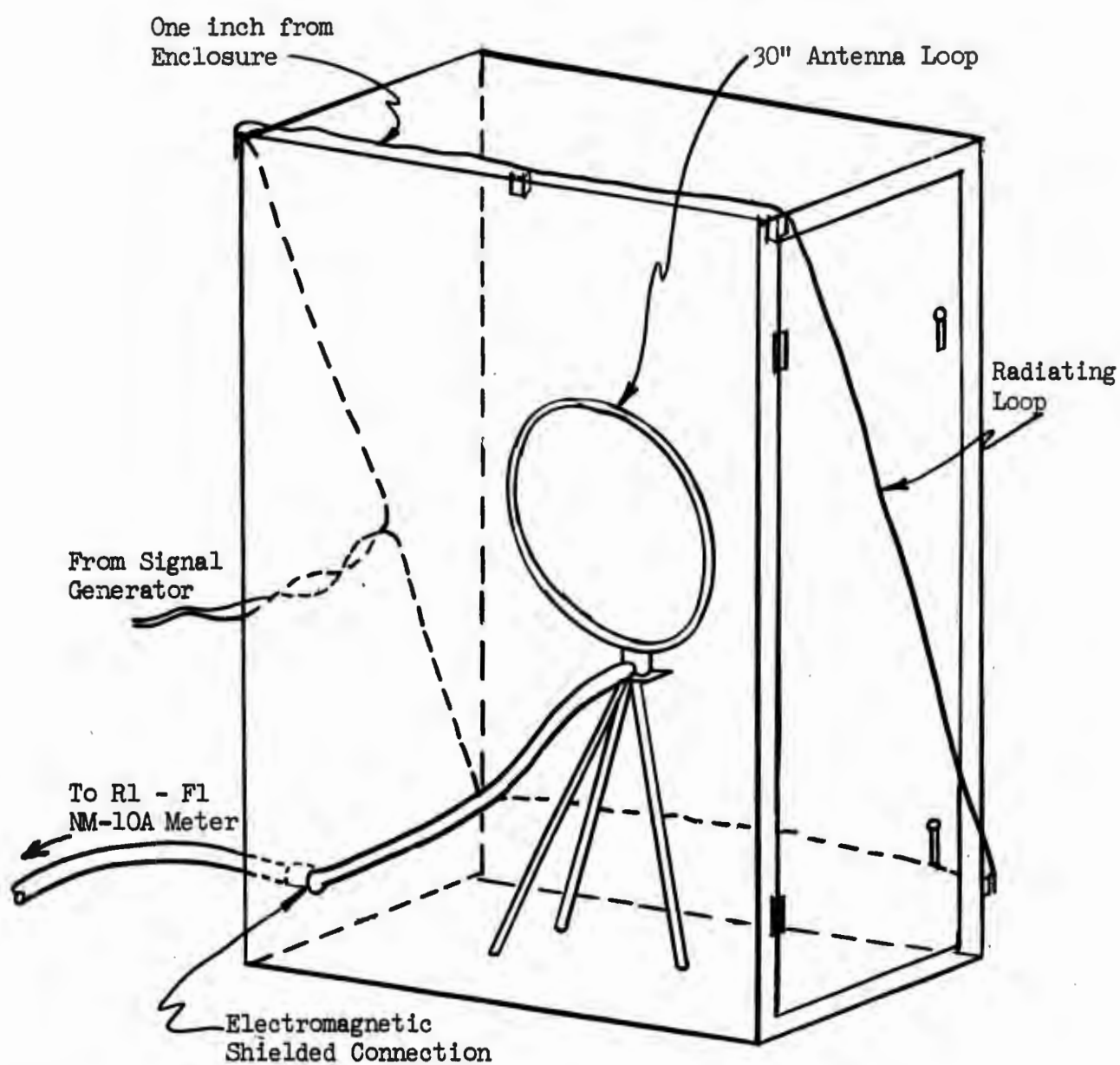
H = amps/meter

E = volts/meter

Ambient values of field intensity were found by placing the antenna loop in space concentric with the larger transmitting loop, as shown in Figure 4.3. To receive attenuated values of field intensity the antenna loop was placed at a fixed position inside the switchgear enclosure. The amount of attenuation, in dB, is calculated the same as in impulse testing.

#### 4.4 Test Results

By varying the frequency of the signal produced by the signal generator



NOTE: Antenna and radiating loop in same plane.

FIGURE 4.2 Test Setup

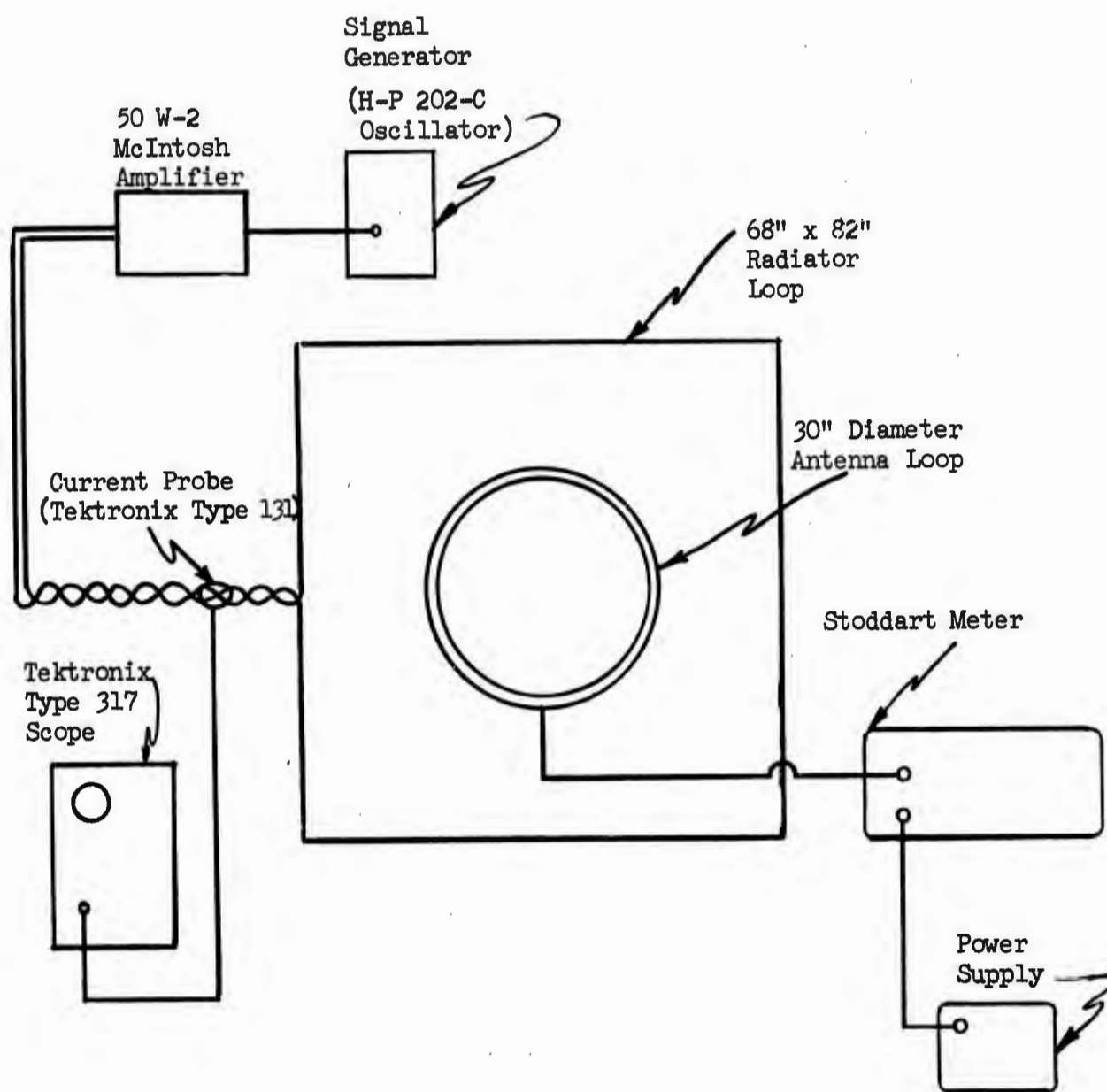


FIGURE 4.3 Wiring Diagram of Continuous Wave Attenuation Measuring Circuit

the amount of attenuation afforded by the enclosure was found to vary from a low of 34.5 dB at 15 kHz to a high of approximately 43 dB at 100 kHz.

The variation in attenuation values is due to the fact that the door of the enclosure was sealed for various stages of susceptibility to electromagnetic field leakage. Figure 4.4 is a comparison of the various levels of attenuation that are afforded by the different methods of sealing the enclosure door. The low attenuation value of 34.5 dB at 15 kHz was recorded with the enclosure door fastened shut by four screws. The higher attenuation value of 43 dB at 100 kHz was recorded with the enclosure door sealed with eight bolts and with a copper braid strip placed between the door and enclosure to seal the inside of the enclosure from the generated electromagnetic field.

In comparing the continuous wave attenuation data with impulse data the period of oscillation, in microseconds, was calculated for the various frequencies. It is at these various times that the levels of attenuation observed by using the two modes of testing are compared. Table 4.1 lists these attenuation values.

TABLE 4.1

SINE WAVE AND IMPULSE WAVE ATTENUATION VALUES

|                      | <u>Attenuation - dB</u>                 |
|----------------------|---|
|                      | <u>10 <math>\mu</math>sec - 100 kHz</u> |
| Sine @ 100 kHz       | 43, 40, 38.5                            |
| Pulse @ 10 $\mu$ sec | 42, 40.5, 40                            |
|                      | <u>40 <math>\mu</math>sec - 25 kHz</u>  |
| Sine @ 25 kHz        | 38.5, 36.5, 35.5                        |
| Pulse @ 40 $\mu$ sec | 35, 33, 31.5                            |
|                      | <u>67 <math>\mu</math>sec - 15 kHz</u>  |
| Sine @ 15 kHz        | 38, 36, 34.5                            |
| Pulse @ 67 $\mu$ sec | 29.5, 27, 26.5                          |

Figure 4.5 shows a graphical comparison of the recorded attenuation values.

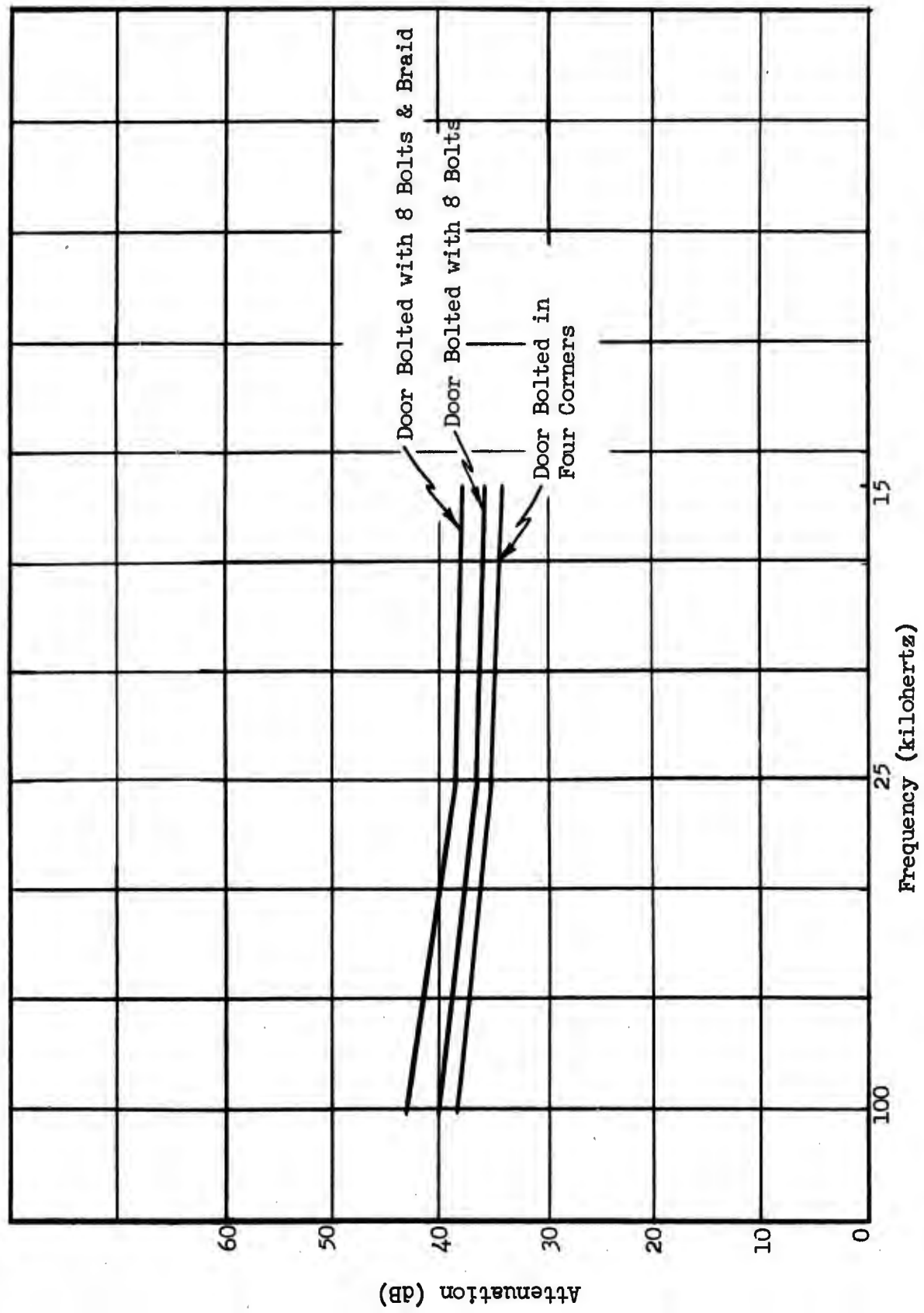
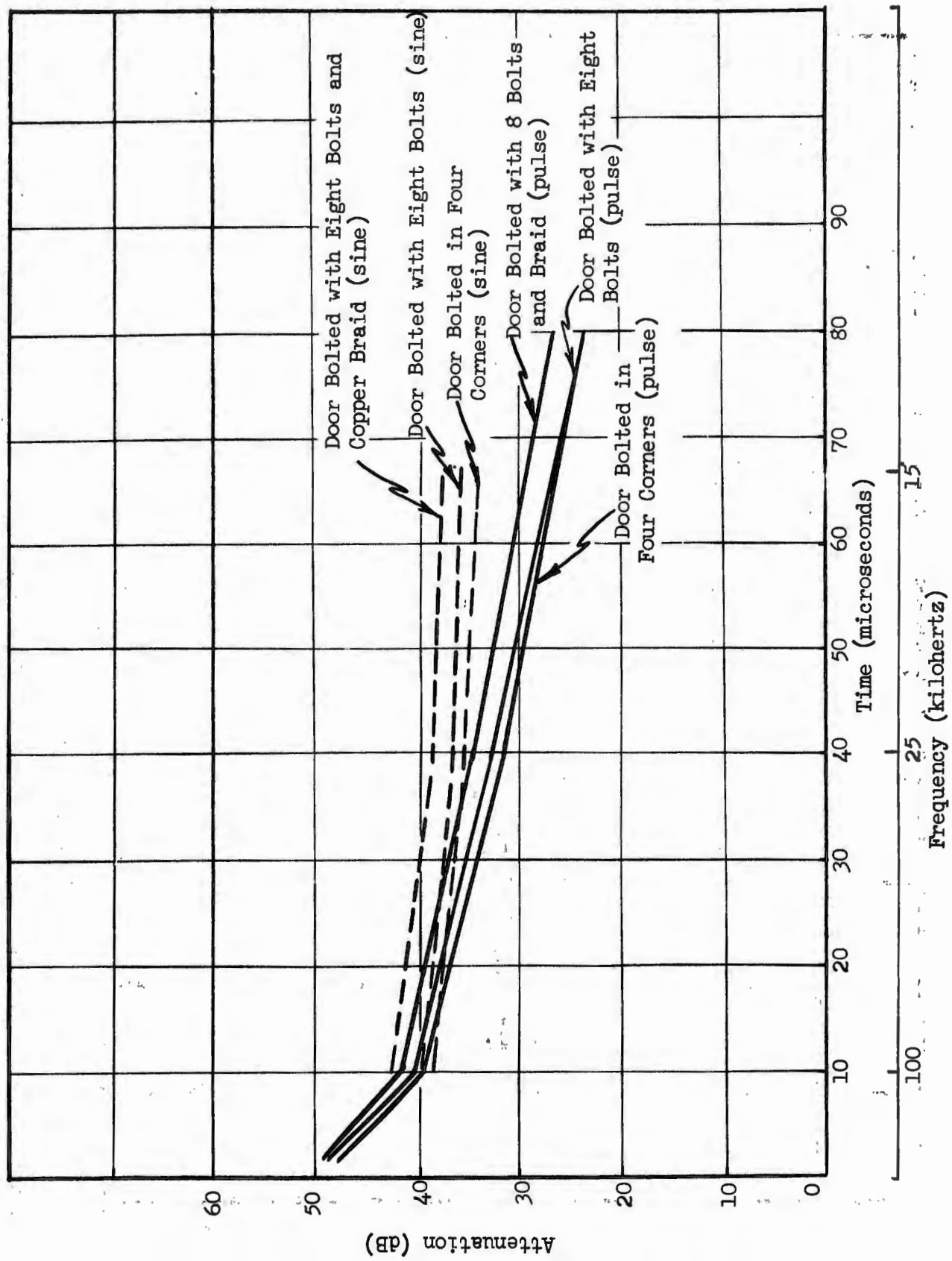


FIGURE 4.4 Continuous Wave Attenuation vs. Frequency for Various Methods of Sealing Enclosure Door

FIGURE 4.5 Comparison of Impulse Tests to Sine Wave Tests vs. Time and Frequency



In the short time period, or higher frequency level, the H-field attenuation values observed in the continuous wave tests and the impulse wave tests are in close agreement with each other. However, at longer times and lower frequencies the decrease in attenuation is more rapid in the impulse wave tests.

This difference is due to the fact that in impulse testing the attenuated wave measured inside the enclosure is different than the applied wave. The attenuated wave shape is distorted with a longer time-to-peak and a much longer time-to-decay to half of the crest value. The slope of the decaying part of the attenuated impulse wave is smaller than the shape of the ambient impulse wave. As the two decaying slopes approach each other, the calculated attenuation decreases. Therefore, at longer times the impulse attenuation values are seen to decrease.

In the continuous wave tests there is no change in the wave shape of the attenuated sinusoidal wave.

#### 4.5 Conclusions

The results of the continuous wave tests show that this method can be used with fairly good accuracy for observing enclosure shielding properties. The frequency range of the field intensity meter was 15 kHz to 250 kHz. This range was adequate when the periods of oscillation of the various frequencies used were calculated and compared with the time range of the impulse tests. It is within the time range of 0 to 100 microseconds that the most important attenuation data of interest to this particular test is obtained.

REFERENCES

1. Flegel, H. E. and Lyke, A. J., WELDED WIRE FABRIC ENCLOSURE ATTENUATIONS AND ELECTRICAL SYSTEM COMPONENT RESPONSES TO MAGNETIC FIELD PULSES (U), General Electric Company, 5 July 1966.
2. Lyke, A. J., SOLID PANEL ENCLOSURE ATTENUATIONS AND ELECTRICAL SYSTEM RESPONSES TO MAGNETIC FIELD PULSES (U), General Electric Company, 28 February 1967.
3. Bridges, J. E., PROPOSED IEEE STANDARD ON MEASUREMENT OF SHIELDING EFFECTIVENESS OF HIGH-PERFORMANCE SHIELDING ENCLOSURES, The Institute of Electrical and Electronic Engineers, Inc., January 1967.

..

..

## **Section 5.0**

### **Geometric Models for the Investigation of NEMP Induced Currents in Buried Conduits**

..

..

..

..

## 5.0 GEOMETRIC MODELS FOR THE INVESTIGATION OF NEMP INDUCED CURRENTS IN BURIED CONDUITS

### 5.1 Introduction

An important aspect of the OCE program to develop design criteria for protection of NIKE-X power plants and facilities electrical systems against NEMP is the problem related to the determination of the magnitudes of NEMP induced voltages and currents on buried conduits and structures and the extent to which the induced quantities are dependent on design parameters such as grounding arrangements, depth of burial, spacing of structures, etc. This report describes a combined analytical and experimental approach to the problem based on geometric modeling techniques. The particular approach was initiated in an attempt to verify and/or extend the results obtained by experimenters at the General Electric Company as reported by D. W. Caverly<sup>1</sup>. The excellent results obtained to date indicate that the method offers an extremely simple, highly efficient solution to the existing problem.

### 5.2 Geometric Models

#### 5.2.1 Models in General

Geometric models have been used successfully in areas of investigation such as power transmission line response and shielding studies. Generally speaking, it is usually impossible to model exactly a given electrical system or circuit in such a manner as to retain an absolute scale factor for both electrical and physical dimensions. The difficulty usually lies with the stringent requirements imposed by conductivity scale factors. However, in situations in which it is desired to study only the effects of variations of physical parameters on the magnitude or nature of the quantities of interest, the geometric model is a powerful tool. The usefulness of the model in such situations is greatly exemplified by the quantity and quality of information obtained in studies concerned with the shielding effectiveness of various geometric structures<sup>2,3</sup>.

### 5.2.2 Modeling for the Buried Conduit Problem

The problem considered here is one that lends itself to solution by modeling techniques when it is viewed in terms of the ultimate objective of the investigation; namely, the development of design criteria for NIKE-X electrical systems installations. For that purpose there exists the need to investigate the manner in which the magnitudes of induced currents in buried conduit are affected by such factors as:

1. the length and depth of the conduit.
2. the geometry of the grounding elements and structures at the conduit terminations.
3. the proximity of conduits with a group.
4. the electrical contact between the conduit and surrounding earth.
5. discontinuities or breaks in the conduit.

Toward that end, an experimental modeling facility was constructed and experiments performed with various geometric grounding arrangements and spacings. The remainder of this report is a detailed description of the entire experiment and conclusions drawn therefrom.

## 5.3 Modeling Facility

### 5.3.1 Experimental Tank

In order to establish a controlled ground environment in which to bury configurations of interest, a 3' x 3' x 5' tank was constructed and filled with sand which was doped with ordinary salt. Details of the tank are shown in Figure 5.1a and Figure 5.1b. The tank is of all wood construction and filled with clean builders sand. As delivered, the sand had an average resistivity of approximately 7500 ohm-meters. This value was found to be inconveniently high; therefore, a salt-water solution was added and mixed thoroughly in order to lower the resistivity to approximately 18 ohm-meters. Mounted on one side of the tank near the top, center, and bottom are three pairs of electrodes of 2" x 2" x 1/8" aluminum, each pair separated by 2". These electrodes are for the purpose of monitoring the relative conductivity of the sand throughout the box.

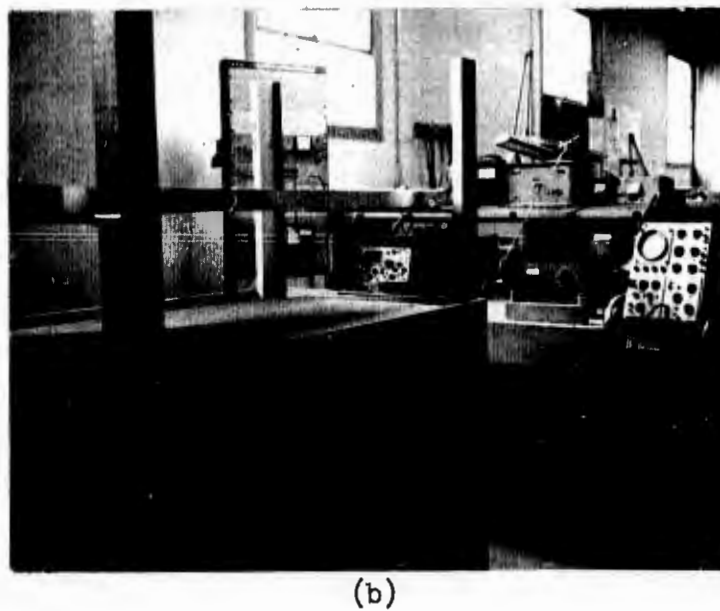
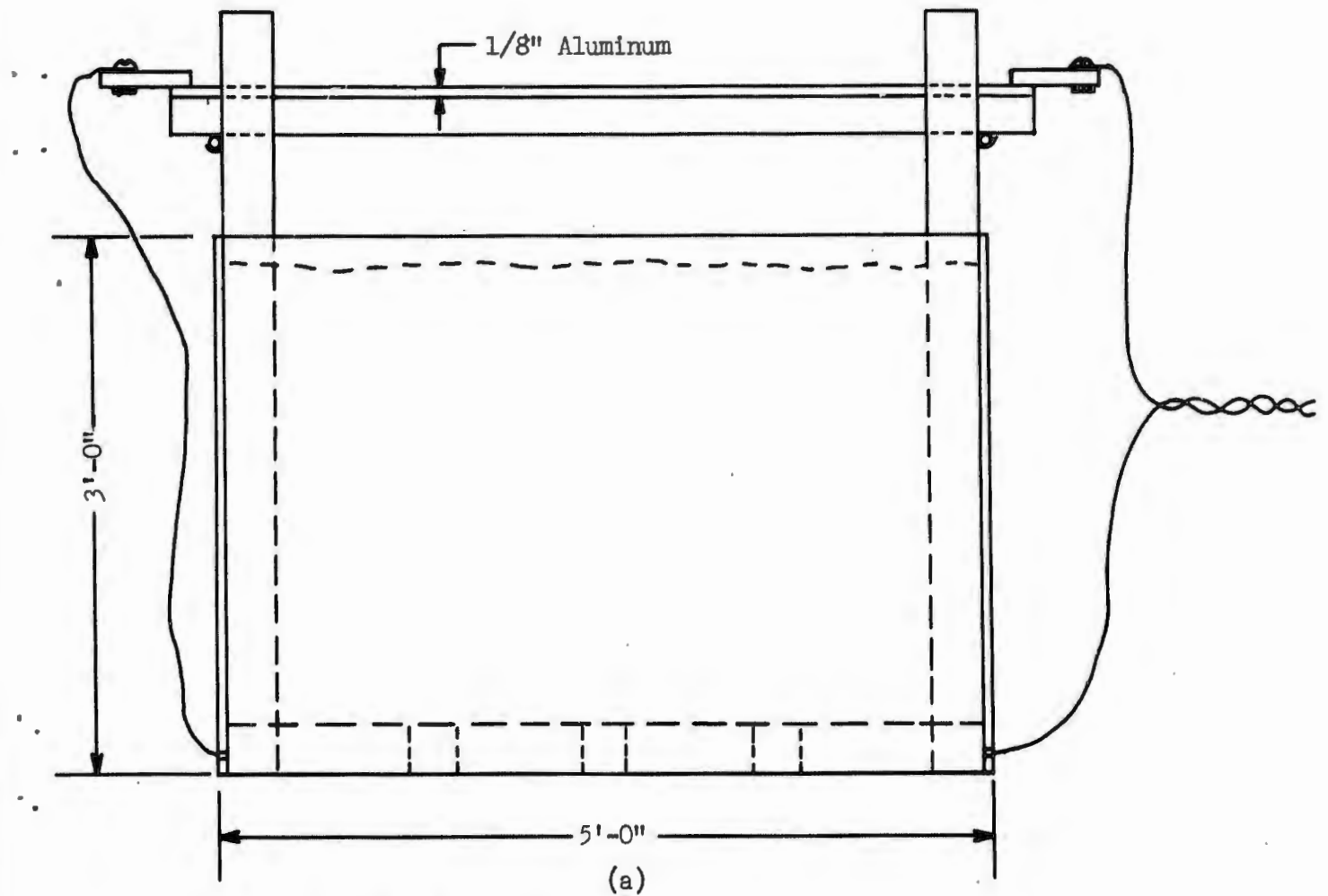


FIGURE 5.1

(a) Details of Tank and Magnetic Field Generator

(b) Photo of Tank, Field Generator, and Instrumentation

### 5.3.2 Conductivity Measurement Apparatus

Measurements of conductivity were made by two different methods. In the first, an insulated box of inside dimensions 2" x 2" x 12" fitted with flat electrodes over the 2" x 2" surfaces was constructed and the resistivity of the sand determined from the resistance between electrodes as measured with an ESI resistance bridge when the box is filled with sand. For this configuration, the current distribution through the box is fairly uniform and the resistivity of the sand is given by  $\rho = 0.85 R_{\text{box}}$  ohm-meters. The second method utilizes a Wenner array consisting of four, one-foot lengths of 3/8" copper tubing spaced in line on 6" centers. The resistivity was measured by inserting the array in the sand, applying a current to the outer rods and measuring the voltage across the inside rods. Details on the method are given in a report by A. J. Lyke<sup>4</sup> and it is easily shown that  $\rho = 1.63 R$  ohm-meters where  $R = \frac{\text{measured voltage}}{\text{applied current}}$ . Details of both devices are shown in Figure 5.2.

### 5.3.3 Magnetic Field Generator

A pulsed magnetic field, uniform over and tangential to the surface of the tank, is developed by means of a flat conducting sheet over the tank supplied by a repetitive current pulser delivering 80 amperes peak. The sheet consists of an aluminum plate 2' x 5-1/2' x 18" fitted with 1/4" plates, 6" long on each end for the purpose of uniformly distributing the current over the 5' segment directly above the tank. Details of the sheet can be seen in Figure 5.1 and wave forms of the current and derivative of the magnetic field (B) are shown in Figure 5.3.

### 5.3.4 Instrumentation

The following subsections describe the instrumentation used for the various quantities measured.

#### 5.3.4.1 Resistance

All resistance measurements were made with one or both of the following:

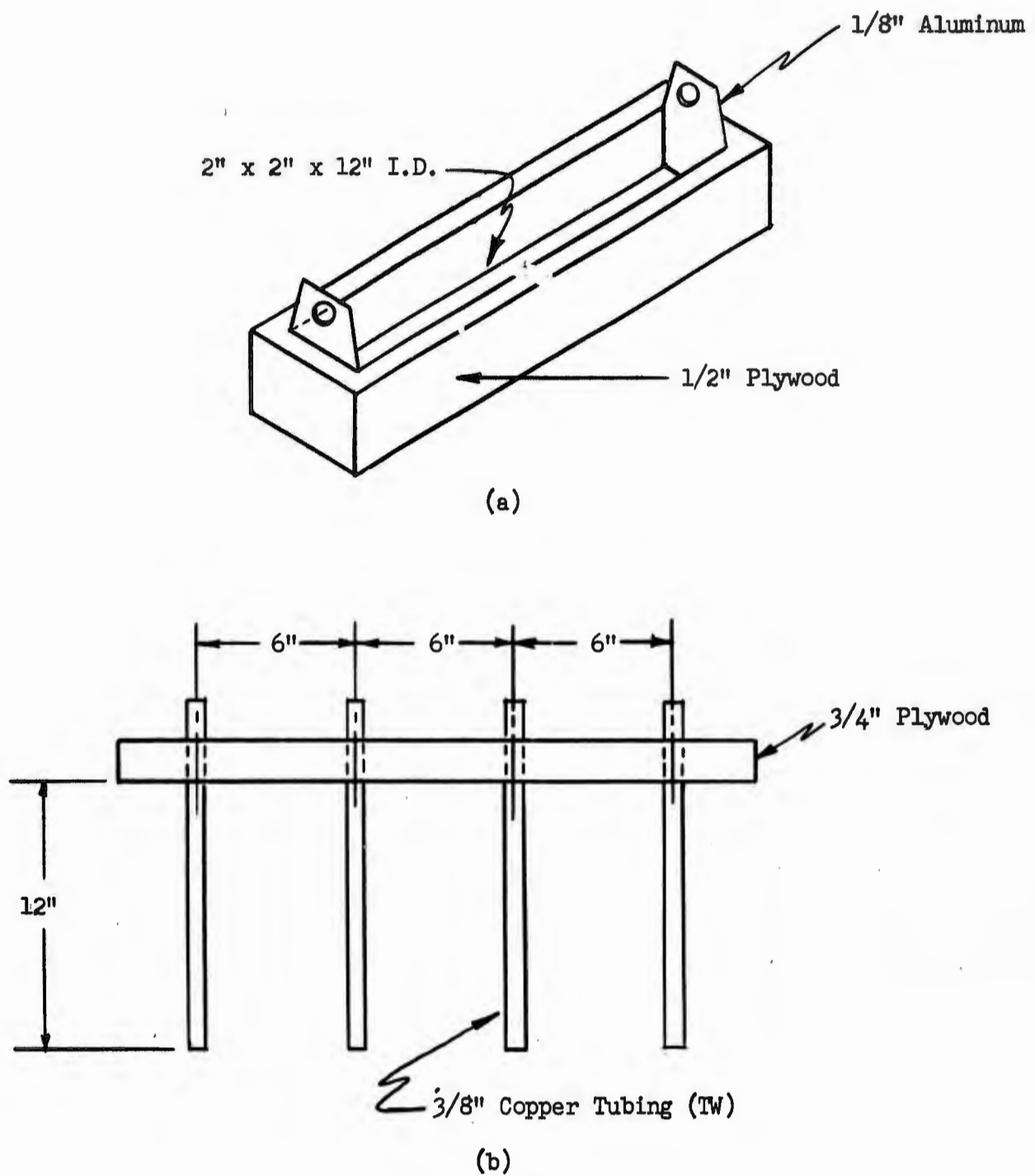
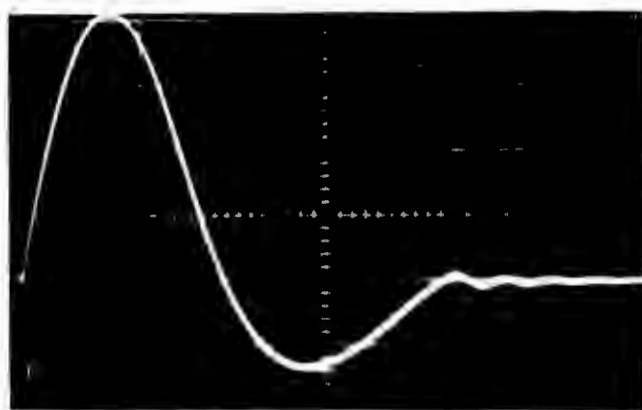
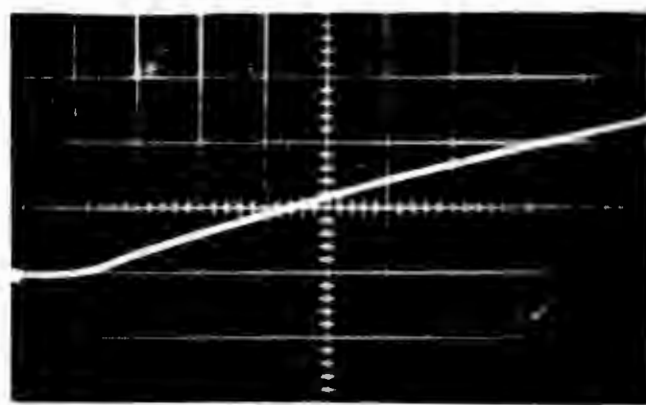


FIGURE 5.2 (a) Box for Measurement of Sand Resistivity  
(b) Wenner Array

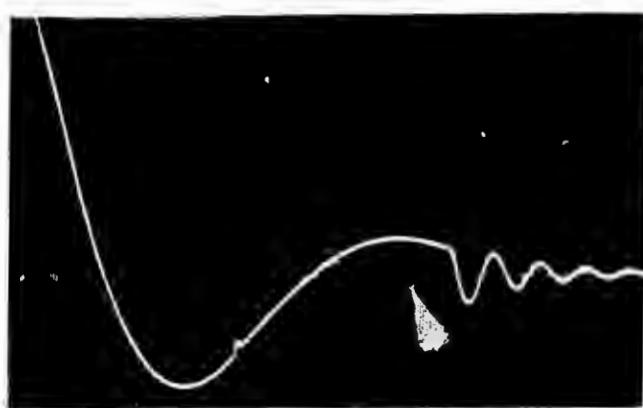


10  $\mu\text{s}/\text{cm}$

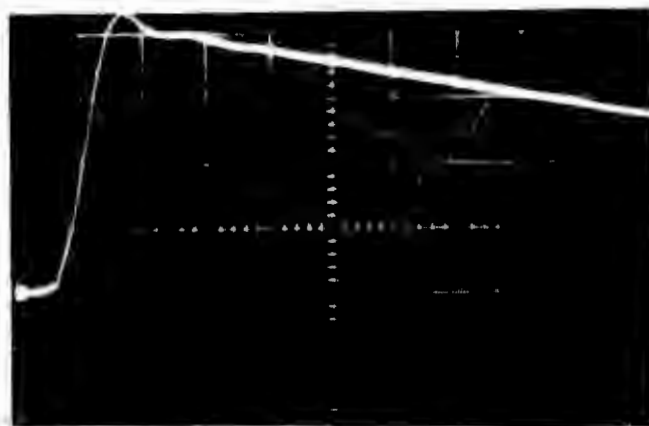


0.5  $\mu\text{s}/\text{cm}$

a) Current into magnetic field generator. Vertical Scale = 20 amp/cm



10  $\mu\text{s}/\text{cm}$



0.5  $\mu\text{s}/\text{cm}$

b) Derivative of magnetic field,  $B$ , at surface of sand.  
Vertical Scale = 50 mV/cm

FIGURE 5.3 Generator Current and Derivative of Magnetic Field

- a) Electro Scientific Ind. Model PVB 300 potentiometric bridge
- b) Voltmeter-Ammeter method using a Simpson 260 milliammeter and an HP 410C VTVM.

#### 5.3.4.2 Time-Varying Current

All time-varying current measurements were made with a Tektronix Model P6016 current probe and one of the oscilloscopes described below. Maximum current sensitivity with this arrangement is 12 ma/cm on either scope.

#### 5.3.4.3 Magnetic Field

The derivative of magnetic field (b) was measured using a one-turn loop detector of 100 cm<sup>2</sup> cross section and resonant frequency well above 100 Mc. The magnetic field was held constant for most measurements and, by graphical integration of the  $\dot{B}$  curve, was calculated to be about 35 A/m peak.

#### 5.3.4.4 Oscilloscopes

The following oscilloscopes were used for all pulsed measurements:

- a) Fairchild Models 777 (Dual Beam) and 776H with wide band amplifiers
- b) Tektronix type 453.

#### 5.3.4.5 Frequency Response

All frequency response curves were obtained using an HP Model 606A, 50 kHz-65 MHz signal generator to drive the circuit under test and a Millivac Model MV 928A RF voltmeter and probe for response measurements.

### 5.4 Experiments Performed

#### 5.4.1 Objective

The primary objective of the experimental work performed was to:

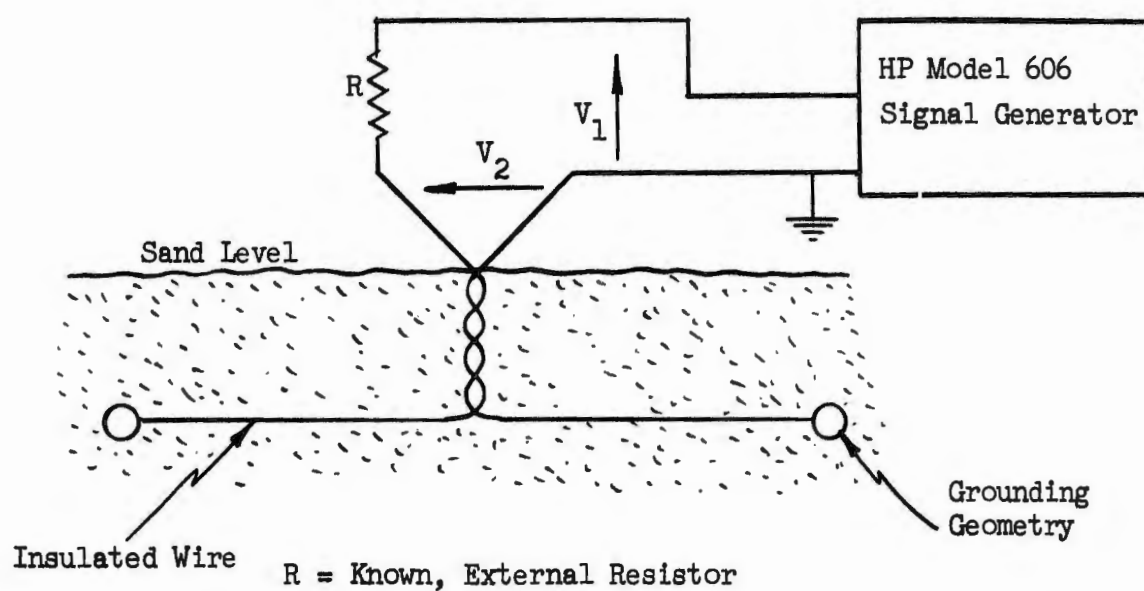
1. Establish an equivalent resistance-inductance circuit for a loop consisting of a buried conductor with given end grounding conditions from which the magnitude of current induced in the conductor by a pulsed magnetic field at the surface could be determined.

2. Investigate the possibility of the existence of relationships between the magnitude of current induced in the conductor by a pulsed field, the effective area of the pickup loop calculated on the basis of an equivalent R-L circuit representation for the loop, and the circuit parameters measured at the terminals of a break in the conductor-ground loop.

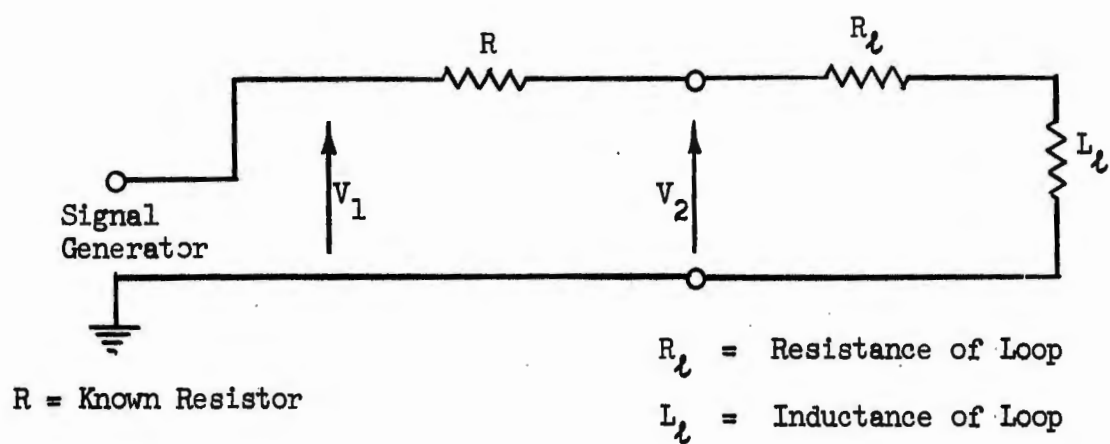
#### 5.4.2 Procedure

All experiments were performed with simple grounding geometries which included spheres, rods, and flat plates. The overall program was divided into three parts as follows:

1. Resistance measurements. In order to establish the validity of the modeling technique, resistance measurements were made on spheres, hemispheres, and cylinders and compared to calculated values. These experiments were performed prior to doping the sand with salt.
2. Circuit parameters. For various geometries and separations, an attempt was made to determine the circuit parameters for the loop under consideration using frequency response methods. With a known resistance in series with the loop, the applied voltage and voltage at the loop terminals was measured as a function of frequency (See Figure 5.4). Anticipating an R-L equivalent circuit, the inductance could be calculated from the 3 dB point on the frequency response plot since the resistance could be measured independently.
3. Induced currents. The magnitude and wave forms of currents induced in conductors when a pulsed field was applied at the surface were recorded for various geometries and separations. From this information, the effective area of the pickup loop was calculated based upon a postulated R-L model for the loop and measured values of resistance.



(a)



(b)

FIGURE 5.4 (a) Typical Arrangement for Frequency-Response Measurement  
(b) Equivalent Circuit for (a) Based on an Assumed R-L Model for the Underground Loop

### 5.4.3 Results

#### 5.4.3.1 Resistance Measurements

In Appendix A, the equations for the resistance between pairs of spheres, hemispheres, and rods are derived. Comparisons of the measured values of resistance for various configurations with values calculated from the derived expressions are given in Tables 5.1, 5.2, and 5.3.

#### 5.4.3.2 Circuit Parameters

During initial attempts to determine the equivalent circuit parameters for the loop by frequency response techniques, some difficulties were encountered due to the high resistance and low reactance of a typical loop. Upon refinement of the measuring technique, usable results were obtained for parallel rods (two) and spheres separated by two feet. The frequency response curves for each case are shown in Figures 5.5 and 5.6.

#### 5.4.3.3 Induced Currents

Oscillographic data of induced current and applied magnetic field was obtained for the parallel rods and flat-plate grounds for various separations and depths. A typical set of data for the rods is shown in Figure 5.7. The purpose of these tests was to determine the effective area of the pickup loop corresponding to a particular geometry and, as shown in Section 5.5.3.1, it is only necessary to obtain values of induced current and  $\dot{B}$  at one instant of time in order to calculate the area. For this reason, it was not necessary to record the entire current-wave form for each test. Figure 5.8 shows the arrangement for three types of tests performed and data obtained is presented in Tables 5.4, 5.5, and 5.6.

One experiment was performed to determine the effect of the insulation on the wire. The parallel rods four feet apart just below the surface and connected by a bare wire laying on the surface were used in this test. First the wire was insulated from the sand by a thin sheet of polyethylene and the peak induced current measured. Then the insulation was removed, the wire covered with sand, and current at various points along the wire was measured. The results of this test are shown in Table 5.7.

TABLE 5.1

Calculated and Measured Resistance between Two Cylinders 12" Apart.

Ground resistivity,  $\rho = 5,100$  ohm-meters.

| <u>Depth (inches)</u> | <u>R<sub>calc</sub> (kilohms)</u> | <u>R<sub>meas</sub> (kilohms)</u> |
|-----------------------|-----------------------------------|-----------------------------------|
| 6                     | 46                                | 50                                |
| 12                    | 23                                | 28                                |

TABLE 5.2

Calculated and Measured Resistance between Two Spheres 3" Deep.

Ground resistivity,  $\rho = 7,600$  ohm-meters

| <u>Separation (inches)</u> | <u>R<sub>calc</sub> (kilohms)</u> | <u>R<sub>meas</sub> (kilohms)</u> |
|----------------------------|-----------------------------------|-----------------------------------|
| 3                          | 173                               | 190                               |
| 6                          | 182                               | 200                               |
| 12                         | 190                               | 200                               |

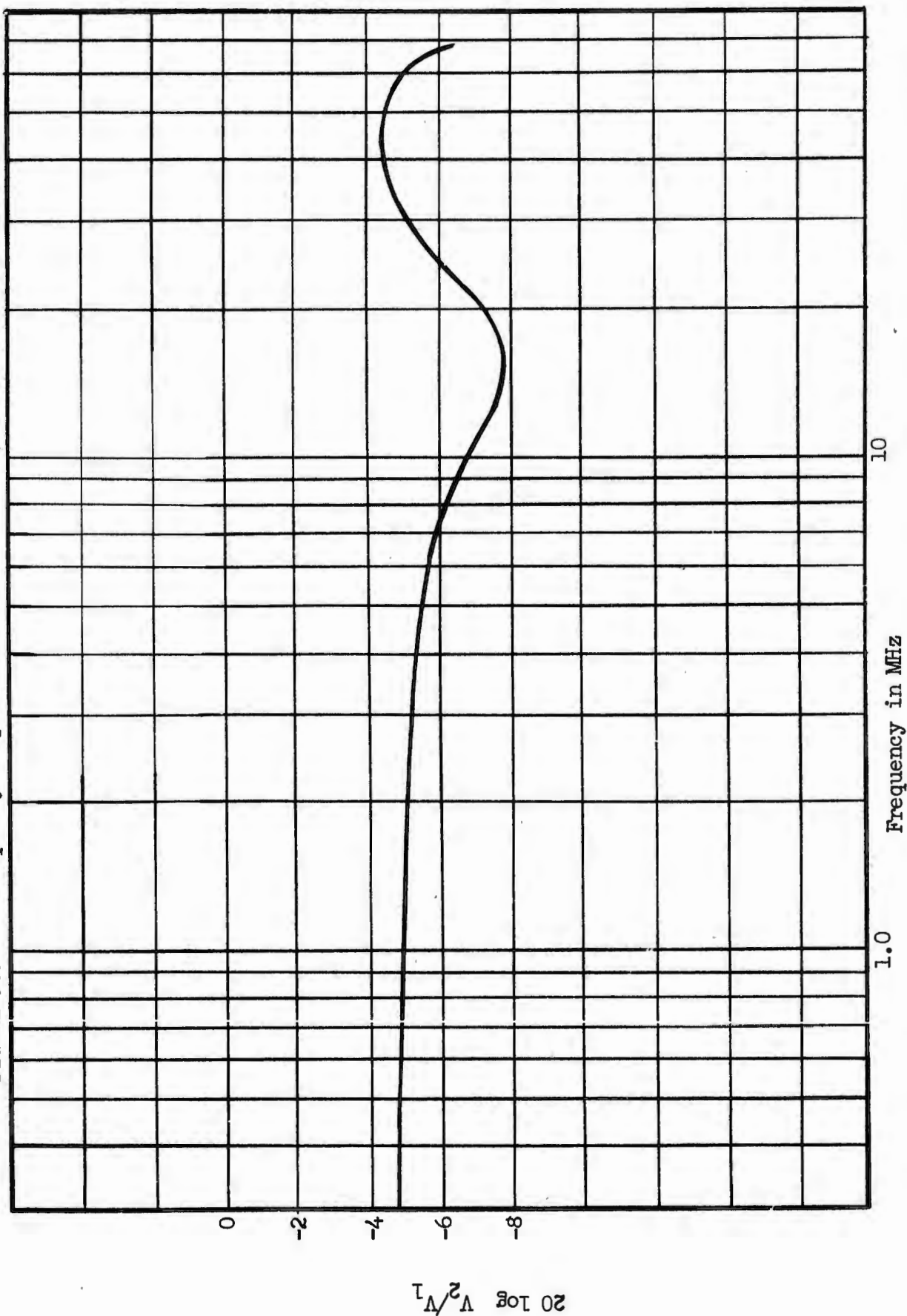
TABLE 5.3

Calculated and Measured Resistance between Two Hemispheres on the Surface.

Ground Resistivity,  $\rho = 7,600$  ohm-meters

| <u>Separation (inches)</u> | <u>R<sub>calc</sub> (kilohms)</u> | <u>R<sub>meas</sub> (kilohms)</u> |
|----------------------------|-----------------------------------|-----------------------------------|
| 1                          | 253                               | 220                               |
| 3                          | 346                               | 310                               |
| 6                          | 364                               | 380                               |

FIGURE 5.5 Frequency Response for Parallel Rods, Two Feet Apart.  $R = 100 \mu$



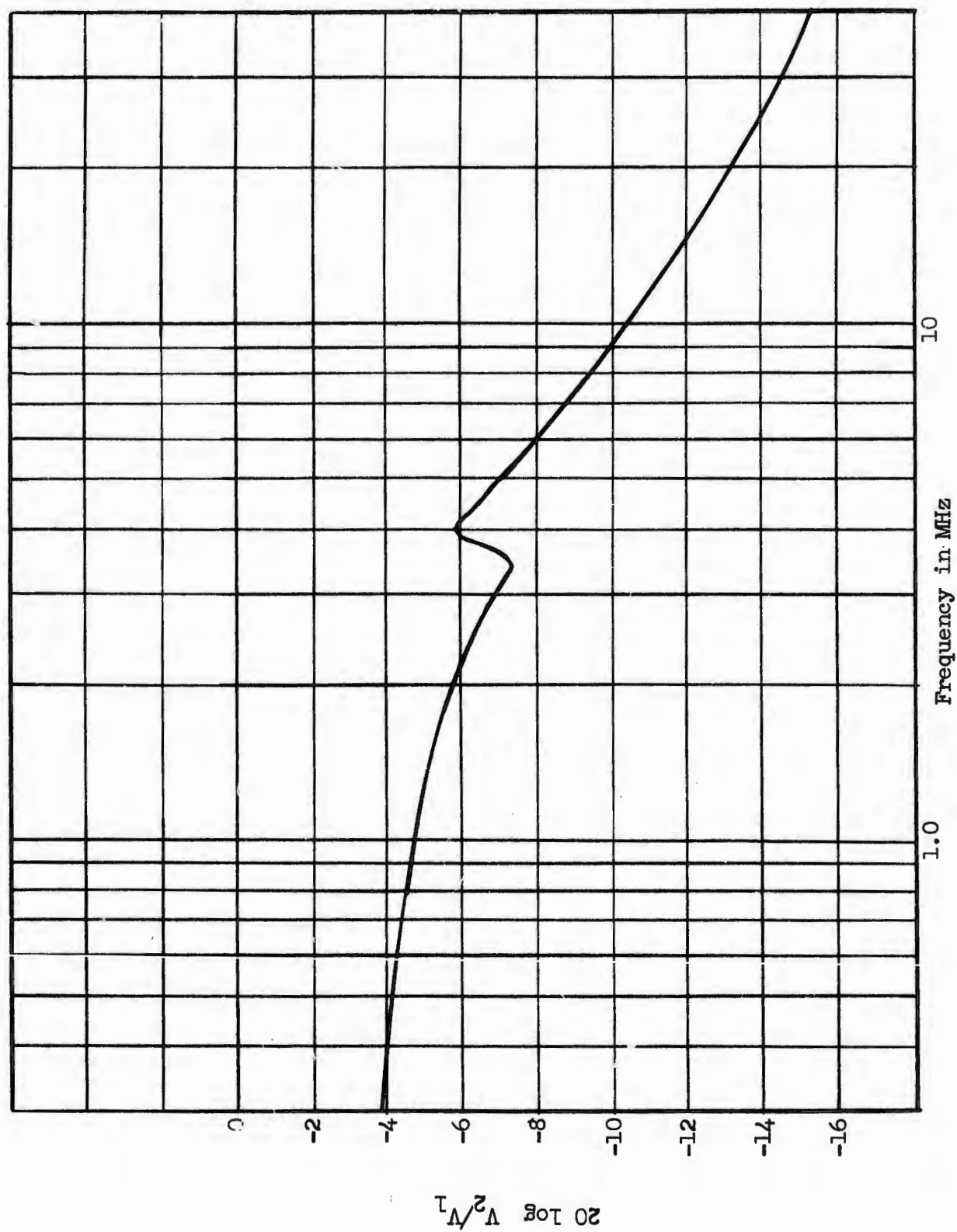


FIGURE 5.6 Frequency Response for Two Spheres, Two Feet Apart.  $R = 500 \text{ n}$

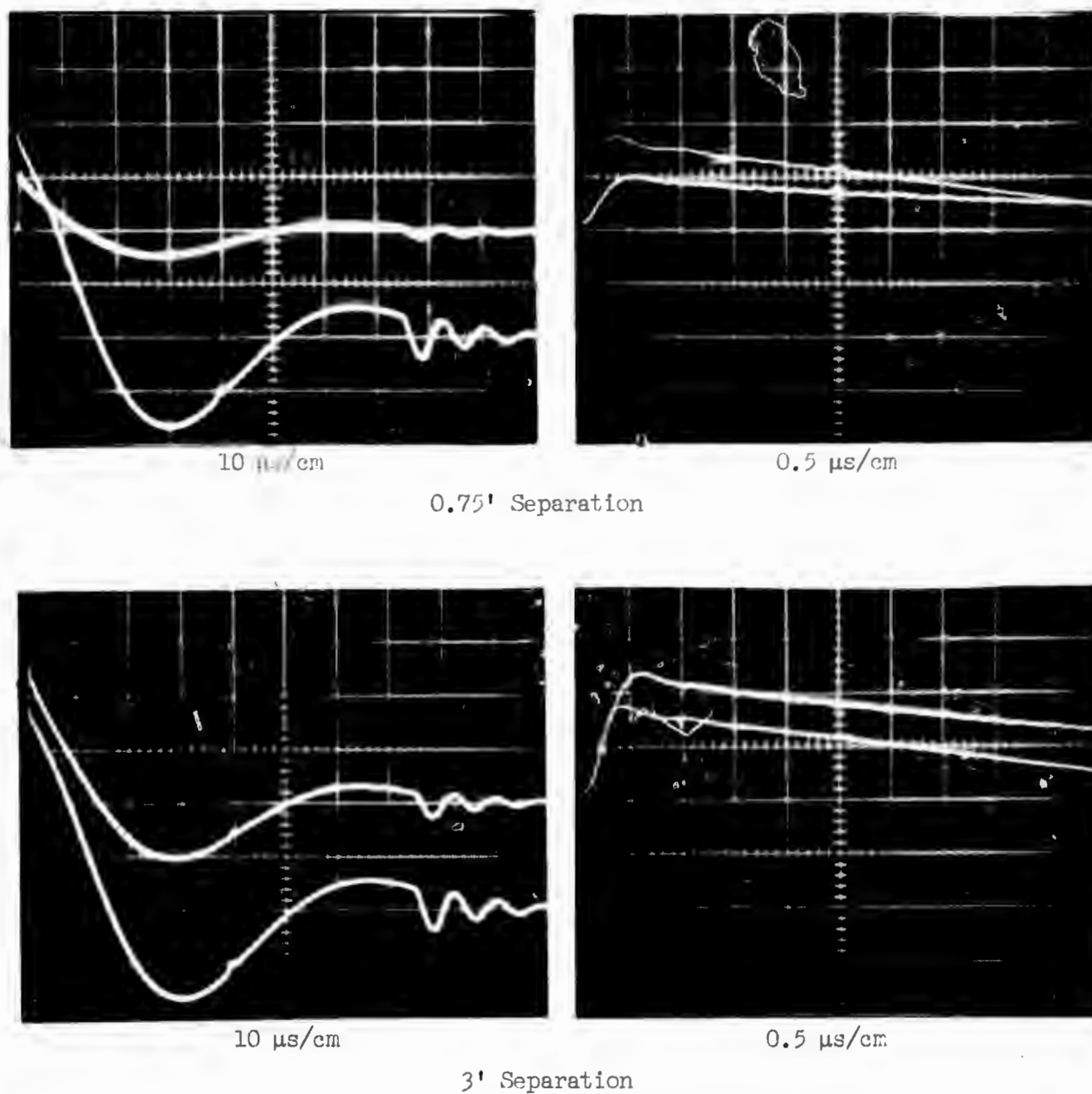


FIGURE 5.7 Induced Current in Underground Conductor (upper trace) and  $\dot{B}$  at Surface (lower trace) for Parallel Rod Grounds at Ends of Conductor. Current Axis - 6.5 mA/cm.  $\dot{B}$  Axis - 47.5 mV/cm

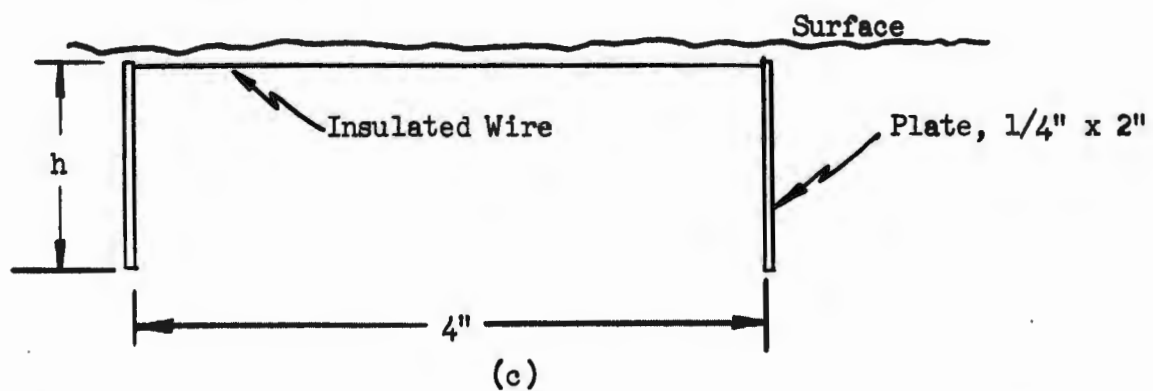
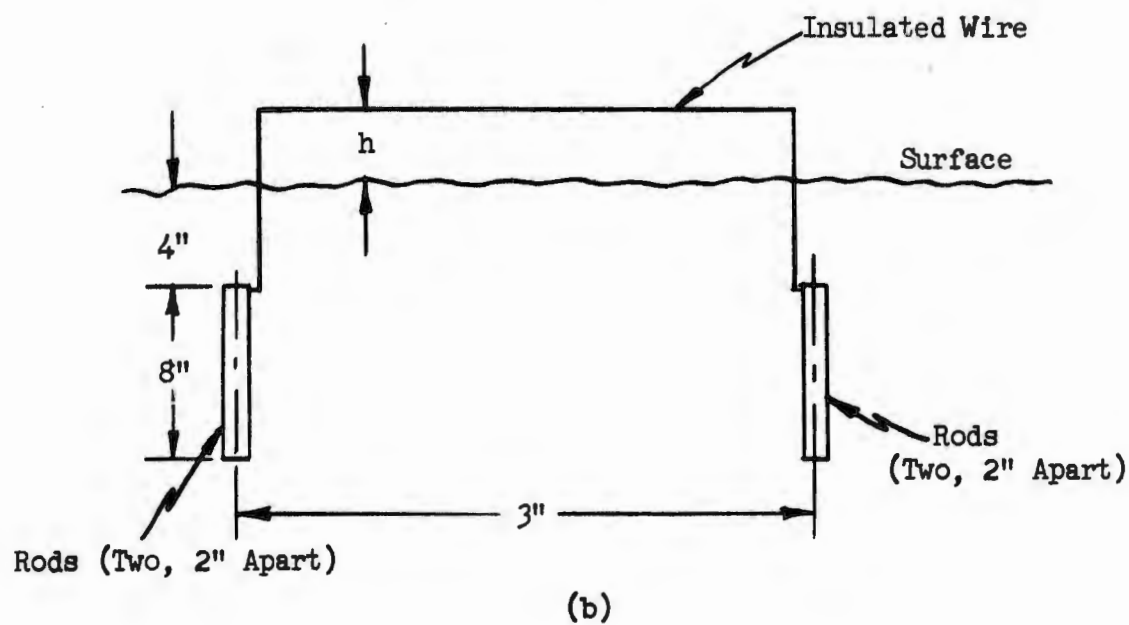
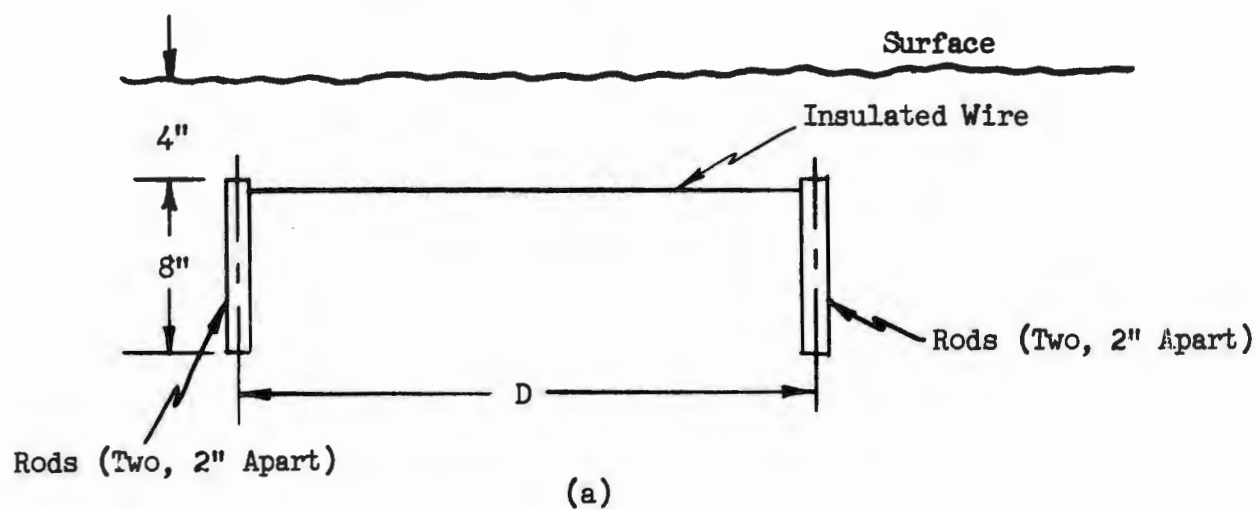


FIGURE 5.8 (a) Parallel Rods. (b) Parallel Rods, Conductor Above Surface. (c) Flat Plates

TABLE 5.4

Conditions: As per Figure 5.8a, measured  $\dot{B}(t)$  and induced current  $i(t)$  at  $t = 2.5 \mu s$ .  $\dot{B}(2.5 \mu s)$  constant =  $7.24 \text{ web/m}^2/\text{sec}$ , resistance measured immediately after each current measurement.

| <u>D (feet)</u> | <u>i(2.5 <math>\mu s</math>) ma</u> | <u>R (ohms)</u> |
|-----------------|-------------------------------------|-----------------|
| 4               | 18.8                                | 150             |
| 3               | 11.7                                | 140             |
| 1.5             | 7.2                                 | 105             |
| 0.75            | 4.3                                 | 86              |

TABLE 5.5

Conditions: As per Figure 5.8c. Length of plates,  $h$ , varied. Measured  $i(t)$  and  $\dot{B}(t)$  at time of  $i_{\text{peak}}$ .  $\dot{B}(T) = 9.75 \text{ web/m}^2/\text{sec}$ , resistance measured immediately after each current measurement.

| <u>Length of Plates,<br/>h, feet</u> | <u>i<sub>peak</sub> ma</u> | <u>R</u> |
|--------------------------------------|----------------------------|----------|
| 2.0                                  | 35.7                       | 115      |
| 1.5                                  | 25.7                       | 130      |
| 1.0                                  | 21                         | 155      |
| 0.5                                  | 15                         | 195      |
| 0.25                                 | 11.4                       | 250      |

TABLE 5.6

Conditions: As per Figure 5.8b.  $B(2.5 \mu s) = 6.66 \text{ web/m}^2/\text{sec}$ ,  $R = 150 \text{ ohms}$

| <u>h (inches)</u> | <u>i (2.5 <math>\mu s</math>) ma</u> |
|-------------------|--------------------------------------|
| 0                 | 14.4                                 |
| 6                 | 20                                   |

TABLE 5.7

Conditions: Parallel rods, tops near surface, separated four feet and connected by bare wire. Measured peak current,  $I_p$ , for wire insulated from sand and buried in sand.

A. Wire Insulated  $I_p = 18 \text{ ma}$

B. Wire in Sand

| <u>Position of current probe</u> | <u><math>I_p</math> ma</u> |
|----------------------------------|----------------------------|
| Left end                         | 15.3                       |
| One foot from left end           | 17.7                       |
| Center                           | 18.6                       |
| One foot from right end          | 17.7                       |
| Right end                        | 15.3                       |

## 5.5 Analysis of Results

### 5.5.1 Resistance Measurements

The resistance measurements with simple geometries were made primarily for the purpose of establishing correlation between measurements with models and theoretical predictions. The analytical expressions for the resistance between cylindrical, spherical, and hemispherical electrodes in a conducting medium are derived in Appendix A. The equations derived were used to calculate the values of resistance shown as  $R_{calc}$  in Tables 5.1, 5.2, and 5.3. At most, the calculated and measured values of resistance differ by 10 to 15%. Considering such factors as non-uniformities in the conductance of the sand, errors in both the measurement of resistance and conductivity, discontinuities in the sand-electrode contact surfaces, etc., the results are considered satisfactory for the purpose.

### 5.5.2 Circuit Parameters

It is obvious from the frequency response curves in Figures 5.5 and 5.6 that the driving point impedance of the circuits considered cannot be represented by a simple R-L equivalent. In fact, the circuits are far more capacitive than inductive, as evidenced by the decrease in voltage across the terminals with increasing frequency. The results indicate that the equivalent circuit for the underground loop is quite complex and, therefore, of questionable value for predicting the nature of induced currents from a surface EMP. This conclusion is not surprising when one considers the fact that in general, the equivalent circuit for a system of coupled circuits is not merely a simple composition of the individual circuits in the system. An excellent example of this being the ordinary power transformer in which the equivalent circuit for any one winding may be a simple series R-L, but the driving point impedance of that same winding measured with the other winding open-circuited will be at least a series-parallel combination of resistances and inductances.

## 5.5.3 Induced Currents

Utilizing the measurements of induced current, resistance of the loop, and applied field, the effective area of the underground induction loop was calculated on the basis of an assumed R-L circuit representation for the loop.

## 5.5.3.1 Calculation for Effective Area

From the wave forms of current and field intensity, it is obvious that the circuit representing the loop is almost purely resistive. Slight differences in the current and field wave forms are discernable only for early times. The effective area of the loop,  $A_e$ , is determined as follows:

For an R-L circuit representation of the loop

$$Ri + L \frac{di}{dt} = \frac{d\phi}{dt} = A_e \frac{dB}{dt} = A_e \dot{B} \quad (5.1)$$

where

$R$  = resistance of the loop

$L$  = inductance of the loop

$\phi$  = flux linking the loop

$A_e$  = effective area of the loop

From the observed wave forms of  $\dot{B}(t)$ , a good approximation for  $\dot{B}$  is:

$$\dot{B} \approx K e^{-at} \quad (5.2)$$

Substituting Equation 5.2 in Equation 5.1 and solving for  $i(t)$

$$i(t) = \frac{A_e K}{L (a - R/L)} \left[ e^{-R/L t} - e^{-at} \right] \quad (5.3)$$

It is observed from the data that  $R/L \gg a$ . Therefore, for  $t \gg 0$

$$i(t) \approx \frac{A_e K}{R} e^{-at} \quad t \gg 0 \quad (5.4)$$

Taking the ratio of Equation 5.4 to Equation 5.2

$$\frac{i(t)}{\dot{B}(t)} = \frac{A_e}{R} \quad (5.5)$$

$$A_e = \frac{i(t) R}{\dot{B}(t)} \quad (5.6)$$

In essence, Equation 5.6 states that the voltage induced in the loop is equal to the resistive drop in the loop after the short transient corresponding to the large  $R/L$  decays. This equation was used in all area calculations for the three experiments described below.

#### 5.5.3.2 Variation in Current and Effective Area with Separation of Grounds

For the parallel-rod grounds the effective area for various separations was calculated utilizing the data of Table 5.5. Values of current and field derivative at ( $t = T = 2.5 \mu s$ ) were used as this time is sufficiently long for the approximations used in establishing Equation 5.6. The calculated area and induced current,  $i(T)$ , are shown as a function of separation,  $d$ , in Figure 5.9. It is observed that for small separation (short conductor) the area appears to increase linearly with separation and for large separations, both the area and current increase as the square of the separation. These results suggest the following explanation.

For small separation, the pickup loop is essentially defined by the area of the plane perpendicular to the field bounded by the length of the rods and the separation, and that the current density below the rods (fringing) is negligible. In fact, this area calculated for the 8" rods separated by 9" (0.75") is  $0.047 \text{ m}^2$  and the effective area calculated is  $0.05 \text{ m}^2$ . This explanation would account for the variation of current shown. For small separation it can be assumed that the resistance between cylinders will vary logarithmically with separation. Therefore, from Equation 5.6 the current should increase less than linearly with separation if the fringing is negligible.

For large separations, it appears that the pickup loop could be defined in terms of two components, one which increases directly with separation and the other as the square of separation. This suggests representation of the pickup area by a rectangular area perpendicular to the field bounded by the

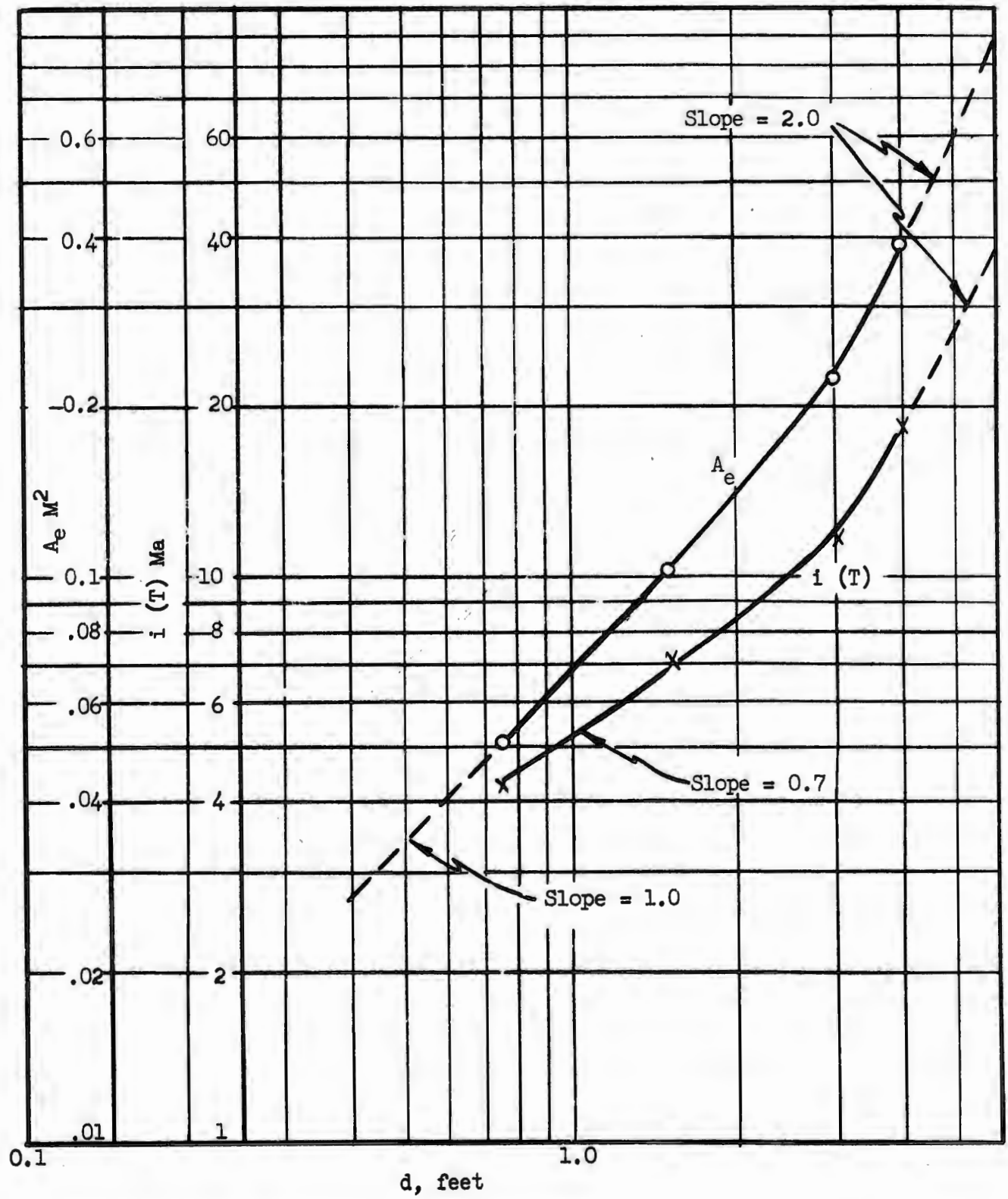


FIGURE 5.9 Effective Area,  $A_e$ , and Induced Current,  $i$  (T), at  $T = 25$  s for Parallel Rods Separated by  $d$  Feet

conductor and ground rods plus another of circular cross section. Indeed, when the grounding geometry is small compared to the separation, it is intuitively obvious that the grounding geometry could be represented by an equivalent sphere. This is evidenced by the small increase in resistance with separation for the rods with the larger separations, as is the case for spherical grounds (see Appendix A). Thus, for large separation the current would be expected to increase as the square of the separation since the resistance tends to be constant and the pickup area varies as the square of the separation.

It is interesting to consider the possibility of representing the pickup area in terms of some function of the electric field or current density distribution. The parabolic increase of area with separation indicates the possibility of representing the loop by an equivalent circular section in the plane of the grounds. It seems reasonable that the center of the current density distribution could be used to define such an area. In Appendix B, the center of current density distribution for a widely separated pair of spheres is determined and found to lie in the plane of the spheres on a hemispherical path of radius equal to one-half the separation. Although the area of such a path cannot be related directly to any of those measured, it does appear likely that such a representation may be adequate to describe variations of pickup with separation.

#### 5.5.3.3 Variation of Current and Effective Area with Vertical Length of Grounds

Similar calculations were performed for the flat plate grounds of various lengths separated by a fixed distance of four feet, utilizing the data of Table 5.6. It was observed that the time at which the current reached its peak value was adequately long for the approximations used in establishing Equation 5.6. The results are shown plotted as a function of length in Figure 5.10.

It is observed that there is very little increase in effective area with length whereas the induced current increases steadily with length to

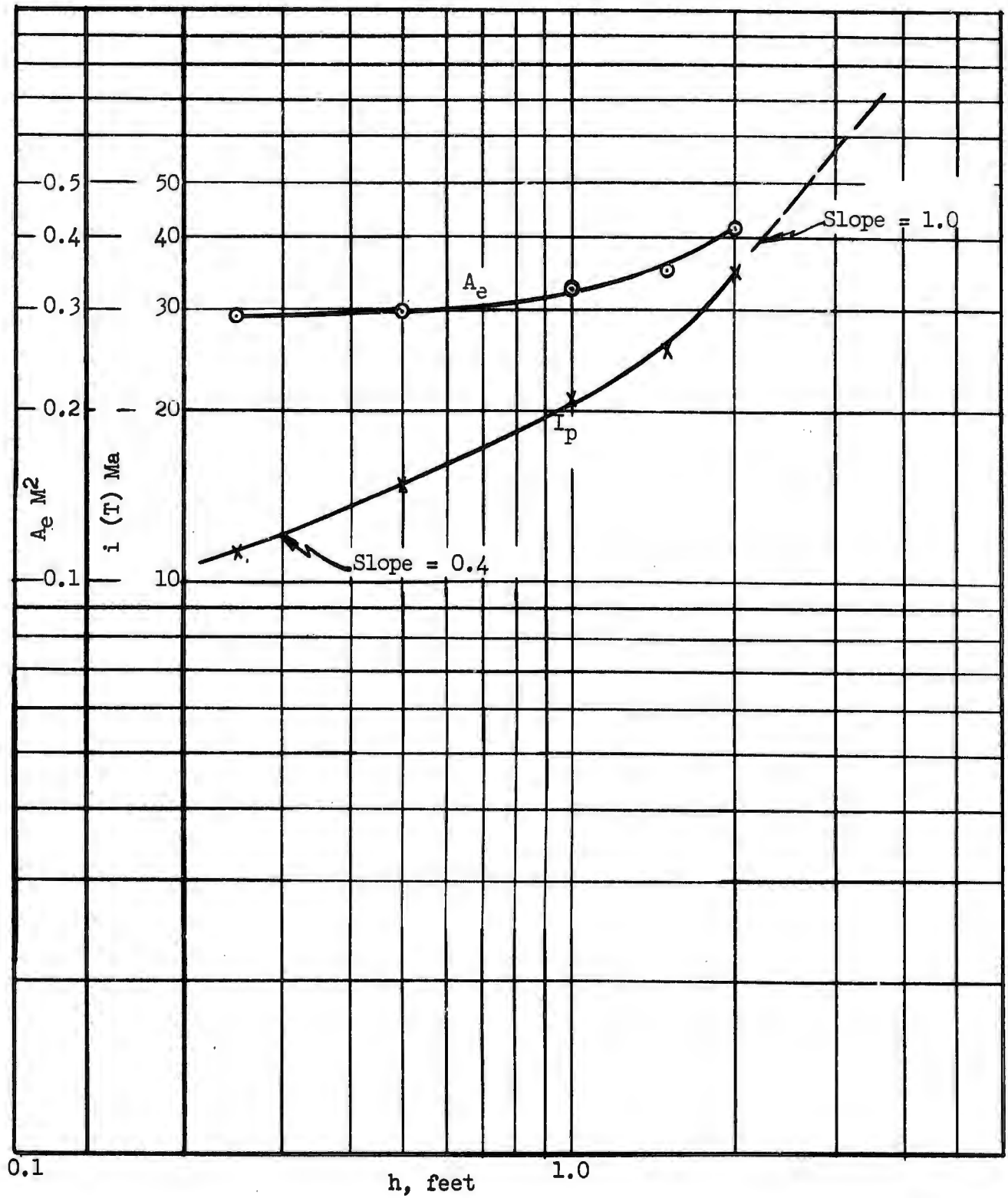


FIGURE 5.10 Effective Area,  $A_e$ , and Induced Current,  $I_{peak}$ , for Flat Plates  $h$ -feet Long

the point where it appears to increase linearly. On the basis of the area calculated, it appears that most of the current flows from the upper portion of the ground plate and the contribution to the total pickup area by increasing length is rather small. However, the resistance of the loop decreases markedly with length. Therefore, on the basis of the assumed R-L circuit for the loop, the current induced should increase with length. There is an apparent contradiction in this explanation in that the resistance should be related to the area if the loop is truly representable by the R-L circuit whose parameters are measured at the terminals of a break in the loop. As in Section 5.5.2, it is concluded that the underground configuration cannot be adequately represented by a simple lumped-parameter model for the investigation of currents induced by a surface EMP.

#### 5.5.3.4 Variation of Current and Effective Area with Height of Conductor Above Surface

The purpose of this test was to investigate the accuracy of the area calculated on the basis of the assumed R-L circuit. With the wire above ground, the difference in pickup area for two different conductor heights is simply the rectangular area bounded by the separation distance and the change in height. The effective areas calculated for the two heights of Table 5.6 are  $0.325 \text{ m}^2$  for the wire on the surface and  $0.450 \text{ m}^2$  for the wire 6" above the surface. The area corresponding to a rectangle 6" x 36" is  $0.140 \text{ m}^2$  which is in close agreement with the difference of  $0.450 - 0.325 = 0.125 \text{ m}^2$  in the effective areas calculated.

#### 5.5.3.5 Effect of the Isolation of the Conductor from the Ground

The data presented in Table 5.7 is self-explanatory. No attempt was made to break the bare wire and make resistance measurements as the current is not uniformly distributed along the wire. It is interesting to note that the peak current in the center of the bare wire is about the same as that in the insulated wire and that the current drops off with distance from the center. This might be explained on the basis of an assumed R-L model for the

loop. For the bare wire, the effective area and resistance of the loop are smaller than for the insulated wire. For a proportionate decrease in both parameters, Equation 5.6 states that the current should remain constant for a given magnetic field pulse. However, such an explanation cannot be substantiated on the basis of one simple experiment.

#### 5.6 Conclusions

The two most important conclusions that may be drawn from this work are:

1. A lumped-parameter R-L equivalent circuit is an inadequate representation for the prediction of induced current in a buried conductor with a given grounding arrangement.
2. Relatively simple geometric modeling techniques may be used to efficiently determine the extent to which EMP-induced currents in buried conduits and structures are influenced by design parameters of the system.

## APPENDIX 5 A

### 5A.1 Resistance between Pairs of Conducting Spheres and Hemispheres

The required resistance relationships are obtained by deriving the capacitance between conductors and then using the well-known resistance-capacitance analog of electrostatics<sup>5</sup>:

$$RC = \epsilon/\sigma \quad (5A.1)$$

where  $\epsilon$  and  $\sigma$  are the permittivity and conductivity of the space.

Consider two charged, conducting spheres of radius "a" meters, separation "d" meters positioned symmetrically on the x-axis as shown in Figure 5A.1.

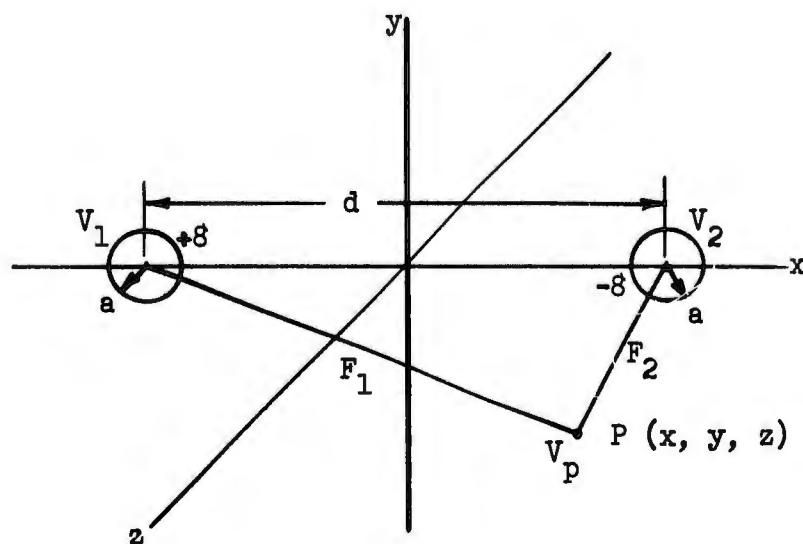


FIGURE A.1

At any point P (x, y, z) the potential  $V_p$  is given by:

$$V_p = \frac{8}{4 \pi \epsilon V_1} - \frac{8}{4 \pi \epsilon V_2} \quad (5A.2)$$

Therefore,

$$V_1 = \frac{8}{4 \pi \epsilon a} - \frac{8}{4 \pi \epsilon (d - a)} \quad (5A.3)$$

$$V_2 = \frac{8}{4 \pi \epsilon (d - a)} - \frac{8}{4 \pi \epsilon a} \quad (5A.4)$$

Then

$$|V_1 - V_2| = 2|V_1| = 2|V_2| \quad (5A.5)$$

or

$$|V_1 - V_2| = \frac{2(8)}{4 \pi \epsilon} \left| \frac{1}{a} - \frac{1}{d - a} \right| \quad (5A.6)$$

Solving for the capacitance between the spheres:

$$C = \frac{8}{|V_1 - V_2|} = \frac{2 \pi \epsilon}{\left| \frac{1}{a} - \frac{1}{d - 2a} \right|} = 2 \pi \epsilon \frac{a(d - a)}{(d - 2a)} \quad (5A.7)$$

The resistance between spheres then, from Equation 5A.1 is

$$R = \frac{1}{2 \pi \sigma} \frac{d - 2a}{a(d - a)} \quad \text{for two spheres} \quad (5A.8)$$

Note that for  $d \gg a$

$$R = \frac{1}{2 \pi \sigma a} \quad (5A.9)$$

For hemispheres, it is sufficient to consider that the upper half space  $y$  to  $0$  is removed and replaced by a nonconducting medium. The resistance between the hemisphere will then be double that for the spheres or:

$$R = \frac{1}{\pi \sigma} \frac{d - 2a}{a(d - a)} \quad (5A.10)$$

or, for  $d \gg a$

$$R = \frac{1}{\pi \sigma a} \quad (5A.11)$$

## 5A.2 Resistance between a Pair of Conducting Cylinders

Consider a conducting cylinder of radius  $b$ , length  $L$ , parallel to an infinite conducting plane at a distance  $h$  and carrying a line charge of  $\rho_L$  coulombs/meter as shown in Figure 5A.2.

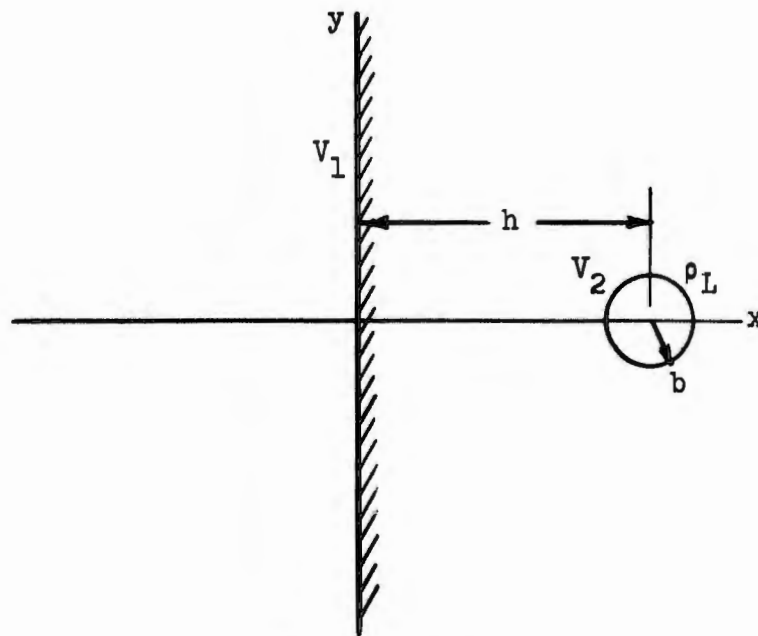


FIGURE 5A.2

The difference in potential between the cylinder and the plane  $V_2 - V_1$  is easily shown to be<sup>5</sup>:

$$V_2 - V_1 = \frac{\rho_L}{2\pi\epsilon} \ln \frac{h + \sqrt{h^2 - b^2}}{b} \quad (5A.12)$$

The capacitance per unit of length  $L$  is, therefore:

$$C = \frac{2\pi\epsilon}{\ln \frac{h + \sqrt{h^2 - b^2}}{b}} \quad \text{farad/meter} \quad (5A.13)$$

For cylinders of small radius located far from the plane,  $h \gg b$ , then

$$C = \frac{2\pi\epsilon}{\ln 2h/b} \quad \text{farad/meter} \quad (5A.14)$$

The capacitance between two cylinders separated by  $2h$  meters is one-half the capacitance given by Equation 5A.14. The capacitance for a pair of cylinders of length  $L$ , radius  $b$ , separation  $d$  is, therefore:

$$C = \frac{\pi\epsilon L}{\ln d/b} \quad (5A.15)$$

#### 4 Appendix 5A

Utilizing Equation 5A.1, the resistance between them is:

$$R = \frac{1}{\pi \epsilon L} \ln d/b \quad (5A.16)$$

# APPENDIX 5 B

To determine the center of current for a pair of conducting hemispheres at the interface between a conducting and nonconducting medium, the current distribution is first obtained from Laplace's equation and the centroid of the resulting distribution is located. Using the geometric notation from Figure 5B.1, Laplace's equation is given by:

$$\nabla^2 V = 0 \quad (5B.1)$$

In cartesian coordinate notation, the solution is obtained as

$$V_p(x, y, z) = \frac{A}{|\bar{r}_1|} + \frac{B}{|\bar{r}_2|} \quad (5B.2)$$

where

$$\bar{r}_1 = \sqrt{(x + d/2)^2 + y^2 + z^2} \quad (5B.3a)$$

$$\bar{r}_2 = \sqrt{(x - d/2)^2 + y^2 + z^2} \quad (5B.3b)$$

For the evaluation of A and B, the boundary conditions are, where it is assumed that  $d \gg a$ ,

$$V = V_1; \quad |\bar{r}_1| = a, \quad |\bar{r}_2| \approx d \quad (5B.4a)$$

and

$$V = V_2; \quad |\bar{r}_1| \approx d, \quad |\bar{r}_2| = a \quad (5B.4b)$$

Thus,

$$V_1 = \frac{A}{a} + \frac{B}{d} \quad (5B.5)$$

and

$$V_2 = \frac{A}{d} + \frac{B}{a} \quad (5B.6)$$

Solving for A and B gives

$$A = \frac{a d^2 V_1 - a^2 d V_2}{d^2 - a^2} \approx \frac{a}{d} (d V_1 - a V_2) \quad (5B.7)$$

$$B = \frac{a d^2 V_2 - a^2 d V_1}{d^2 - a^2} \approx \frac{a}{d} (d V_2 - a V_1) \quad (5B.8)$$

Therefore,

$$V_p(x, y, z) = \frac{a}{d} \frac{(d V_1 - a V_2)}{|\bar{r}_1|} + \frac{a}{d} \frac{(d V_2 - a V_1)}{|\bar{r}_2|} \quad (5B.9)$$

To find the current distribution,

$$J = \sigma E = \sigma (-\nabla V) = -\sigma \left( \frac{\partial V}{\partial x} \bar{i} + \frac{\partial V}{\partial y} \bar{j} + \frac{\partial V}{\partial z} \bar{k} \right) \quad (5B.10)$$

which, from Equations 5B.3a, 5B.3b, and 5B.10, becomes

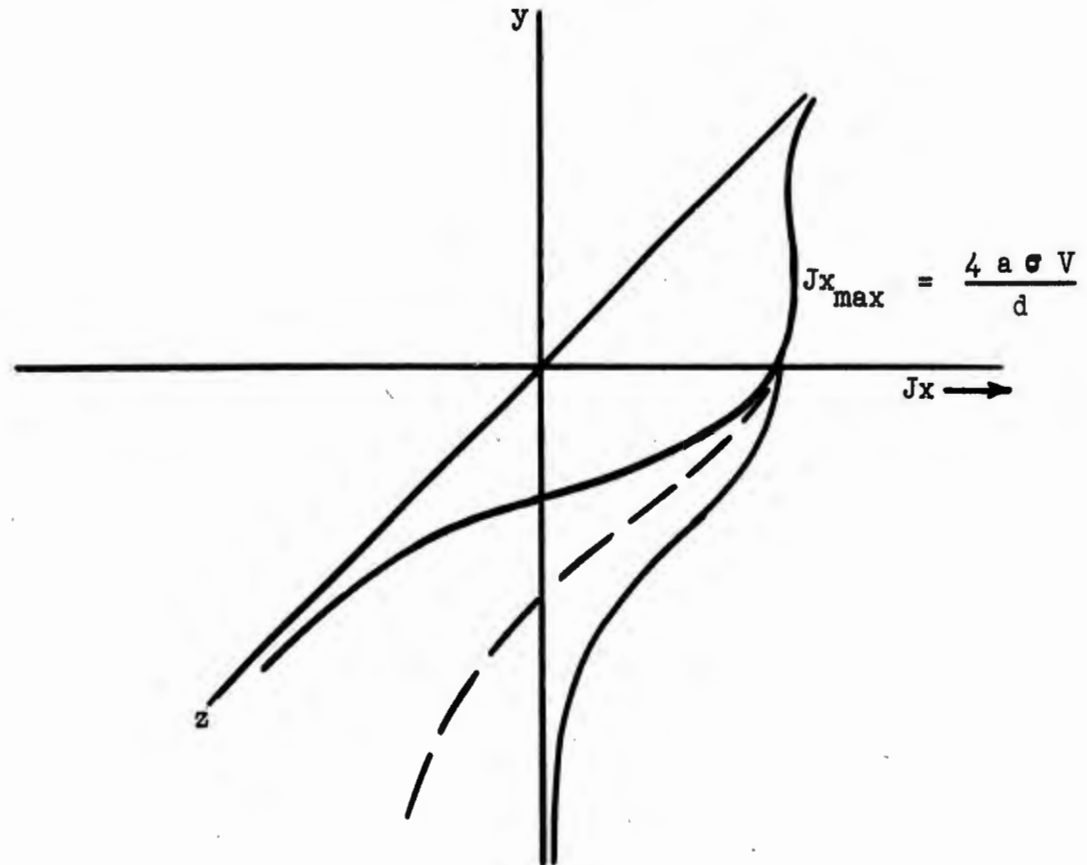
$$\begin{aligned} J(x, y, z) = a \sigma \left[ \left( \frac{(dV_1 - aV_2)(x + d/2)}{|\bar{r}_1|^{3/2}} + \frac{(dV_2 - aV_1)(x - d/2)}{|\bar{r}_2|^{3/2}} \right) \bar{i} \right. \\ \left. + \left( \frac{(dV_1 - aV_2)y}{|\bar{r}_1|^{3/2}} + \frac{(dV_2 - aV_1)y}{|\bar{r}_2|^{3/2}} \right) \bar{j} \right. \\ \left. + \left( \frac{(dV_1 - aV_2)z}{|\bar{r}_1|^{3/2}} + \frac{(dV_2 - aV_1)z}{|\bar{r}_2|^{3/2}} \right) \bar{k} \right] \quad (5B.11) \end{aligned}$$

Since the current distribution is independent of the absolute potential, an arbitrary reference potential can be chosen. Thus,  $V_2 = -V_1 = V$ .

That is,  $V = 0$  at  $x = 0$ , and for  $d \gg a$ ,

$$\begin{aligned} J(x, y, z) = a \sigma V \left[ \left( \frac{x + d/2}{|\bar{r}_1|^{3/2}} - \frac{x - d/2}{|\bar{r}_2|^{3/2}} \right) \bar{i} \right. \\ \left. + \left( \frac{y}{|\bar{r}_1|^{3/2}} - \frac{y}{|\bar{r}_2|^{3/2}} \right) \bar{j} \right. \\ \left. + \left( \frac{z}{|\bar{r}_1|^{3/2}} - \frac{z}{|\bar{r}_2|^{3/2}} \right) \bar{k} \right] \quad (5B.12) \end{aligned}$$

A sketch of the current distribution is given below.



From symmetry, the centroid is located in the plane defined by  $x = 0$ .  
In this plane,

$$J(0, y, z) \simeq a \sigma V \left[ \frac{d}{r_1^{3/2}} \bar{i} \right] \bigg|_{x=0} \quad (5B.13)$$

or

$$J(0, y, z) \simeq \frac{a d \sigma V}{(d^2/4 + y^2 + z^2)^{3/2}} \bar{i} \quad (5B.14)$$

Further symmetry arguments indicate that the centroid is along the

4 Appendix 5B

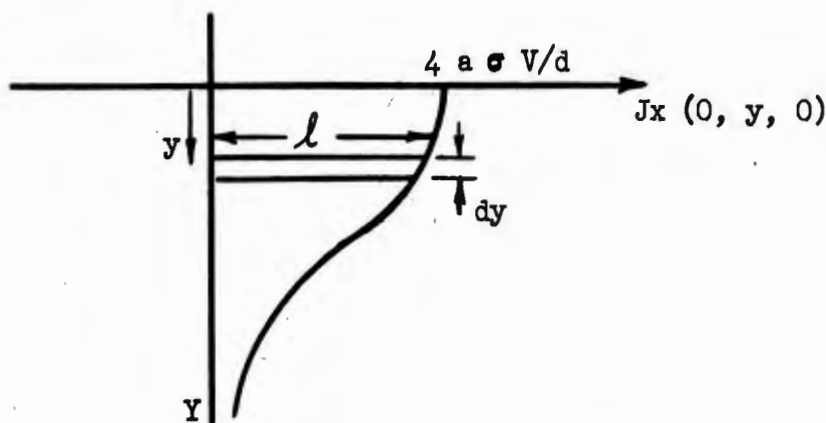
$z = 0$  axis. Thus,

$$J(0, y, 0) = \frac{a d \sigma V}{(d^2/4 + y^2)^{3/2}} \quad (5B.15)$$

For the centroid  $\bar{Y}$

$$A \bar{Y} = \int_0^{\infty} y (l dy) \quad (5B.16)$$

where the geometry is defined below.



$$A = \int_0^{\infty} J_x(0, Y, 0) dy = \lim_{L \rightarrow \infty} \int_0^L \frac{a d \sigma V}{(d^2/4 + Y^2)^{3/2}} dy \quad (5B.17)$$

which simplifies to

$$A = \frac{4 a \sigma V}{d} \quad (5B.18)$$

Therefore, from Equation 5B.16

$$\begin{aligned} \bar{Y} &= \frac{d}{4 a \sigma V} \int_0^{\infty} y J(0, y, 0) dy \\ &= \frac{d}{4 a \sigma V} \lim_{T \rightarrow \infty} \int_0^T \frac{a d \sigma V y}{(d^2/4 + y^2)^{3/2}} dy \end{aligned} \quad (5B.19)$$

$$= \frac{d^2}{4} \lim_{T \rightarrow \infty} \int_0^T \frac{y}{(d^2/4 + y^2)^{3/2}} dy \quad (5B.19)$$

cont.

which becomes, in the limit

$$\bar{Y} = \frac{d}{2} \quad (5B.20)$$

#### SECTION 5.0 REFERENCES

1. Caverly, D. W., EXPERIMENTAL MEASUREMENT OF CURRENT ON BURIED CONDUIT RESULTING FROM ELECTRIC AND MAGNETIC FIELDS, General Electric Company, Pittsfield, Massachusetts, 30 January 1967.
2. Staffin, R., Juels, R., and Basse, P., AN INVESTIGATION OF ELECTROMAGNETIC ENERGY COUPLING AND SHIELDING EFFECTS, Procedyne Corporation, New Brunswick, New Jersey, 1 October 1965.
3. Fisher, F. A., FEASIBILITY OF GEOMETRIC MODELS FOR THE DETERMINATION OF SHIELDING EFFECTIVENESS, General Electric Company, Pittsfield, Massachusetts, 5 September 1966.
4. Lyke, A. J., EXPERIMENTAL MEASUREMENT OF EARTH MAGNETIC FIELD ATTENUATION, General Electric Company, Pittsfield, Massachusetts, 1 October 1966.
5. Smythe, William R., STATIC AND DYNAMIC ELECTRICITY, McGraw-Hill Book Company, New York, 1950.

## **Section 6.0**

### **Experimental Measurement of Current on Buried Conduit Resulting from Electric and Magnetic Fields - Part II**

6.0 EXPERIMENTAL MEASUREMENT OF CURRENT ON BURIED CONDUIT  
RESULTING FROM ELECTRIC AND MAGNETIC FIELDS - Part II

6.1 Introduction

These experiments are a continuation of the tests previously reported in "Experimental Measurement of Current on Buried Conduit Resulting from Electric and Magnetic Fields", 30 January 1967, General Electric Company, Pittsfield, Massachusetts.

6.2 Objective

The purpose of these tests was:

1. to determine the magnitude of current induced on buried conduit of various lengths (100 to 400 feet) from a magnetic field.
2. to assess the conservatism in the analytical methods for calculating conduit current developed from the previous tests on above ground (100 to 200 feet) and underground conduit (100 feet).
3. to show the effects on conduit current from grounding beds (connected to the ends of the conduit) for various lengths of conduit runs.
4. to determine the difference in conduit current between a buried conduit in direct contact with earth and a buried conduit contained in an isolated duct.
5. to investigate the reduction of conduit current afforded by shunting plates, guard wires, or screening.

6.3 Test Facility and Setup

The testing was conducted between Towers #2 and #3 of the General Electric Company's Project UHV. This facility and equipment have been described in a previous report<sup>1</sup>.

6.3.1 Experimental Setup

This experiment consisted of numerous conduit configurations (2-inch diameter rigid steel conduit) below ground located in an H-field radiator.

This radiator was composed of the three phases of a transmission line and earth, Figure 6.1. The three phases were isolated from the rest of the line at both Towers #2 and #3. At Tower #2 the lines were connected together and to an impulse generator (pulse energy source). At the other end of the transmission line, for part of this experiment, the three lines were shorted and connected to ground (by ground rods) at Tower #3. For the other part of the experiment the lines were shorted together and tied to ground halfway between Tower #2 and Tower #3.

The buried conduit in direct earth contact was located 300 to 700 feet from Tower #2. The buried conduit contained within a duct was 450 to 550 feet from Tower #2. In all cases the conduit was directly under the radiator and parallel to the direction of the lines, Figure 6.1 and Figure 6.2.

The 100-foot, isolated 2-inch conduit was centered, by wooden spacers, in a one-foot diameter transite pipe buried three to four feet below ground, Figure 6.3. Test holes at the ends of the conduit contained the ground rods and provided access for measurement of the conduit current. Since these test pits were small compared to conduit length, their effect was assumed negligible.

The 400-foot buried conduit was located three to four feet below ground with test pits at the ends and at the 200-foot, 100-foot, and 50-foot locations. The conduit was disconnected at these pits depending on the experiment and connected to ground rods at the required location, Figure 6.4. Bare copper wire was used to connect the conduit and the ground rods. Copper braid was clamped in layers between the conduit ends at the test pits to connect the different sections of pipe together.

At the middle of the 400-foot conduit the test pit was enlarged for experiments on conduit current reduction by the use of shunting plates, Figure 6.5.

#### 6.3.2 Generator Voltage and Current

The peak current for the radiator loops was approximately 9,000 amps

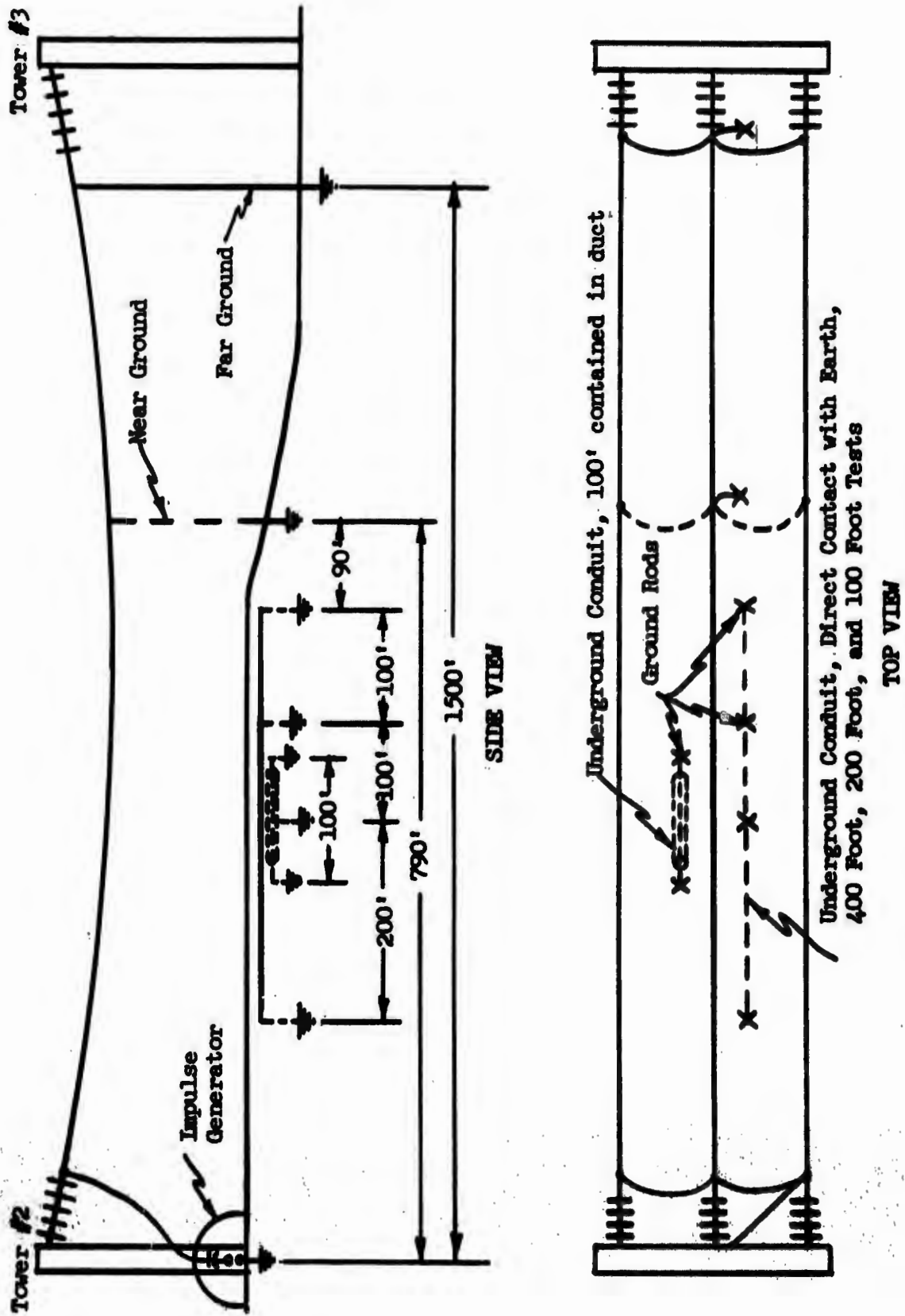


FIGURE 6.1 Test Facility Setup

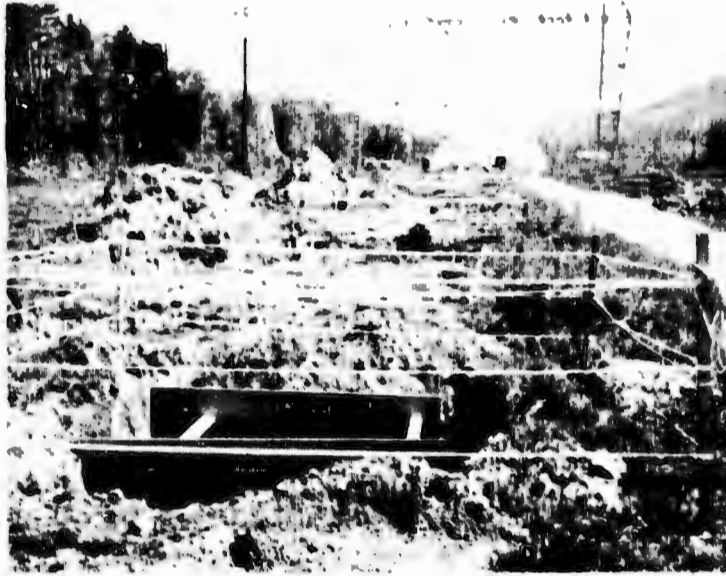


FIGURE 6.2 Four Hundred Foot Buried Conduit Setup

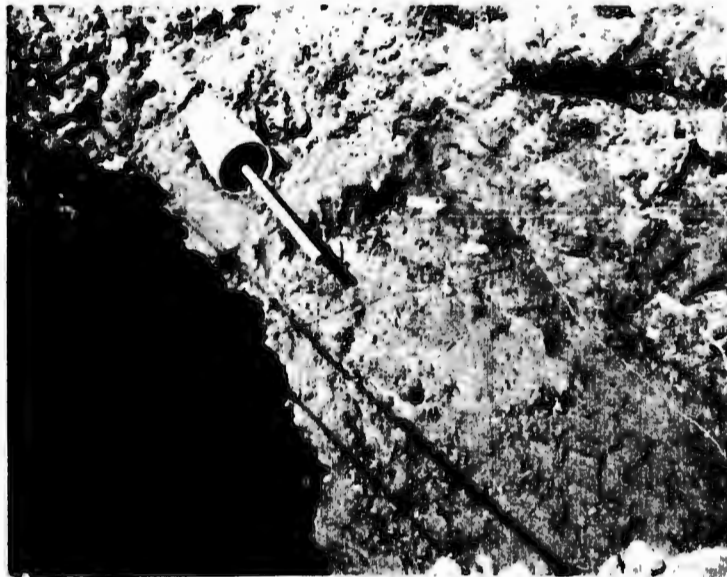


FIGURE 6.3 One Hundred Foot Buried Conduit (isolated) Setup



FIGURE 6.4 Buried Conduit Test Pit

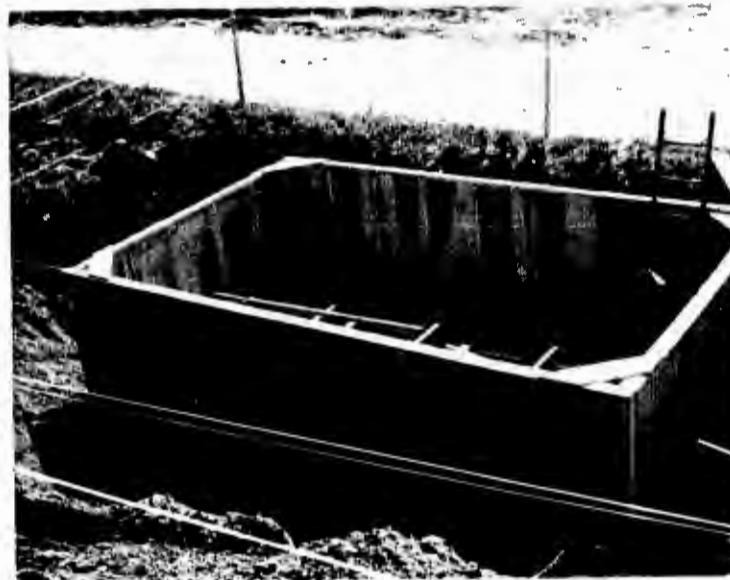


FIGURE 6.5 Four Hundred Foot Conduit Test - Middle Test Pit

as shown in Figure 6.6. With the "far ground" (tied to ground at Tower #3), the H-field produced at the surface was uniform over the 100-foot isolated conduit test area, but varied slightly over the 400-foot conduit test area. The value was constant except near the 400-foot test hole (nearest the pulse generator) where the H-field was 15 percent lower than the rest of the test area. For the "near ground" test, the H-field magnitude varied along the length of the conduit.

#### 6.3.3 Measurements

The H-field, conduit current, resistance, and inductance measurements were the same as in the report, "Experimental Measurement of Current on Buried Conduit Resulting from Electric and Magnetic Fields", 30 January 1967 General Electric Company, Pittsfield, Massachusetts. The measurement systems have been described in other reports<sup>1,2</sup>.

Recent measurement of the soil resistivity (by the four probe method) shows a constant value of 130 ohm-meters is applicable for the length of conduit used in these experiments<sup>5</sup>. Figure 6.7 presents the data from two sets of measurements taken in the area of the experiments.

#### 6.4 Tests

##### 6.4.1 Buried Conduit - 100, 200, and 400 Feet

In previous tests (with "far ground" termination) it was shown that the current flowing on short lengths of conduit (100 and 200 feet supported above ground and 100 feet buried) was induced from the encompassing H-field<sup>3</sup>. By the use of superposition convolution integrals these current wave shapes were calculated from the measured H-field wave shape, conduit loop resistance, and inductance. By assuming an effective area (to provide the best fit) correlation between the calculated and measured current for the various test setups provided empirical data for the inductance and effective areas for buried conduit of longer lengths.

To determine the conservatism of these empirical curves for the

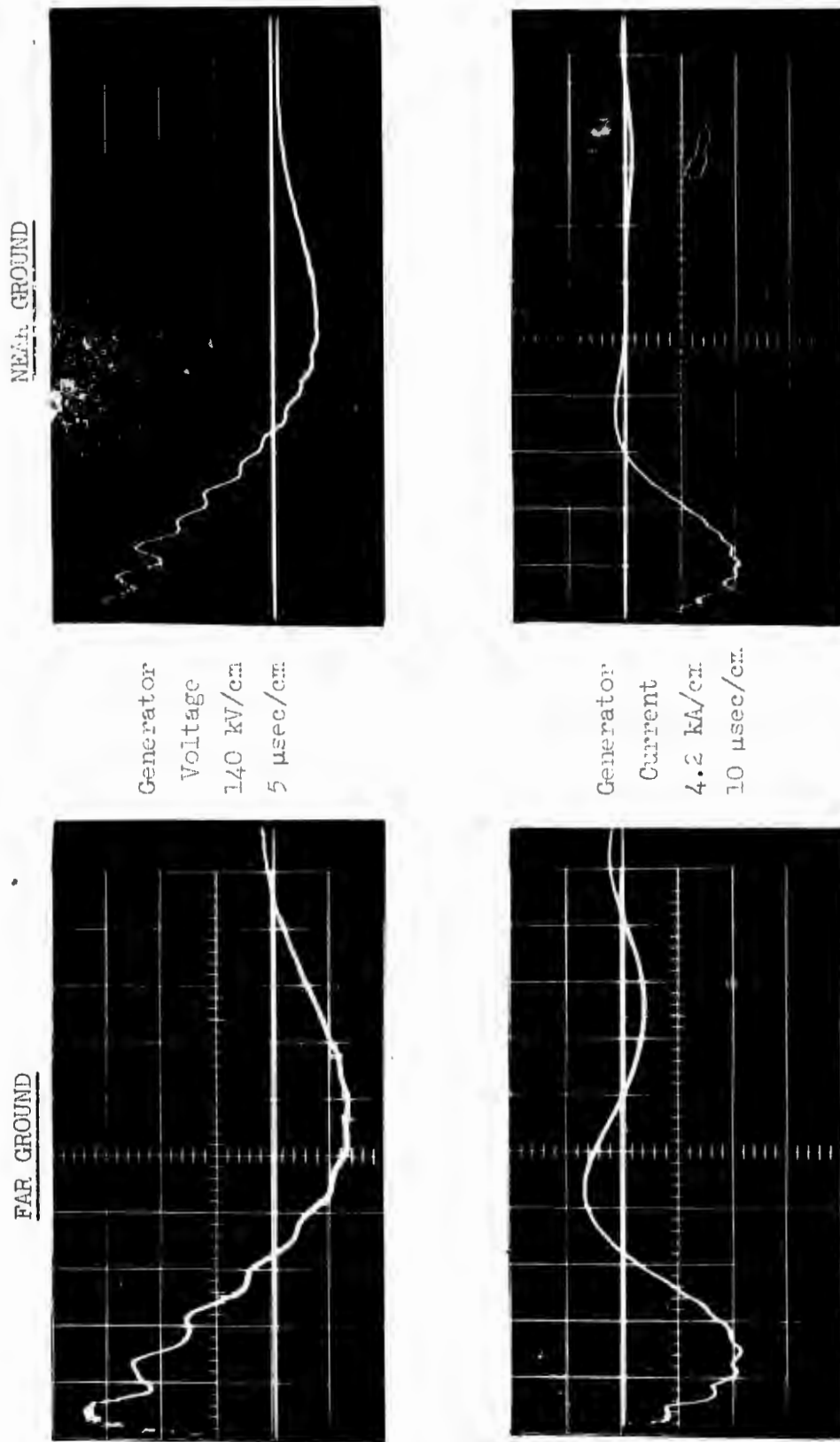


FIGURE 6.6 Generator Voltage and Current

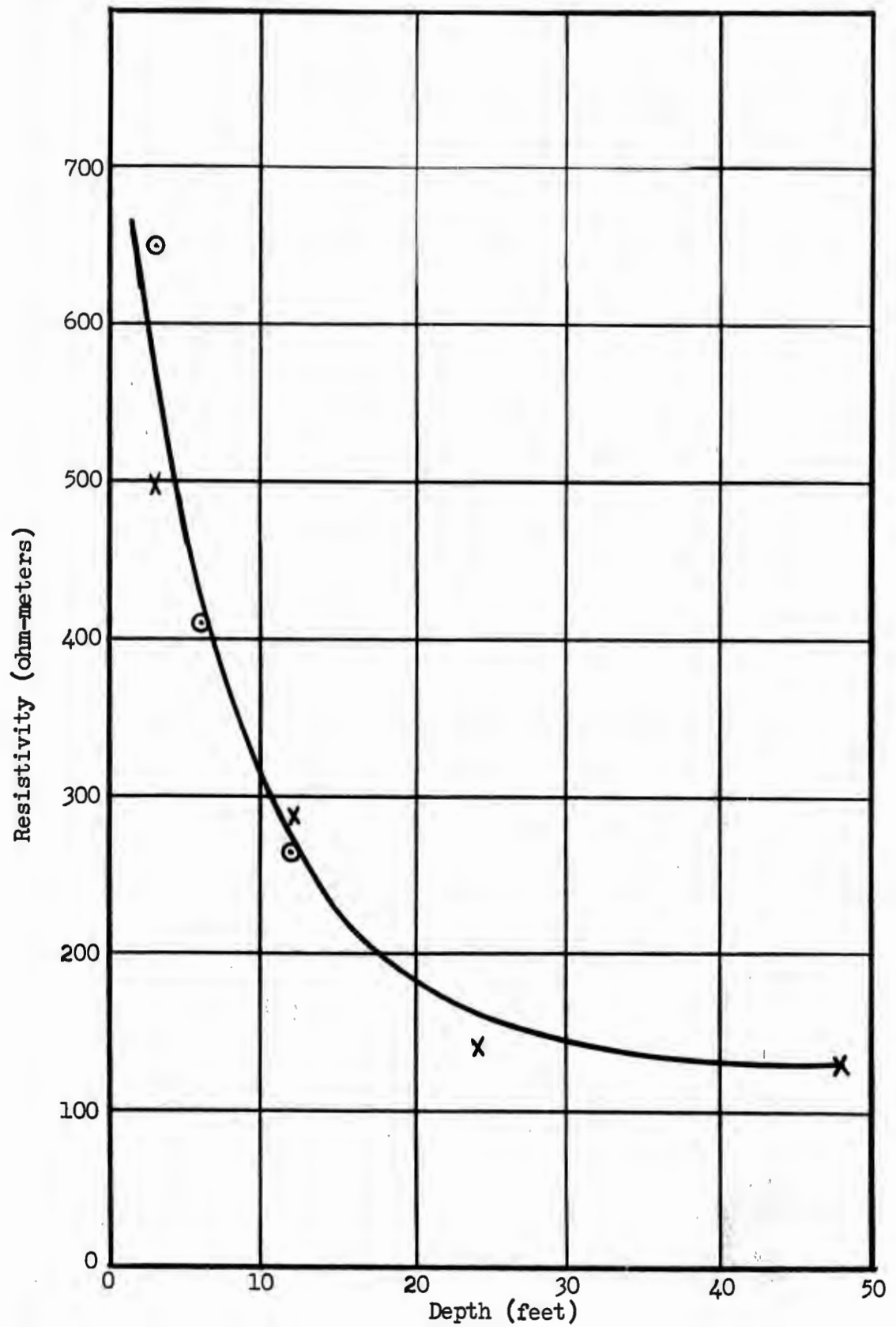


FIGURE 6.7 Average Soil Resistivity over a Hemispherical Volume of Diameter, D, Measured Using the Four Probe Method

calculation of conduit current, 100, 200, and 400 feet of buried conduit were tested with and without ground rod termination. Measurements of the current were made at the center and at each end of the conduit.

This current, as in the previous tests, has a wave shape whose crossover points show the effects of resistance and inductance of the current loop, Figure 6.8. Figure 6.6, the radiator loop current which generates the H-field, has a crossover point at 32 microseconds. The corresponding crossover for the conduit 18.5 microseconds. The effect of the R/L factor is to move the crossover point to a shorter time than the corresponding crossover of the H-field environment. These parameters also affect the magnitude of the pulse.

To calculate the conduit current wave shape from the empirical data of the previous test, values of effective area and inductance were obtained from Figures 22 and 23 of the report<sup>3</sup>. The measured H-field was used as shown in Figure 6.6 and the resistance was approximately the sum of the measured terminating ground rod beds.

The current magnitude measured on the conduit at the center and at the ends was not the same. The center current measurement was maximum when the conduit was terminated to ground at each end. This wave shape is plotted with the calculated value of current in Figure 6.9 for the 200 foot conduit and Figure 6.10 for the 400 foot conduit.

For the 200 foot conduit the calculated value of current fits the measured value with the first peak being slightly larger. The crossover points are within two microseconds.

The calculated current wave shape for the 400 foot conduit has a magnitude that is approximately two times larger than the measured wave shape. The crossover points are between two and four microseconds of the measured value. To show the difference of peak values between the calculated and the measured currents, the first and second crests were plotted for the three lengths of conduit measured (100, 200, and 400 feet), Figure 6.11.

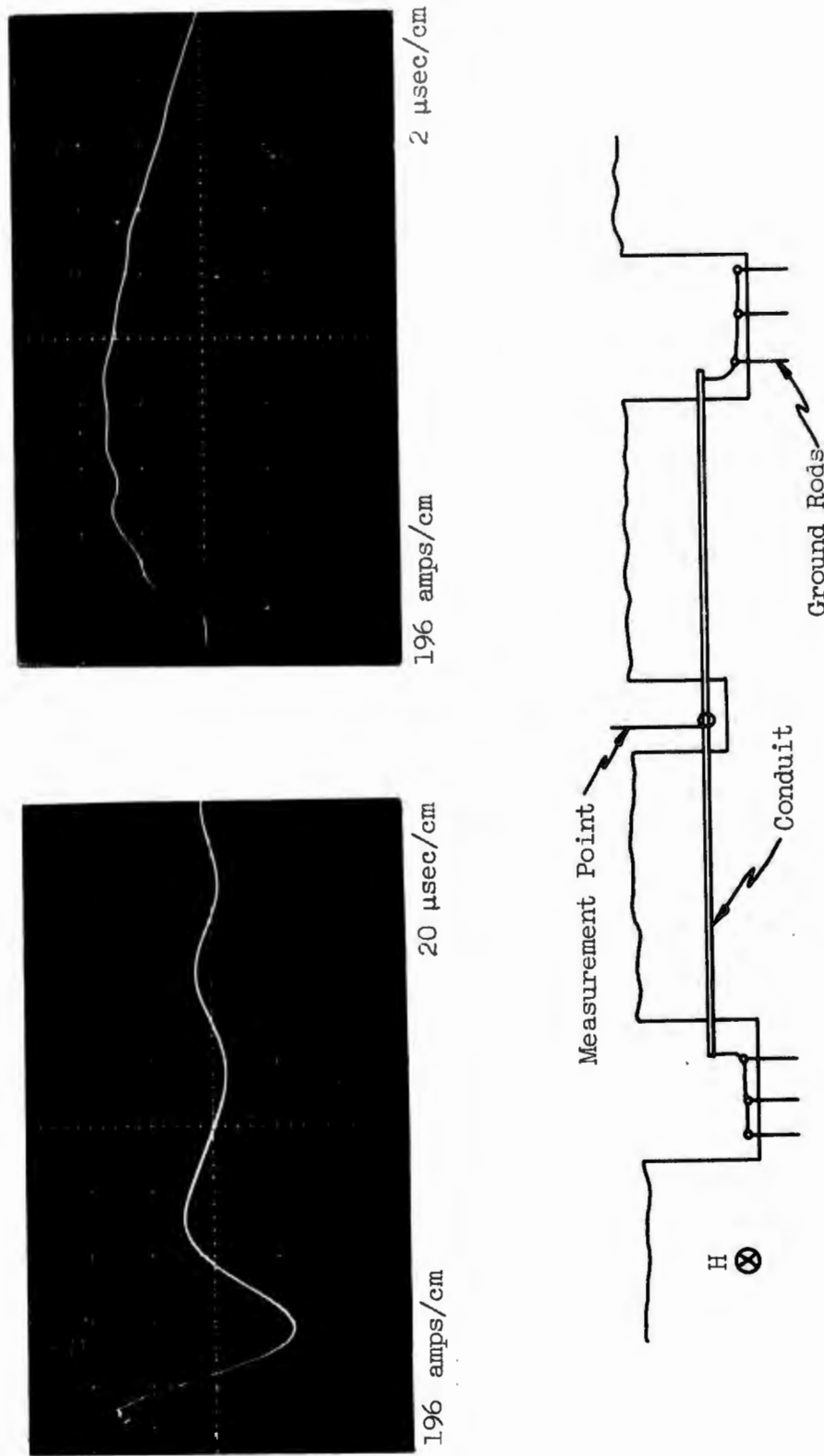


FIGURE 6.8 Conduit Current - Two Hundred Feet, Buried, with Ground Rod Termination

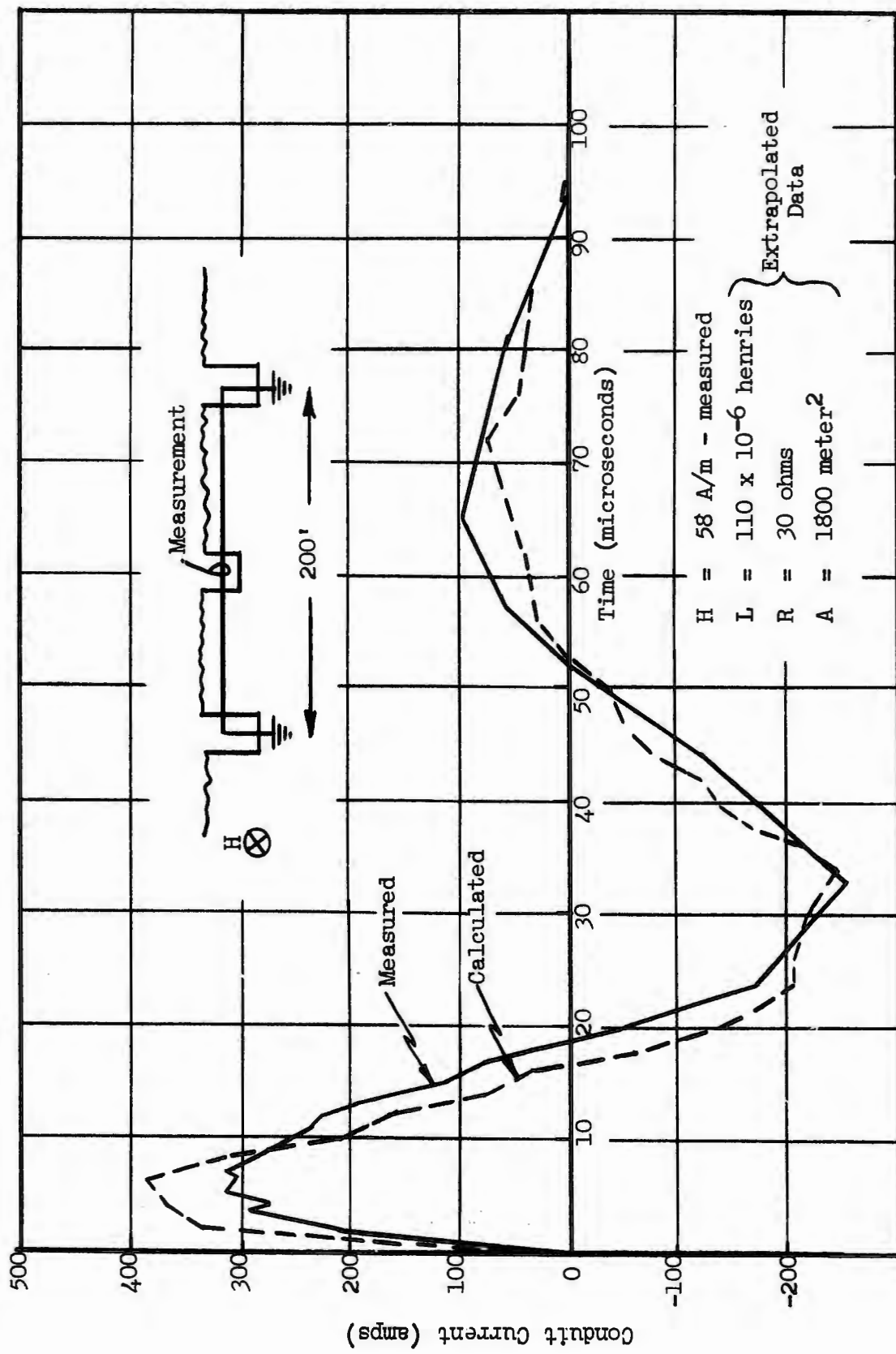
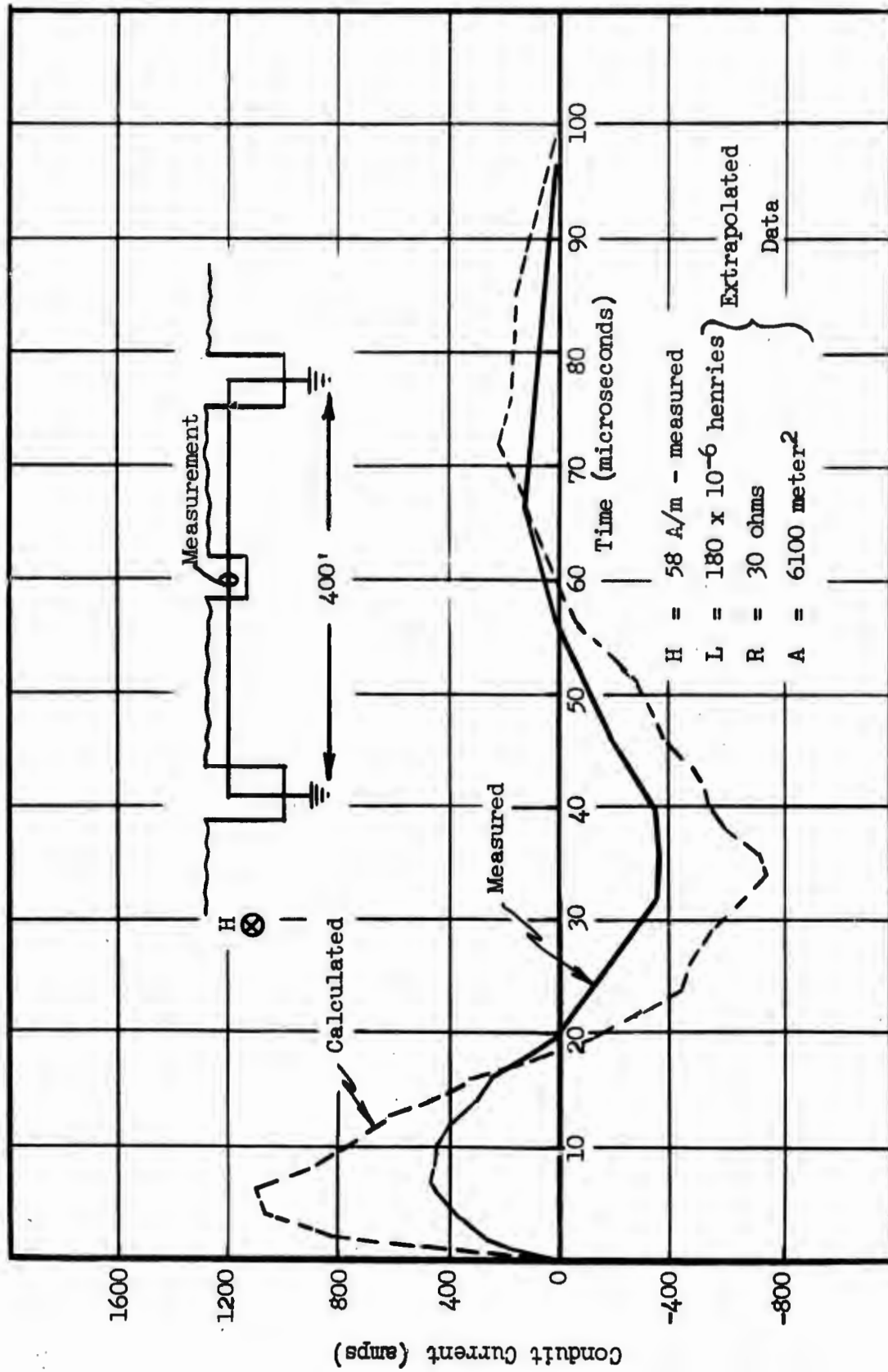


FIGURE 6.9 Conduit Current. 200' Buried Ground Termination at Each End. Measurement at Center.

FIGURE 6.10 Conduit Current. 400' Buried, Ground Termination at Each End. Measurement at Center.



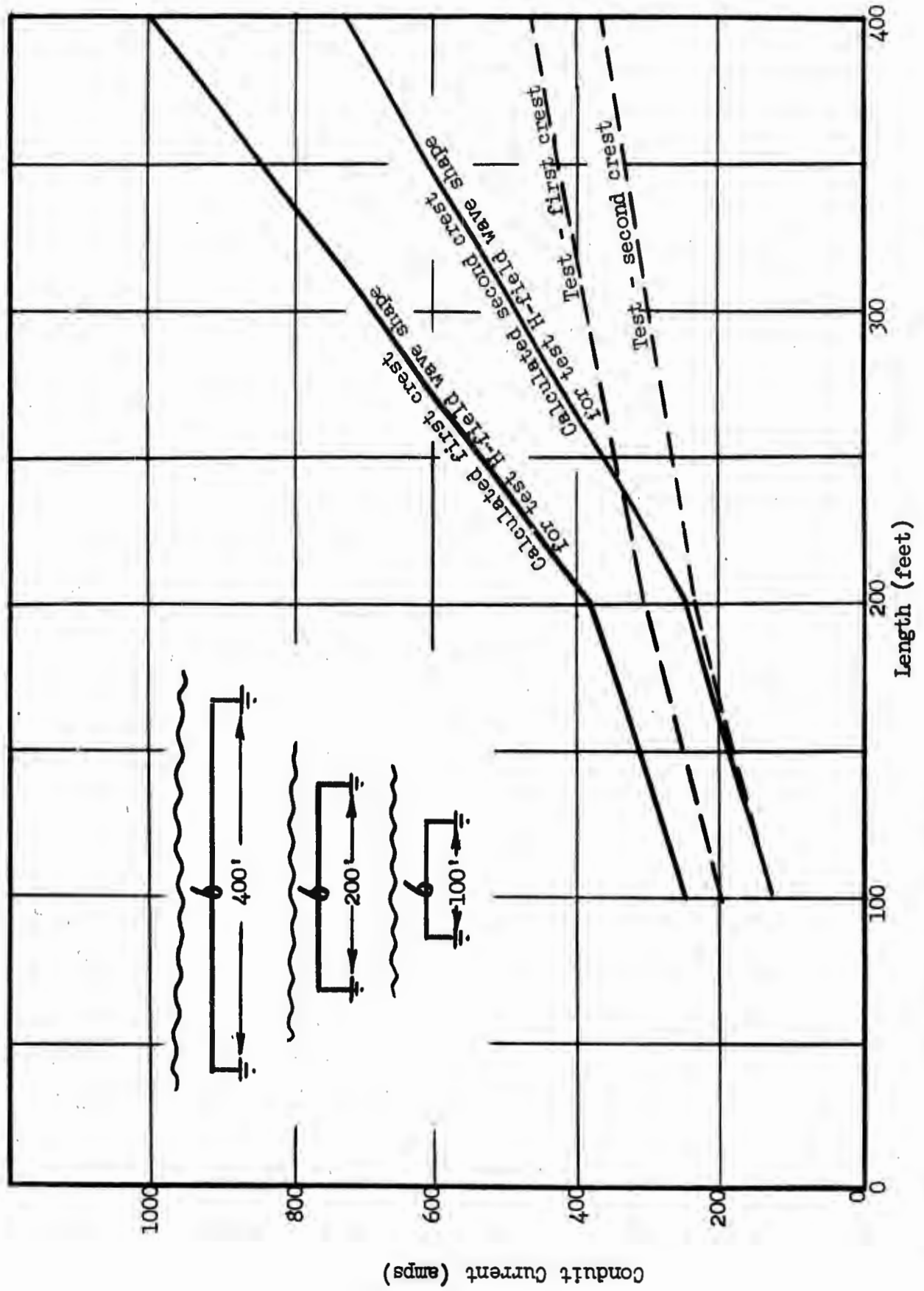


FIGURE 6.11 Peak Conduit Current for the First and Second Crests. Calculated and Measured Values.

This graph indicates that for a ground resistivity of approximately 130 ohm-meters the difference between the calculated current and the measured value will continue to increase rapidly for longer lengths of conduit. At 1,000 feet this ratio has been calculated as approximately 5:1. It, therefore, appears that for long runs of conduit in an H-field the calculated value of current by the lumped parameter model will be larger than the actual current even with various ground resistivities.

The calculating procedure is based on a model which considers that all of the current induced by the H-field flows along the conduit and through the ground via the counterpoise system of the buildings. In the actual installation, for long conduits in direct contact with earth, the current will also travel from the conduit to ground as shown in Figure 6.12 and 6.13. Figures 6.14 and 6.15 show the variation in current between the ends and the center of a buried conduit connected to counterpoise systems. As expected, the current increased at both the center and ends when the conduit was extended from 200 to 400 feet. The percent increase in current for the ends of the conduit were not as large as the percent increase at the center. This indicates that for longer conduit runs a larger variation between these currents will exist with the larger current being at the center of the conduit. This variation will be dependent on the ground resistivity, counterpoise impedance, and the length of the conduit.

#### 6.4.2 Buried Conduit, Isolated from Direct Contact with Ground, Tied to Ground Rod Beds at Each End

In the report on the previous series of experiments (Part I), Tests #3 and #8 were similar except that the conduit in Test #8 was buried in direct contact with ground, Table 6.1. The current, as measured at the end of the conduit, was approximately 2:1 larger for the underground experiment. The measured loop inductance was just the reverse; the inductance above ground being approximately double the value underground. This indicated a possibility of reducing buried conduit current by containing the conduit in an isolated duct (six times the diameter of the conduit).

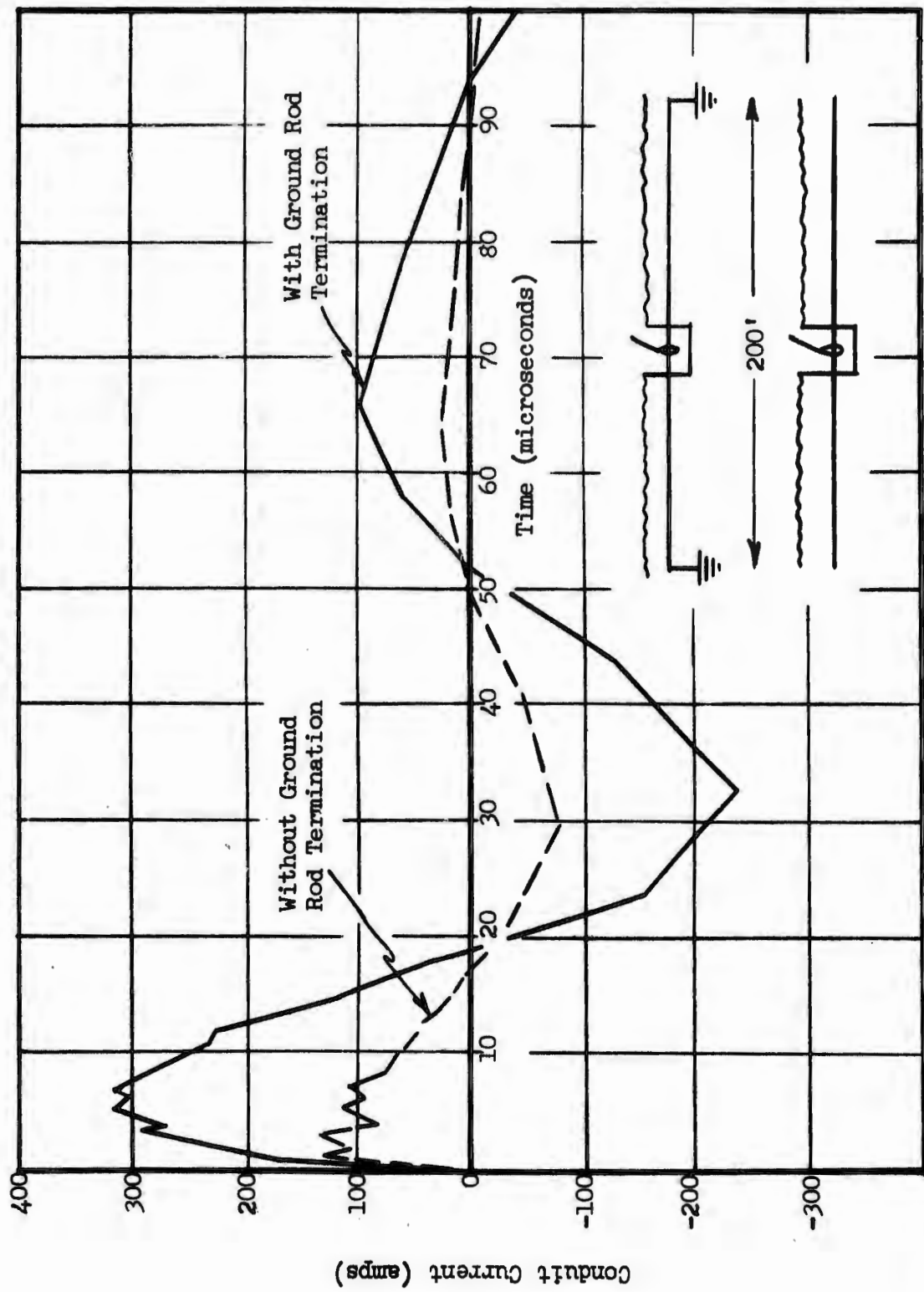


FIGURE 6.12 Conduit Current (center). 200' Conduit with and without Ground Rod Termination.

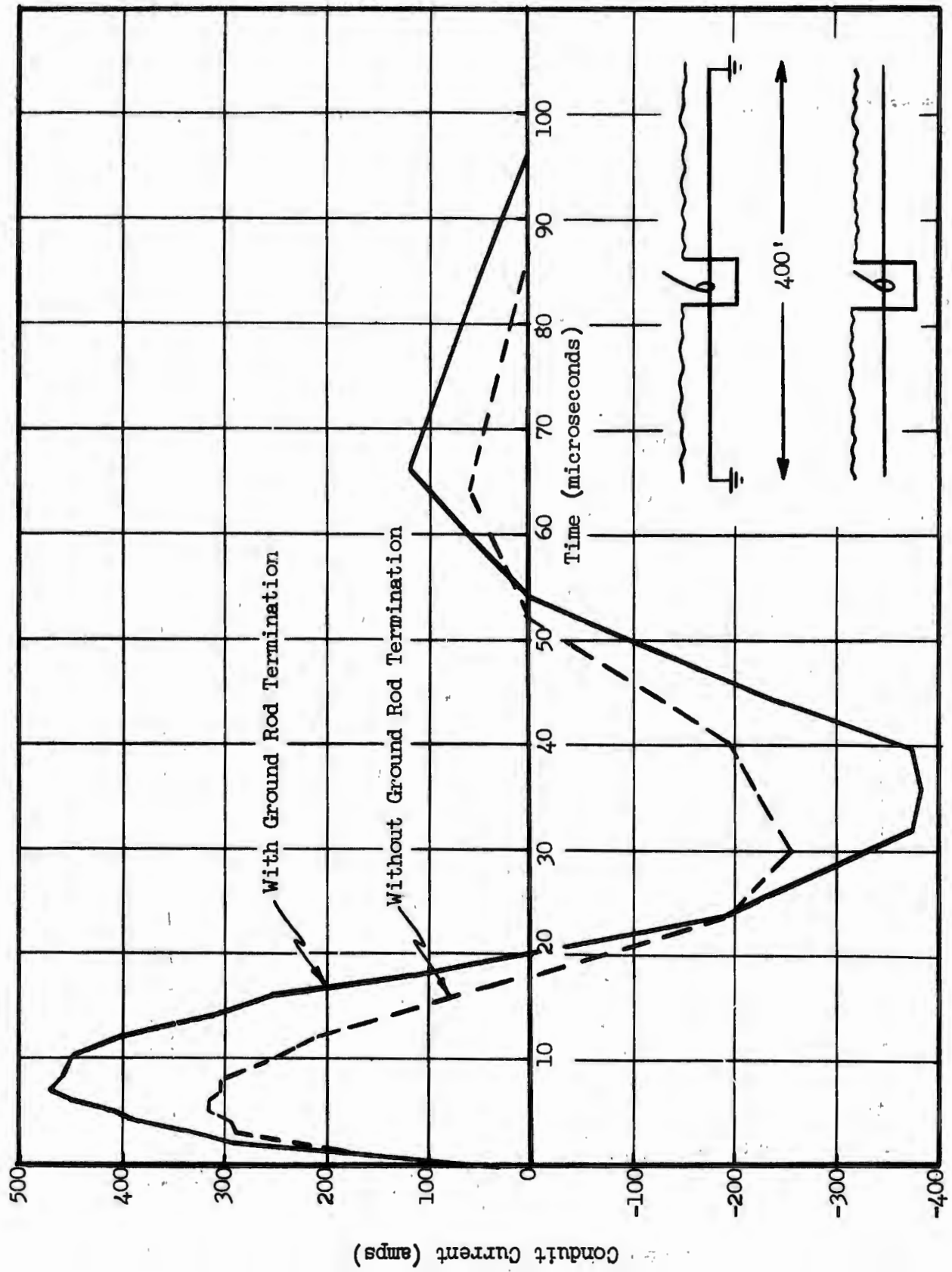


FIGURE 6.13 Conduit Current (center). 400' Conduit with and without Ground Rod Termination.

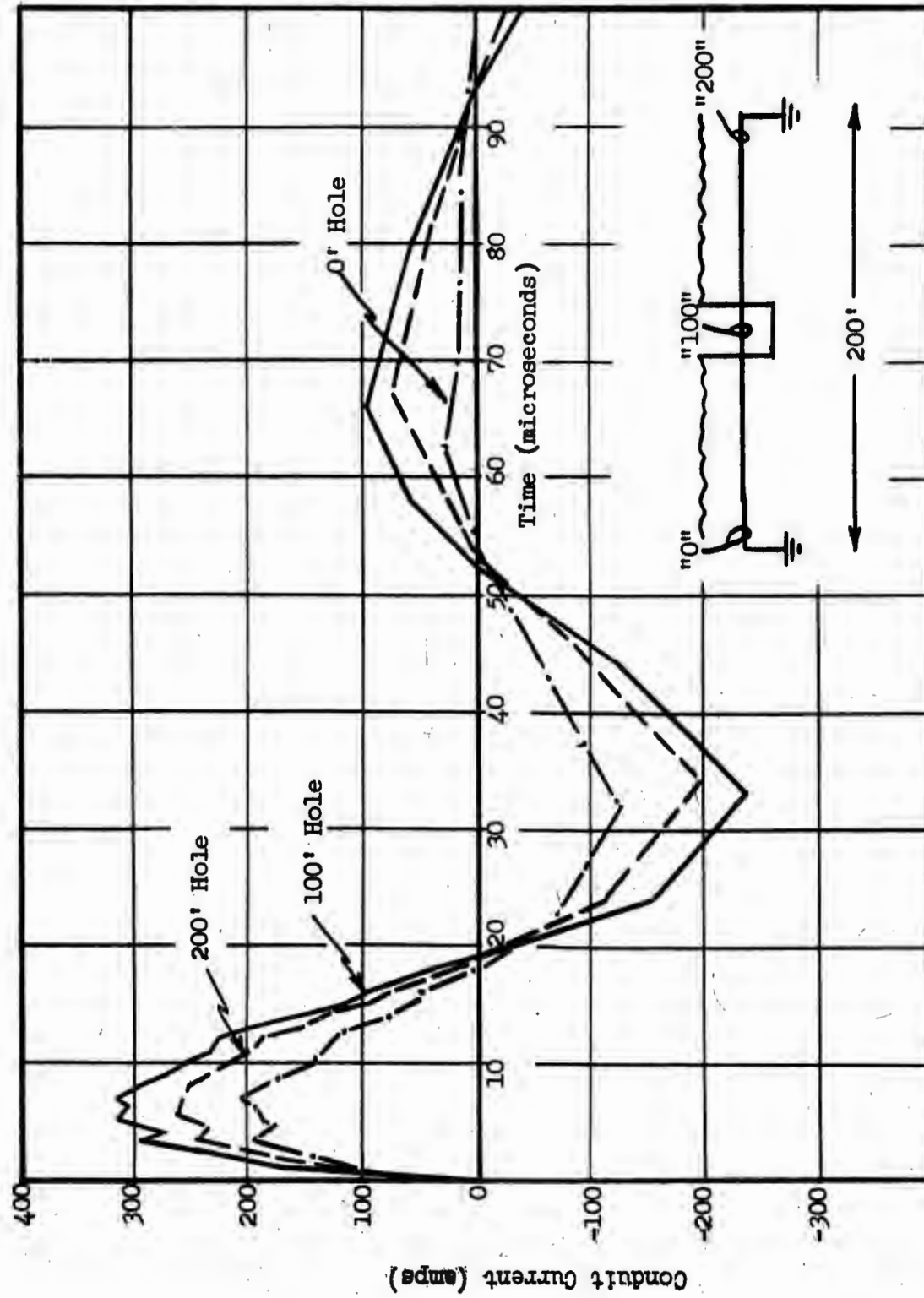


FIGURE 6.14 Conduit Current. 200' Conduit with Ground Rods at Ends. Measurement at Ends and Center.

FIGURE 6.15 Conduit Current. 400' Conduit with Ground Rods at Ends and Center.

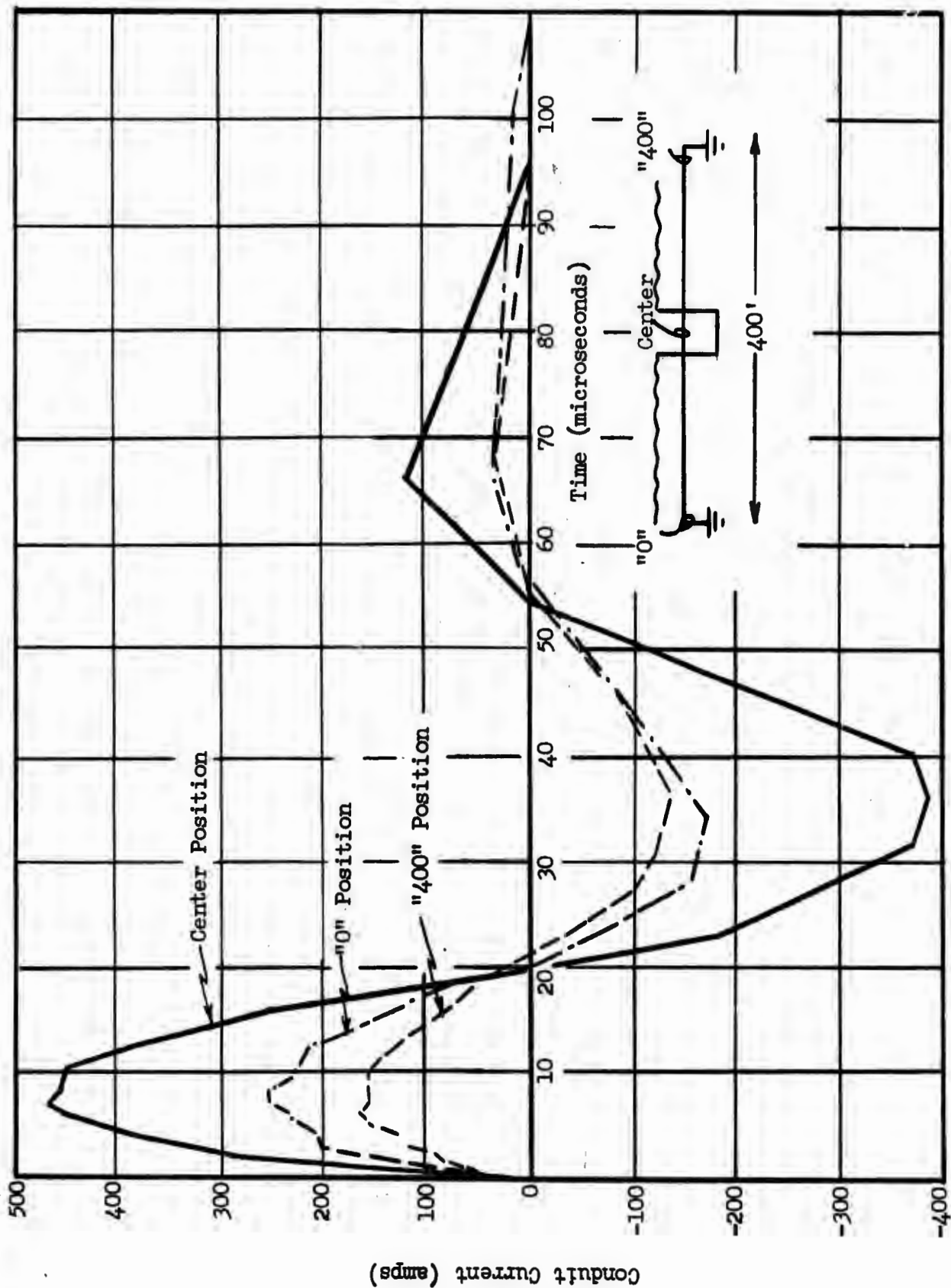

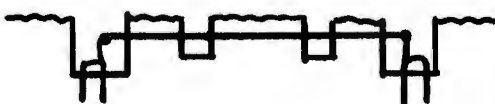


TABLE 6.1

PREVIOUS CONDUIT TESTS

| Test  | Measured |                                 | Conduit Current<br>First Peak |
|---|----------|---------------------------------|-------------------------------|
|   | R        | L                               | Amps                          |
| <p>#3 Above Ground<br/>100' Conduit Tied to Ground<br/>Rods, Far Ground</p>  | 30 ohms  | $140 \times 10^{-6}$<br>henries | 96                            |
| <p>#8 Underground<br/>100' Conduit Tied to Ground<br/>Rods, Far Ground</p>   | 20 ohms  | $75 \times 10^{-6}$             | 165                           |

One hundred feet of conduit (the same as used in Tests #3 and #8) was centered in a transite pipe and buried in earth. The conduit-pipe was located in the same area as the previous test and the same grounding rod beds were attached to the ends of the conduit.

The measured inductance of the loop was  $104 \times 10^{-6}$  henries, a value which lies approximately halfway between the value as measured for the above ground loop and the value of the direct contact underground conduit. The current was approximately halfway between the other current measurements, Figure 6.16. It should be noted that the H-field wave form for the isolated test was slightly different than for the other two tests. This is the reason for the earlier crossover points and the faster rise time of the leading edge of the conduit current wave form.

To investigate the reduction of conduit current provided by guard wire or screening, two tests using each type of material was performed. The wire or screening was placed on top of the earth over the conduit and attached to the ends of the conduit at the ground beds. Current measurements were made on both the guard wire or screen and on the conduit, Figure 6.17. The guard wire and screen reduce the current on the conduit as shown in Figure 6.18. The amount of the reduction depends on the impedance of the guard wire versus the impedance of the conduit and the amount of area between the two. This effect will be discussed in the following section.

#### 6.4.3 Guard Wire and Screening Investigation - Buried Conduit

To understand the reduction in conduit current from screening connected to the ends of a buried conduit, earlier data from the previous report on above ground conduit tests verified the current sharing effect for two parallel conduit, Figure 6.19. The diagram shows the similarity between the two tests and also indicates the various currents which flow in the conduit-earth combination.

When two parallel paths are contained in a conduit loop, the current that flows through each section is the result of the impedance of each

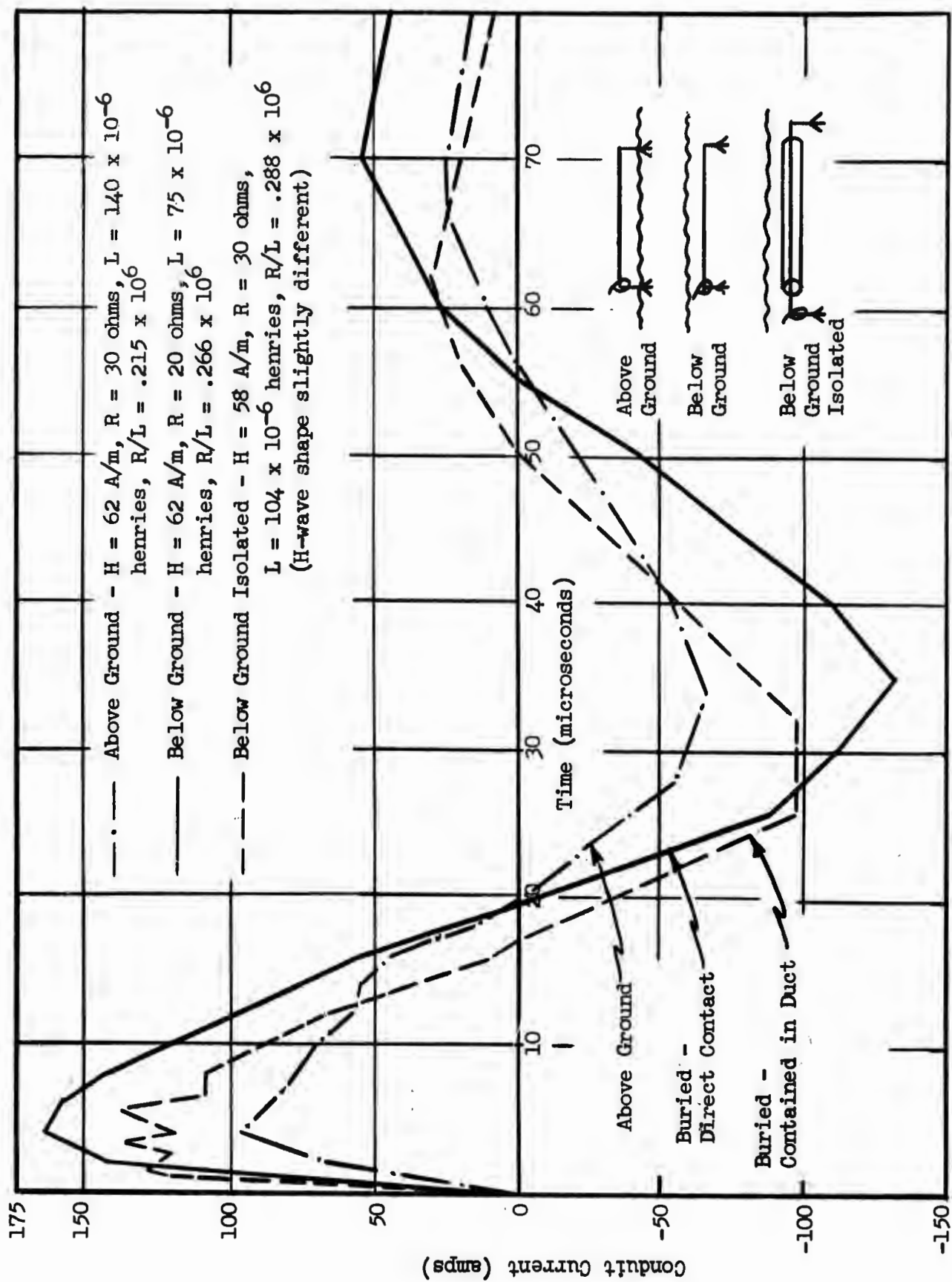


FIGURE 6.16 100 Foot Conduit - Above Ground, Below Ground, and Below Ground Isolated

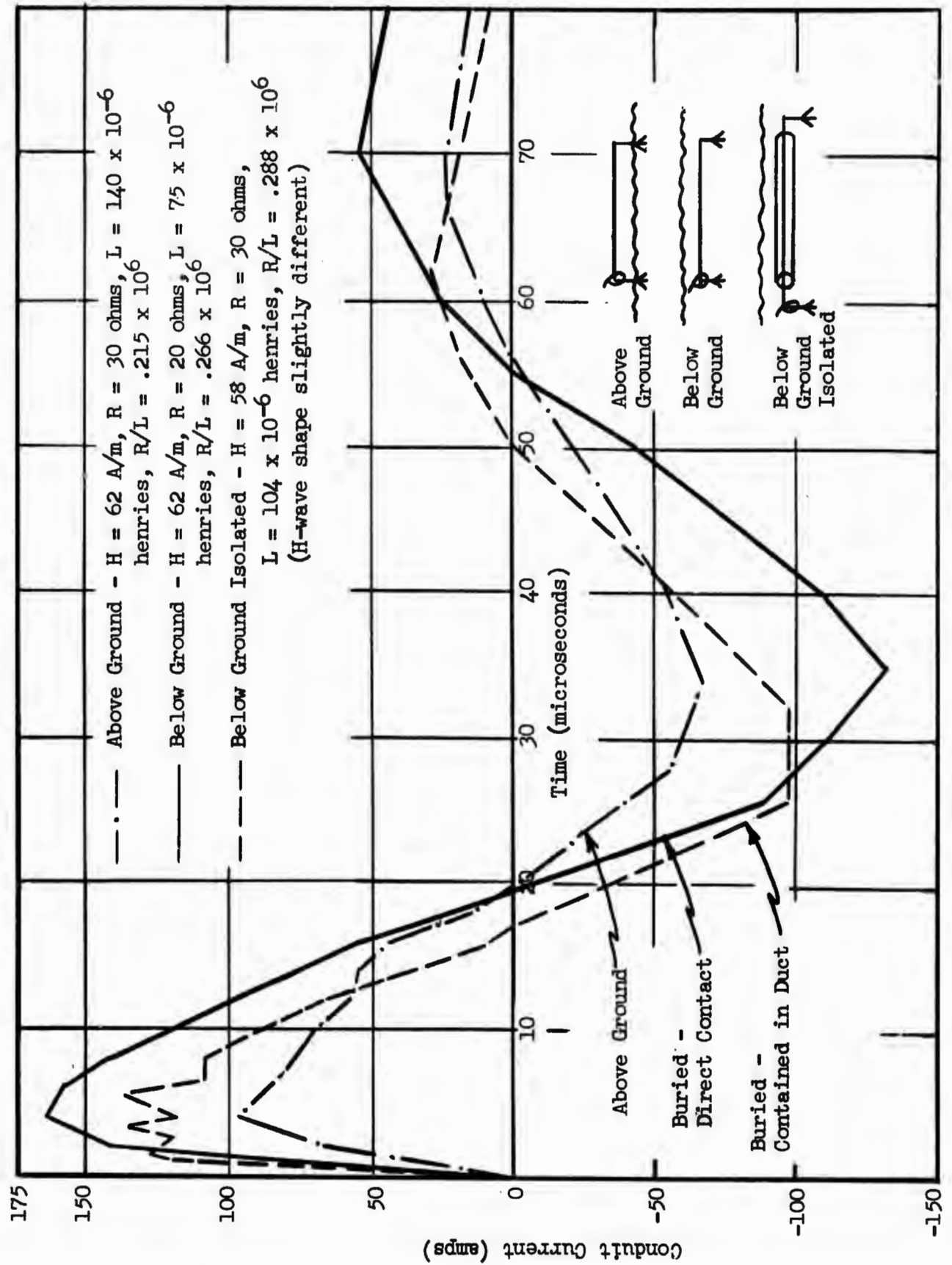


FIGURE 6.16 100 Foot Conduit - Above Ground, Below Ground, and Below Ground Isolated

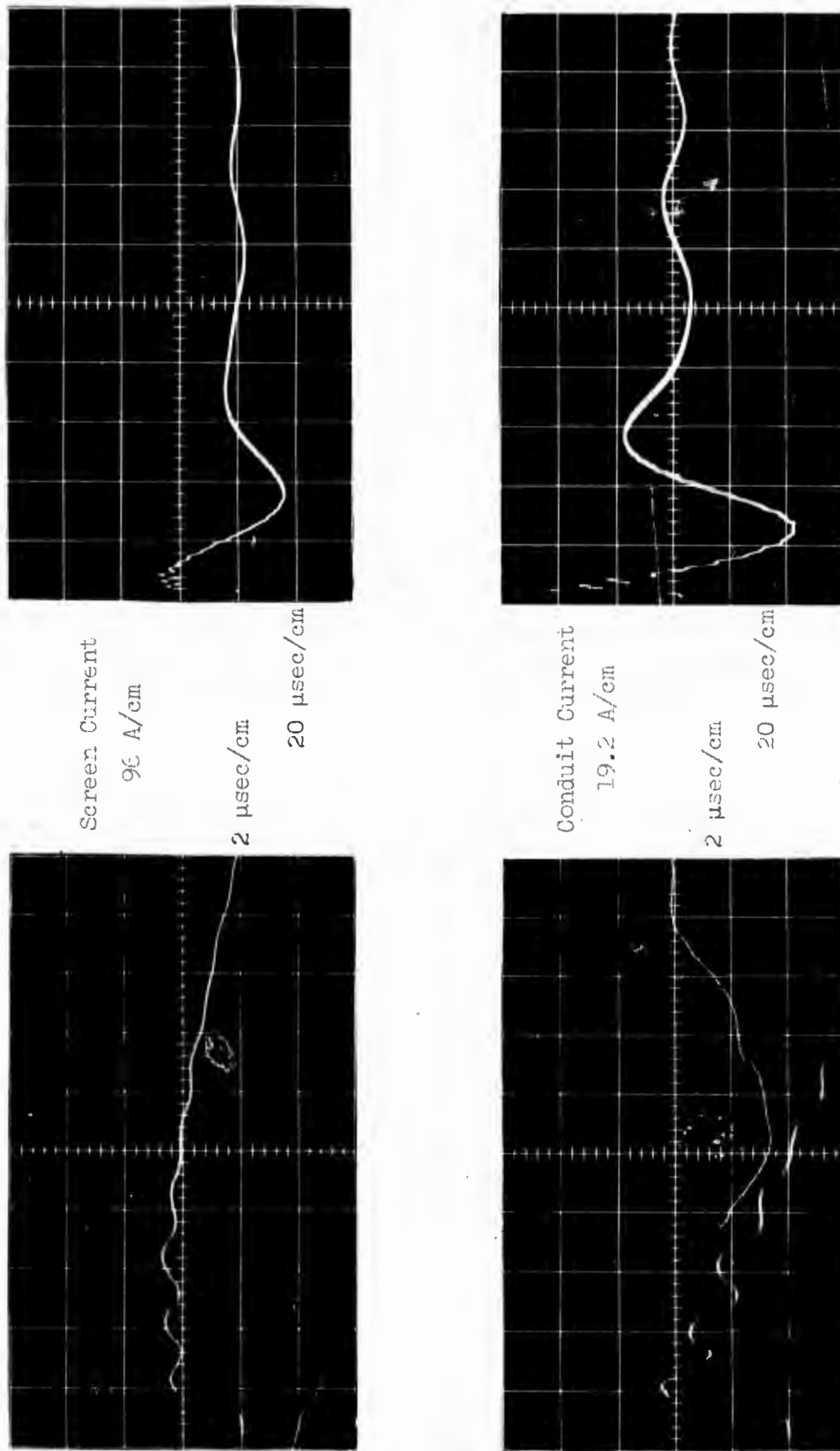


FIGURE 6.17 Buried Conduit, Contained in Duct, Galvanized Screen Guard

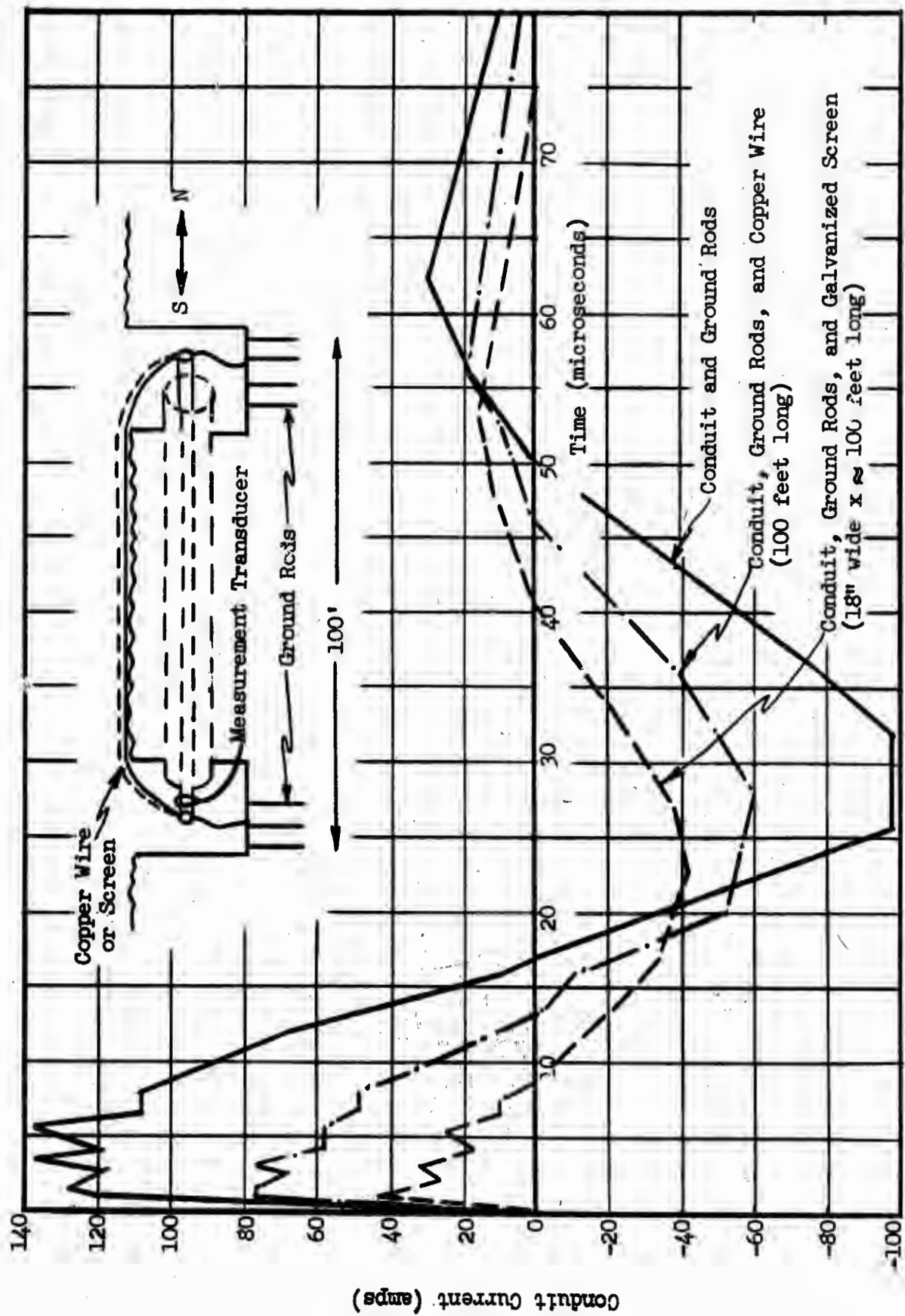


FIGURE 6.18 Measured Conduit Current - Isolated Conduit - Buried

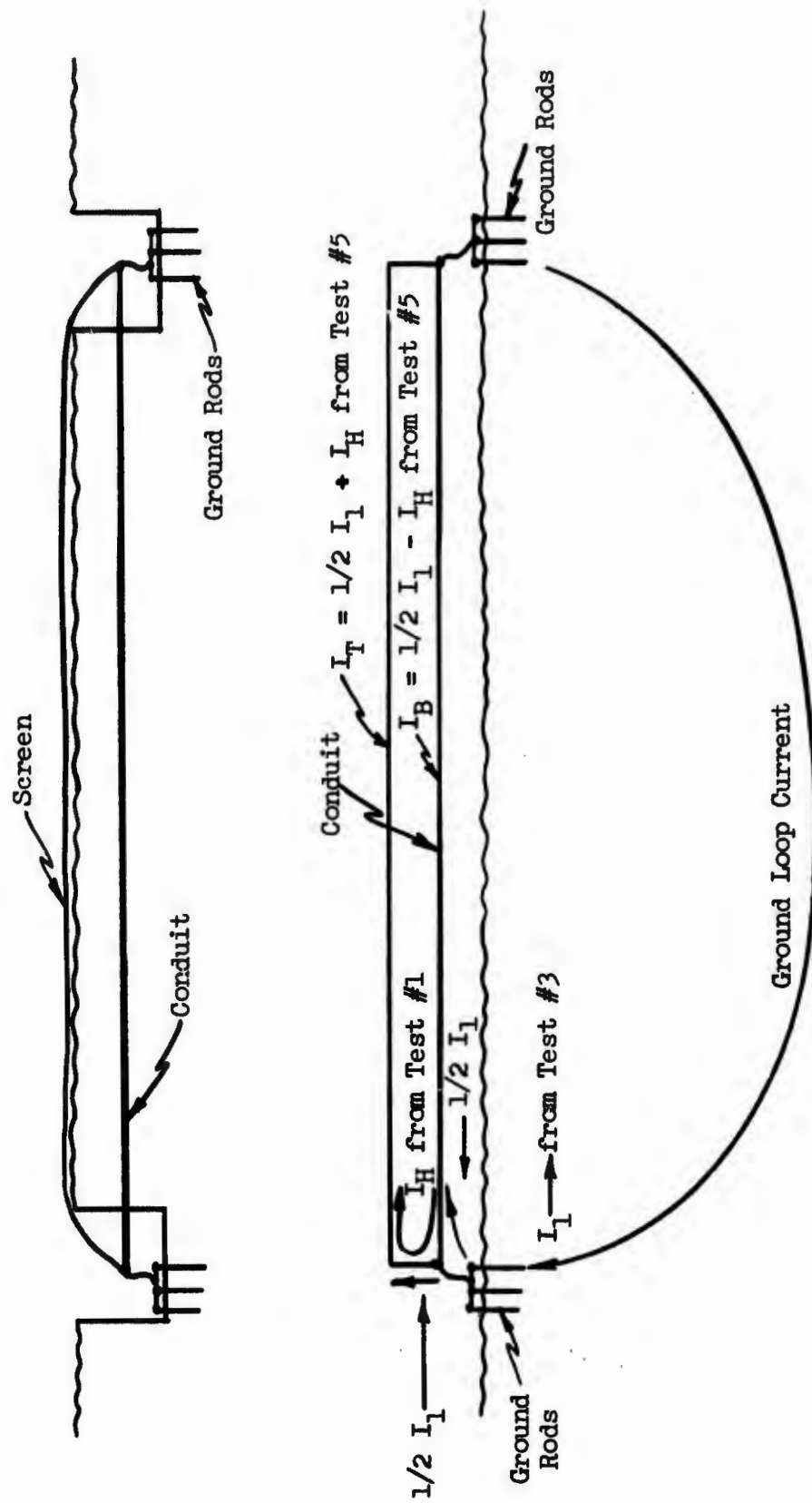


FIGURE 6.19 Conduit Current Reduction

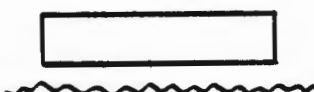
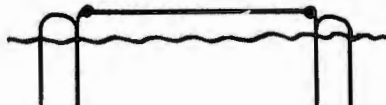
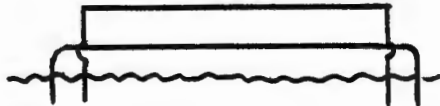
section and the H-field contained within the loop formed by the parallel paths. This was verified from Tests #5, #3, and #1 of the previous test report. The conduit setups and peak current values observed for these tests are shown in Table 6.2. In Test #5 two identical conduits, one above the other, were placed in an H-field and connected electrically in parallel and to ground through ground rods. The impedance of each conduit was the same since the conduits were identical. The current generated by the larger ground-conduit loop would be divided approximately equally between the two above ground conduits if the effect of the H-field between the conduits was not considered. This H-field generates a second current which flows around through the two conduits as measured in Test #1.

To be able to predict the current wave shape in each of the conduits (top and bottom) of Test #5, the current wave shape as measured in Test #3 is divided by two. For the wave shape of the top conduit, current from Test #1 is added to this wave shape. For the bottom conduit, the current wave shape from Test #1 is subtracted from this current wave shape, Figures 6.20 and 6.21.

The calculated current wave shapes for both top and bottom conduits are a close approximation to the measured values. The measured wave forms on the two parallel conduit above ground are very similar to the current wave forms of the isolated conduit under ground with the screening.

To further check the effects of the screening with other ambient parameters, 100 feet of conduit was buried within 75 feet of the radiator ground. This provided a non-linear H- and E-field with an average H-field of 84.5 A/m and an estimated horizontal E-field of 200 volts/meter. The conduit was in direct contact with the earth and attached to ground rods at the ends. Measurements of current were made at the center and ends of the conduit with and without the screen material attached, Figure 6.22 and 6.23. The graphs show that at the ends of the conduit the peak current is reduced approximately 4:1 while at the center the current is reduced 3:1. Again, the wave shapes

TABLE 6.2PREVIOUS CONDUIT TESTS

| Test  | Measured   |  | Conduit Current<br>First Peak |
|---|--|--|-------------------------------|
|   | R  | L  | Amps                          |
| #1 Closed loop above ground , 100'<br>long, 4 feet high, one foot<br>above ground, far ground<br>                  | .085<br>ohms   | $60 \times 10^{-6}$<br>henries   | 41.8                          |
| #3 100' Conduit tied to ground<br>rods, one foot above ground,<br>far ground<br>                                 | 30 ohms  | $140 \times 10^{-6}$<br>henries  | 96                            |
| #5 100' Conduit each tied<br>together and ground rods, one<br>foot and five feet above<br>ground, far ground<br> | <u>upper</u><br>30 ohms<br><br><u>lower</u><br>30 ohms | $140 \times 10^{-6}$<br>henries<br><br>$140 \times 10^{-6}$<br>henries | 77<br><br>35.2                |

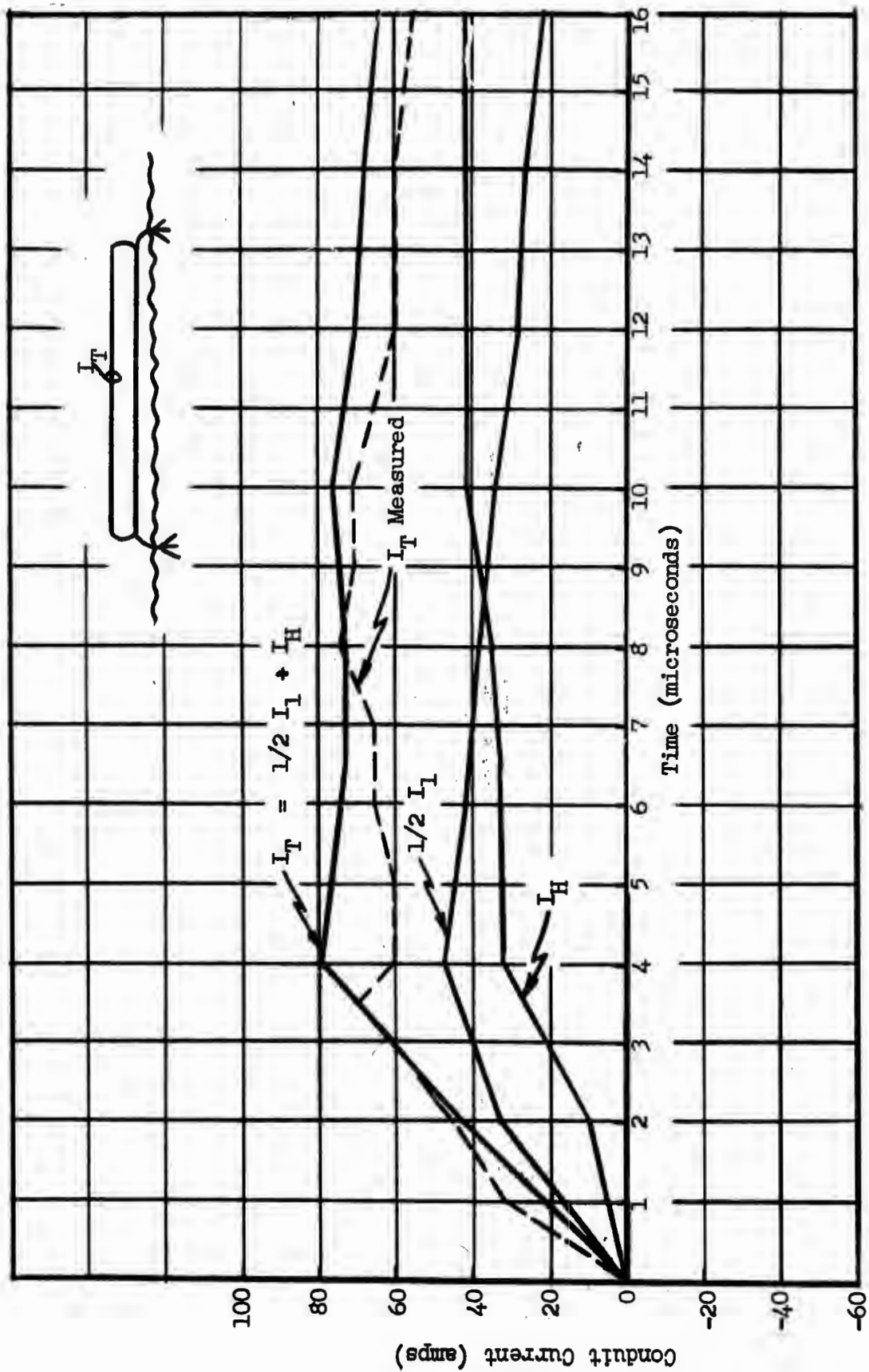


FIGURE 6.20 Top Conduit Current, Measured and Calculated

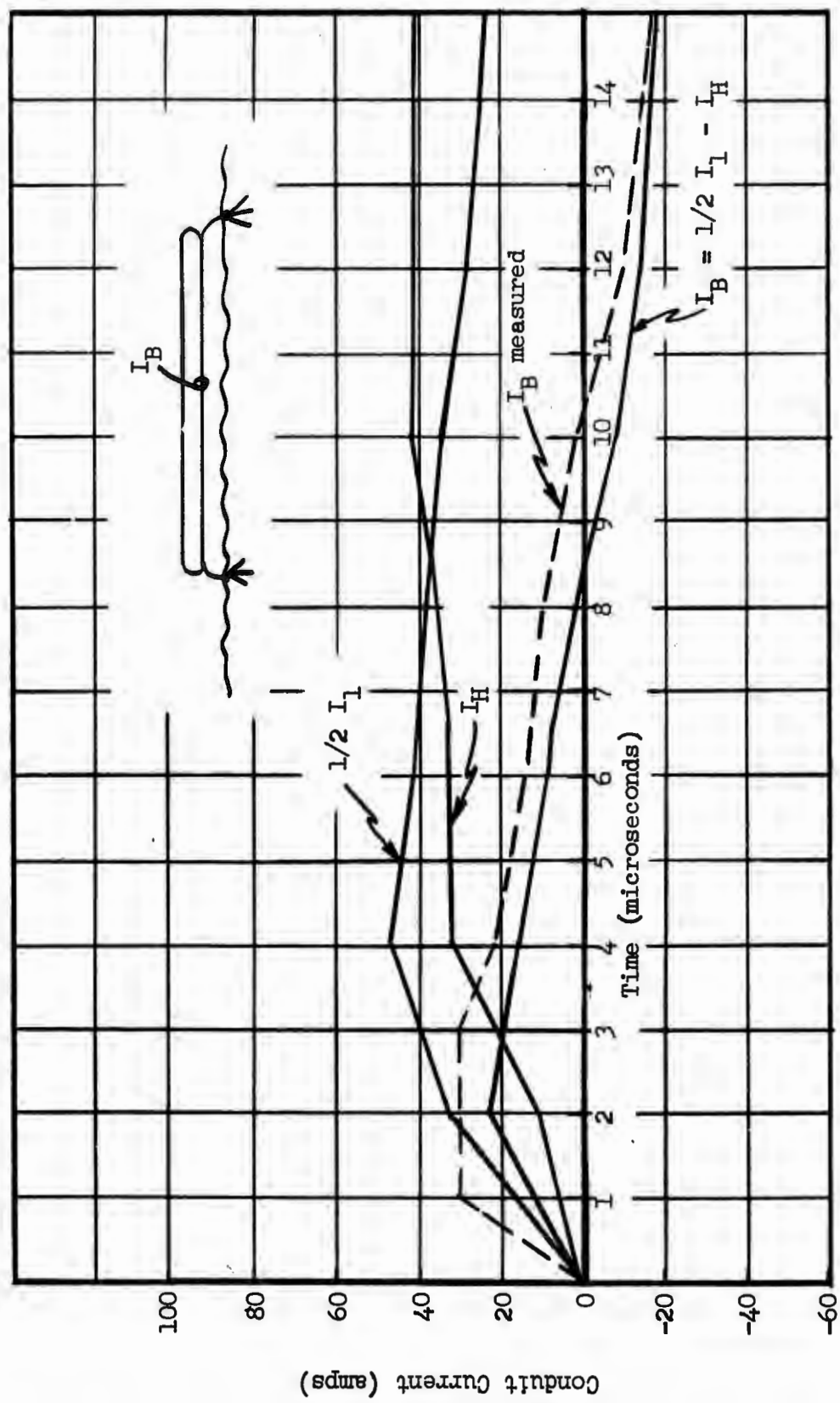


FIGURE 6.21 Bottom Conduit Current, Measured and Calculated

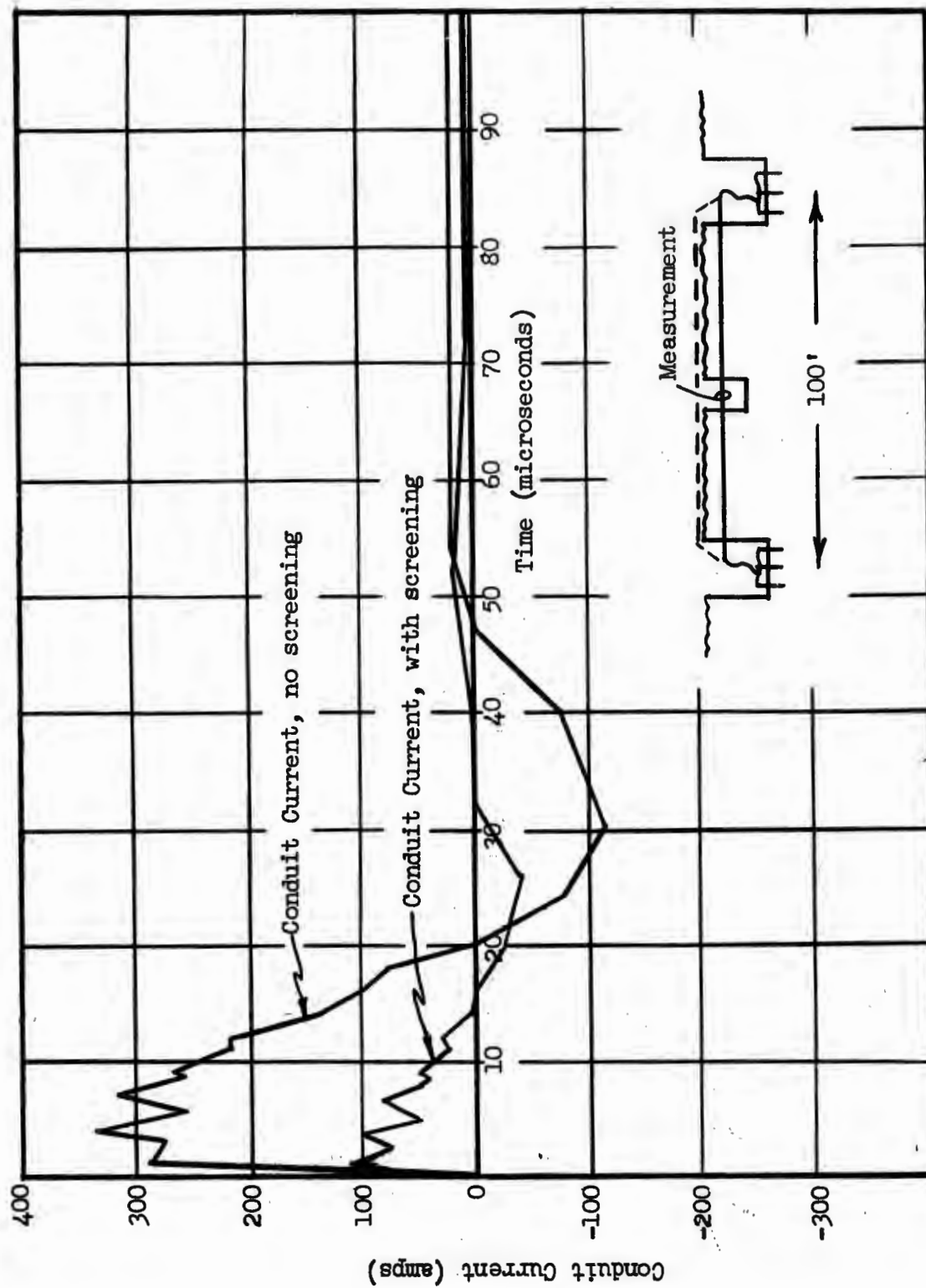


FIGURE 6.22 Center Conduit Current with and Without Screening. Near Field.

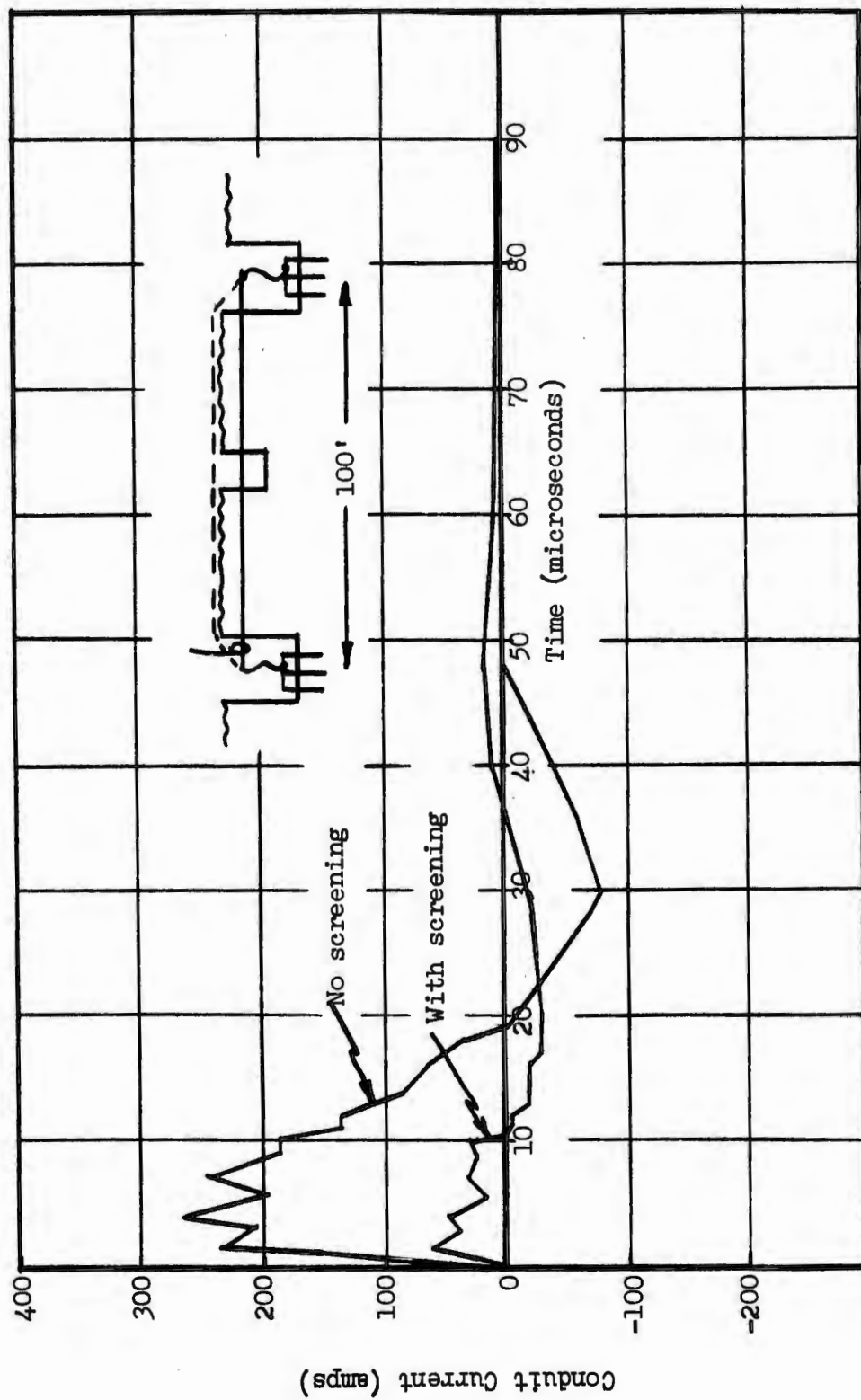


FIGURE 6.23 End Conduit Current with and without Screening. Near Field.

of the current on the conduit and screen are similar to the other tests discussed in this section.

#### 6.4.4 Current Shunt Plates - Buried Conduit

Various current shunting schemes were tested to study the effects of shunting plates and counterpoise systems on the division of current and the resulting H-field attenuation or enhancement within a conduit system. A test hole, 17' x 10' x 9', Figure 6.24, containing shunting plates and a ground rod system, was used at the end of a 200 foot conduit run for several tests and in the middle of a 400 foot conduit run for the remainder of the tests. Shunting plates, one foot wide by four feet long and 1/4-inch thick, were connected from the conduit to the ground rod bed. These plates were located fifteen feet apart within the test hole. The vertical distance between the conduit and ground rod bed was four to five feet. For many of the tests an aluminum sheet, 18 inches wide, was connected from the bottom of one shunt plate to the bottom of the other plate. This reduced the horizontal impedance of the ground bed and helped determine current flow and distribution for the various experiments.

The first series of experiments consisted of the shunt plates and ground rod bed connected to the end of a 200 foot conduit. Measurements on the incoming conduit and on the center conduit between the shunt plates produced a 2.6:1 reduction in the center conduit current, Figure 6.25. Removal of the aluminum sheet from the shunt plates produced insignificant change in center conduit current, Figure 6.26. This indicates that the shunt plate current enters the ground directly with a minimum of current flow across the grounding system. The magnitude of each current is dependent on the impedance of each section (conduit and shunt plate versus shunt plate) and the induced current within this loop. This is the same set of parameters which controlled the current division on the conduit-screen experiments, Section 6.4.3.

The above tests simulated a counterpoise grounding system connected at

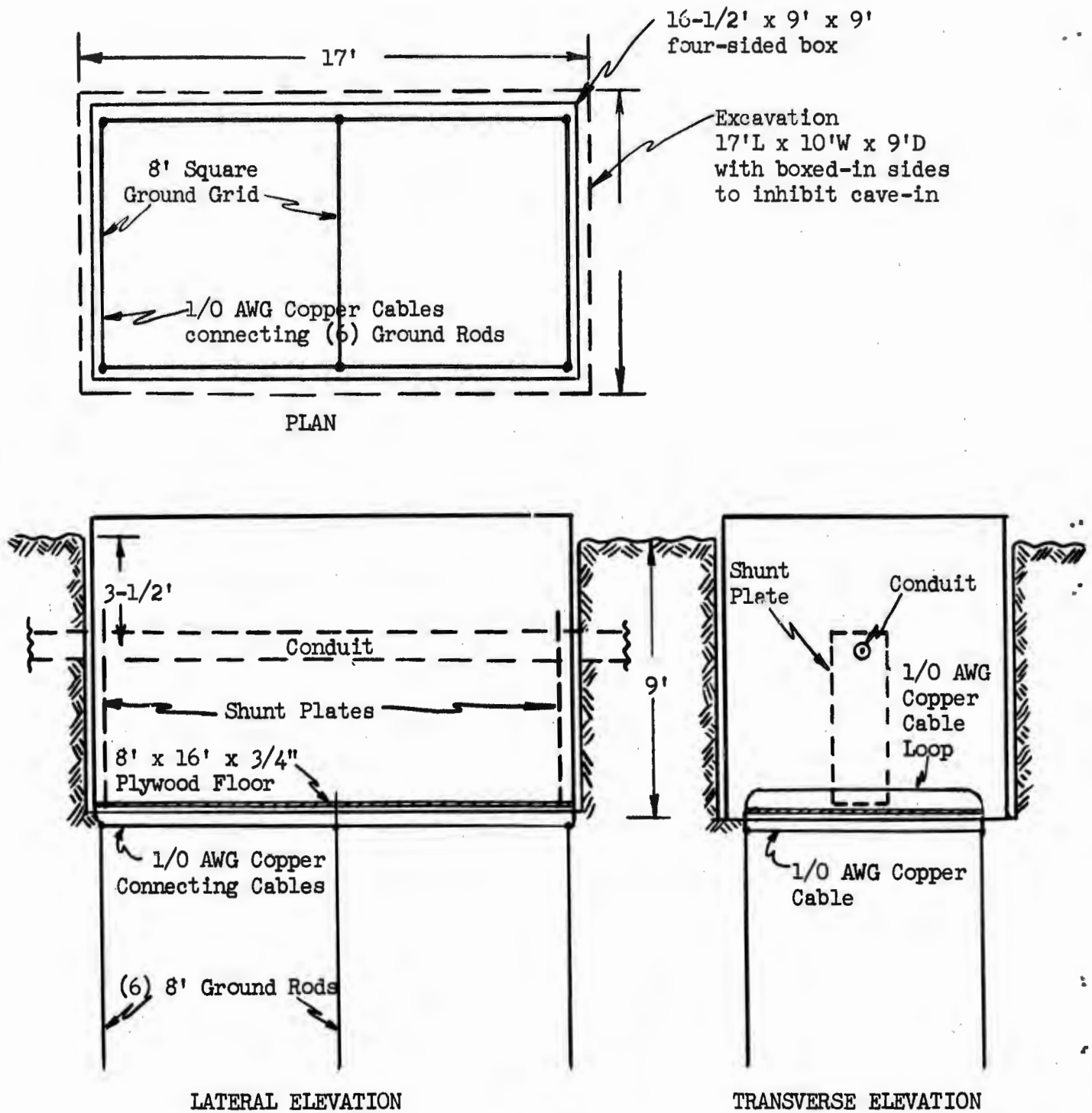


FIGURE 6.24 Grounding System Arrangement in Excavation at Center of Conduit Run

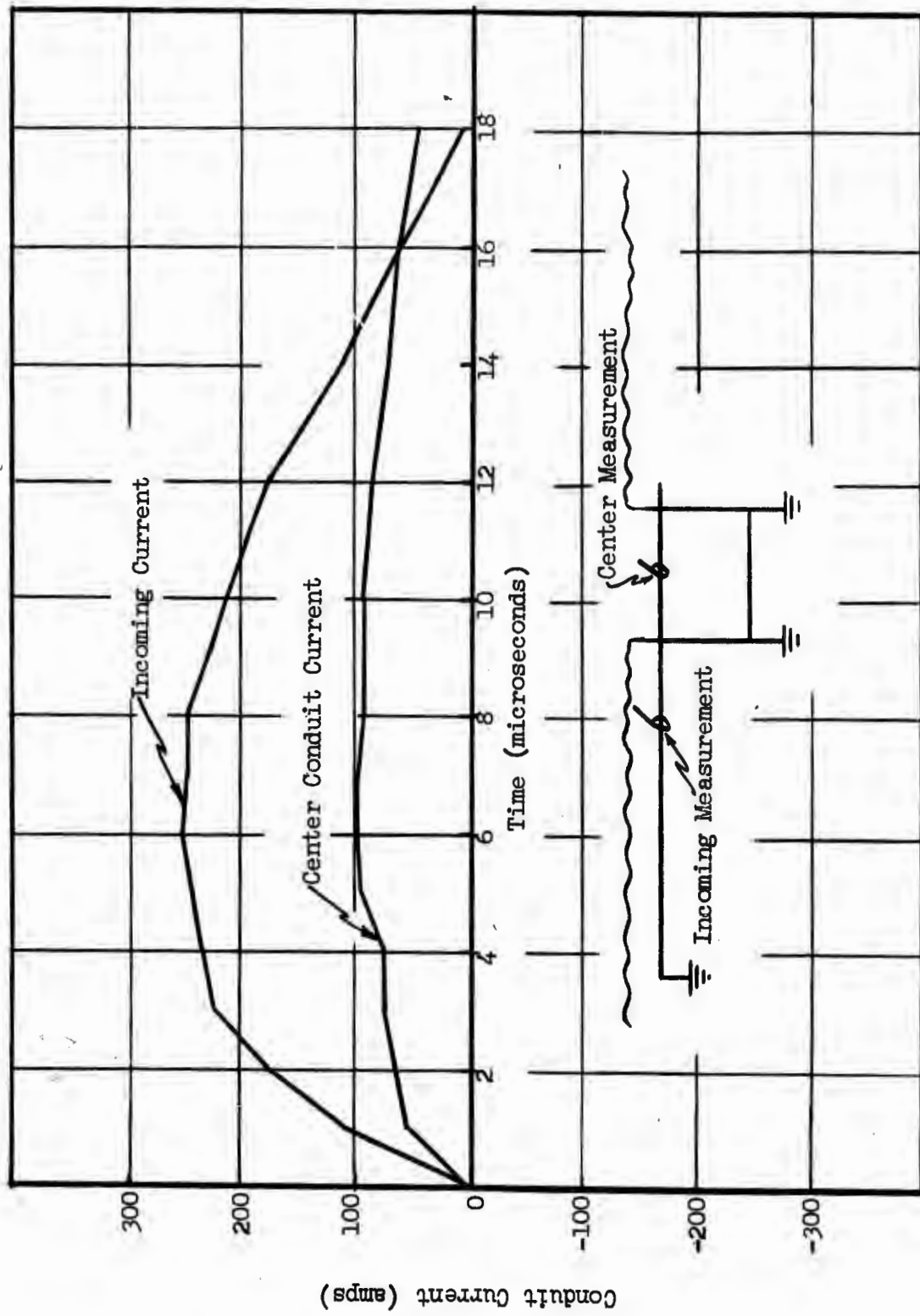
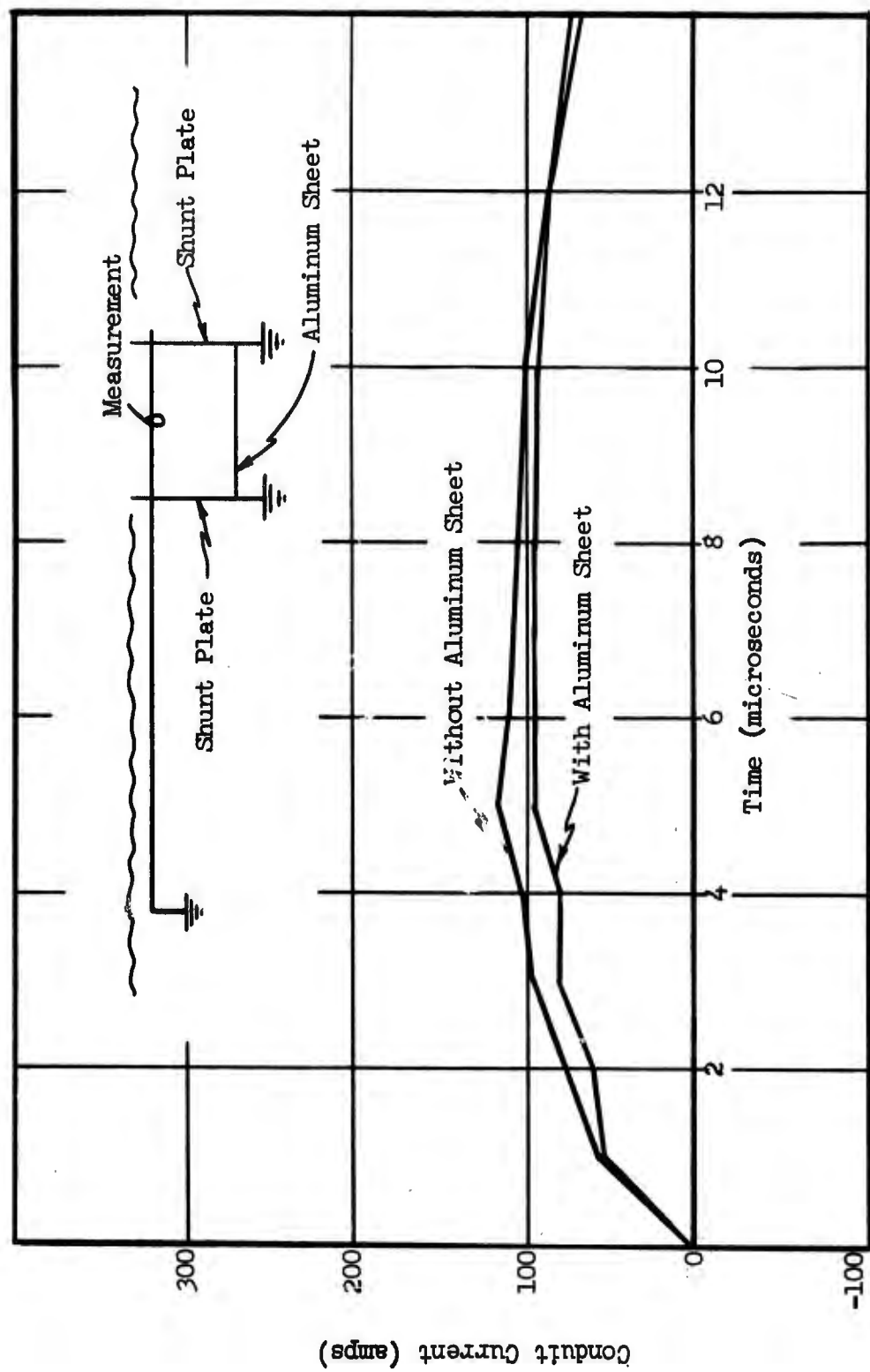


FIGURE 6.25 Conduit Current - Shunting Plates and 200 Feet of Conduit

FIGURE 6.26 Conduit Current - Center Measurement with and without Aluminum Ground Sheet

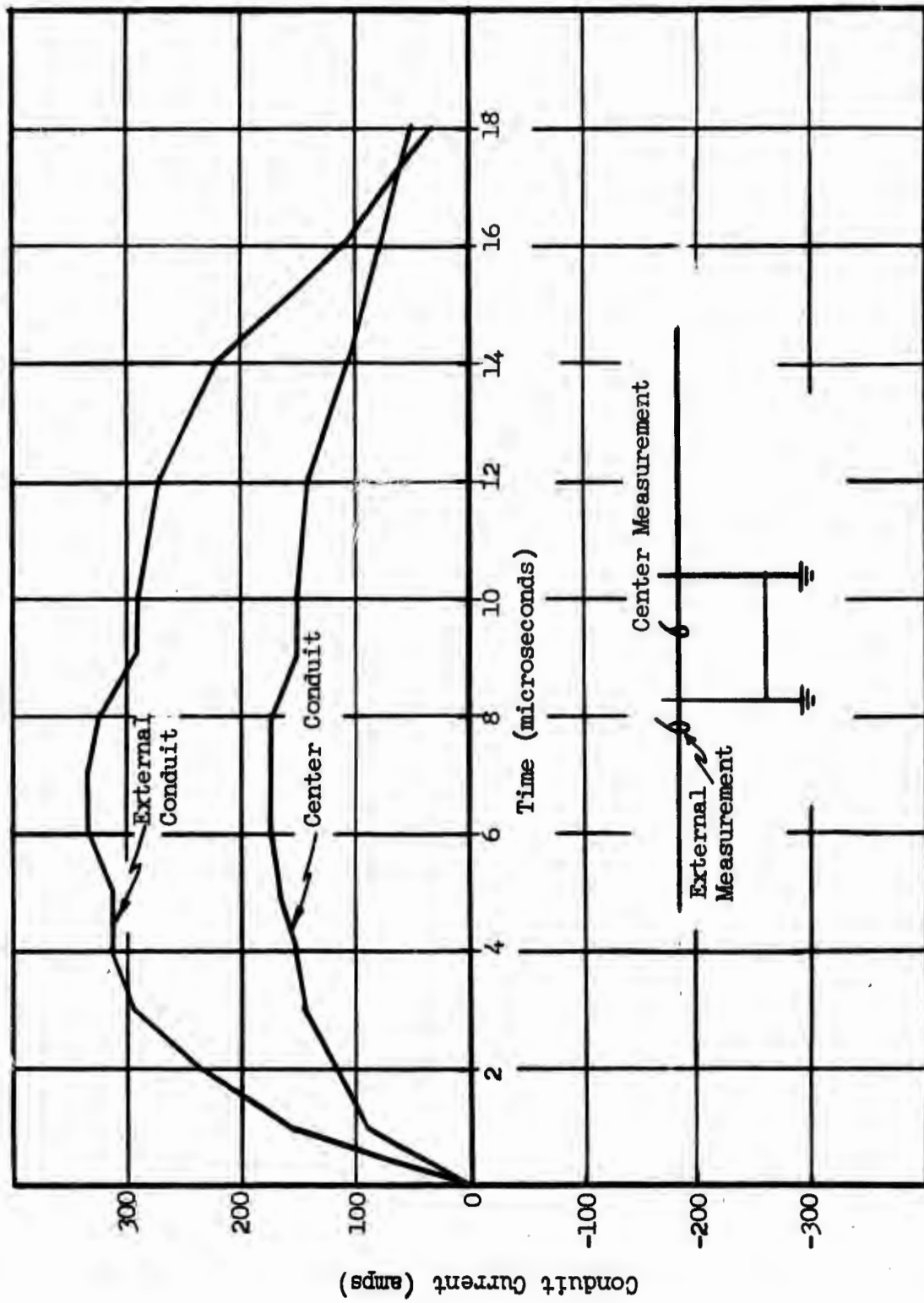


the end of a conduit system. In reality, most counterpoise systems would have conduits connected to all sides. To interpret these conditions, the grounding system was connected in the middle of a 400-foot conduit. In the initial tests the conduit was ungrounded at its ends. Current, as measured on the incoming conduit and at the center between the shunt plates, show a reduction of 2:1 for center conduit, Figure 6.27. In Figure 6.28, the grounds were added to the ends of the conduit and measurements made on both sides of the center hole. These currents are practically identical, even with the H-field being 15 percent smaller at the 400 foot position. This indicates that only a small current at the center position flows to ground, but the major current tends to flow through the center section; fifty percent of the current through the conduit and the other fifty percent down one shunt plate, across the grounding system, and up the other shunt plate. This was also verified by the removal of the aluminum strip at the ground points which changed the value of the current flowing through the center conduit, Figure 6.29. Eliminating the aluminum strip increased the impedance of the ground system horizontal path. Thus, the increase in current in the above conduit.

Figure 6.30 shows the division of current between the conduit and shunt plate. This again is controlled by the impedance of these components and the induced current in the conduit-shunt plate loop.

To show the effects of other parallel circuits (such as other conduits or steel members of a building which are tied to the conduit-counterpoise system), a third current path of screen material was placed above the conduit approximately two feet and connected to the conduit either outside the shunt plates or inside the shunt plates, Figures 6.31 and 6.32. With the adding of another parallel path the conduit current at the center was reduced by a ratio of 4:1. Therefore, the more parallel paths (conduit or structural members) in a counterpoise-building system, the less current on the individual conduits contained within.

FIGURE 6.27 Conduit Current - Stunt Plates, 400 Feet of Conduit



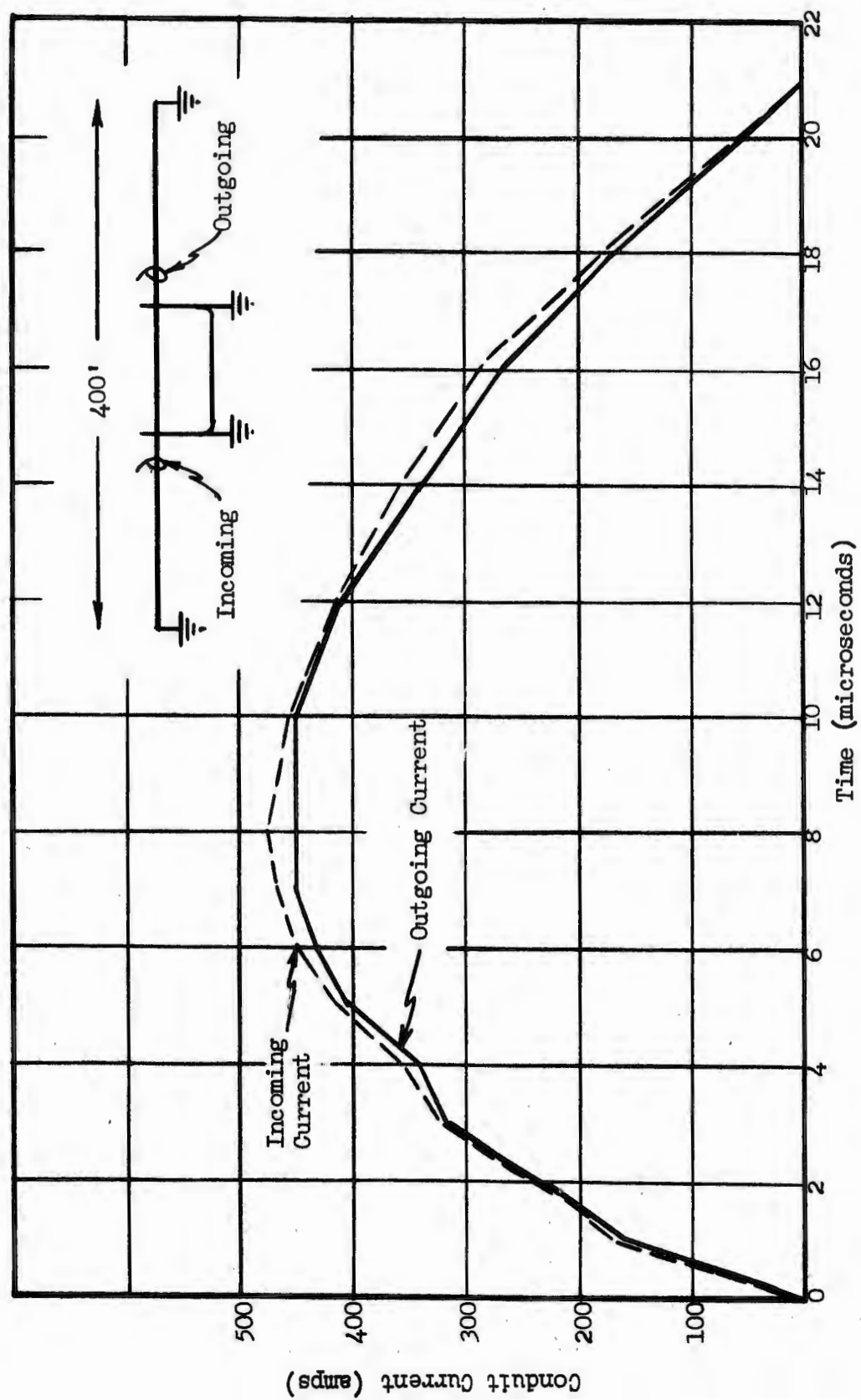


FIGURE 6.28 Conduit Current - Shunt Plates, 400 Feet of Conduit

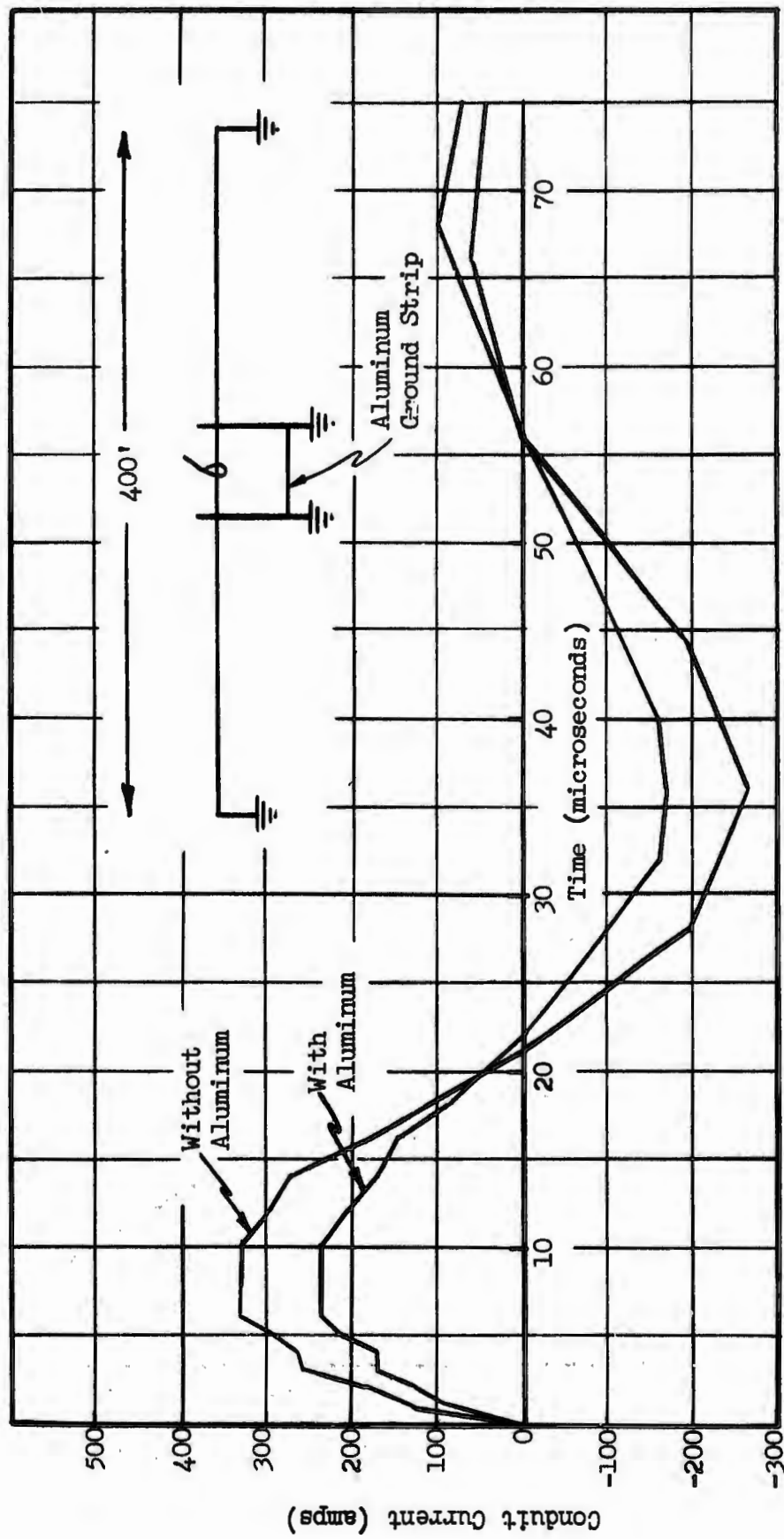


FIGURE 6.29 Conduit Current - Shunt Plates, with and without Aluminum, Ground Strip, 400' of Conduit

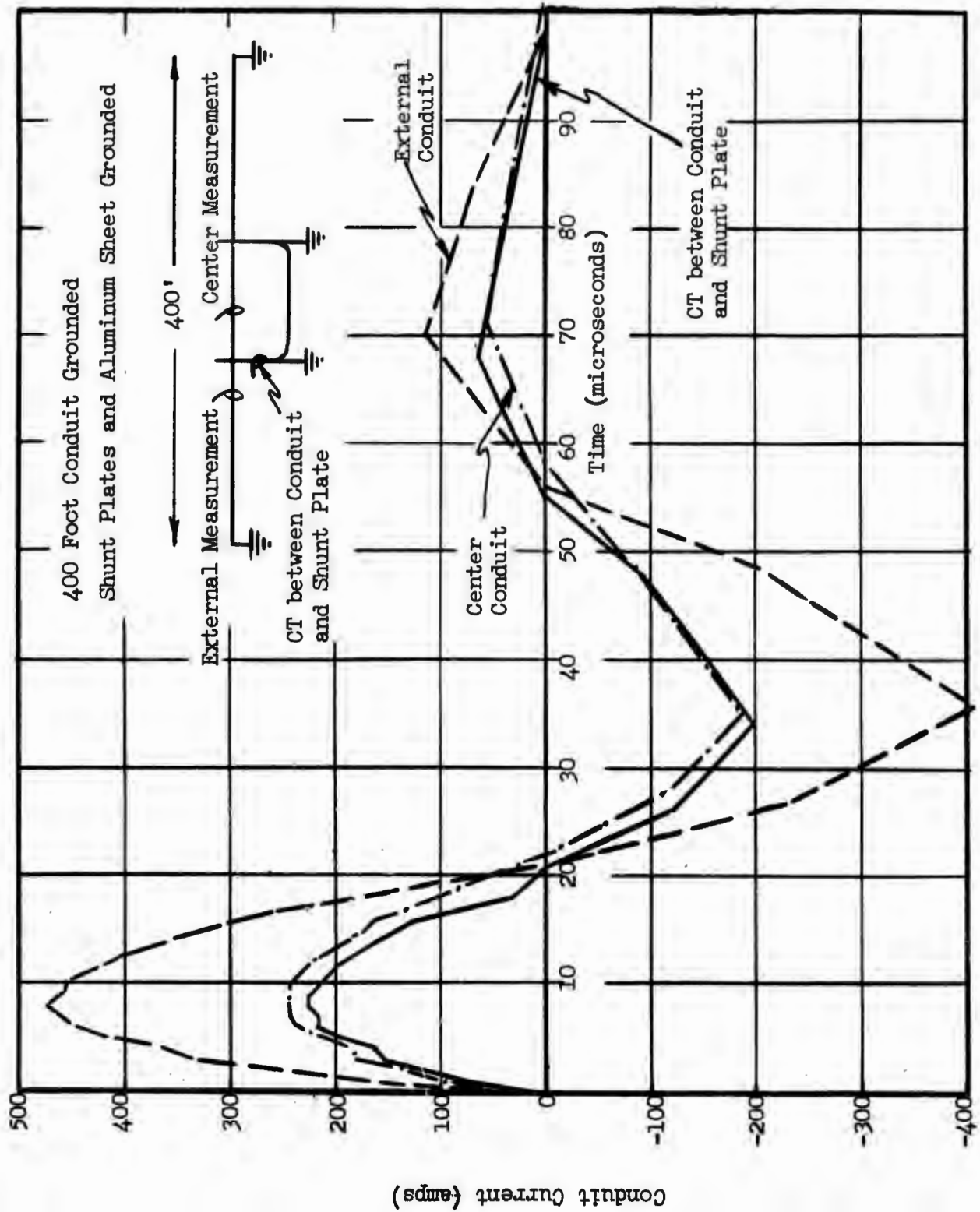
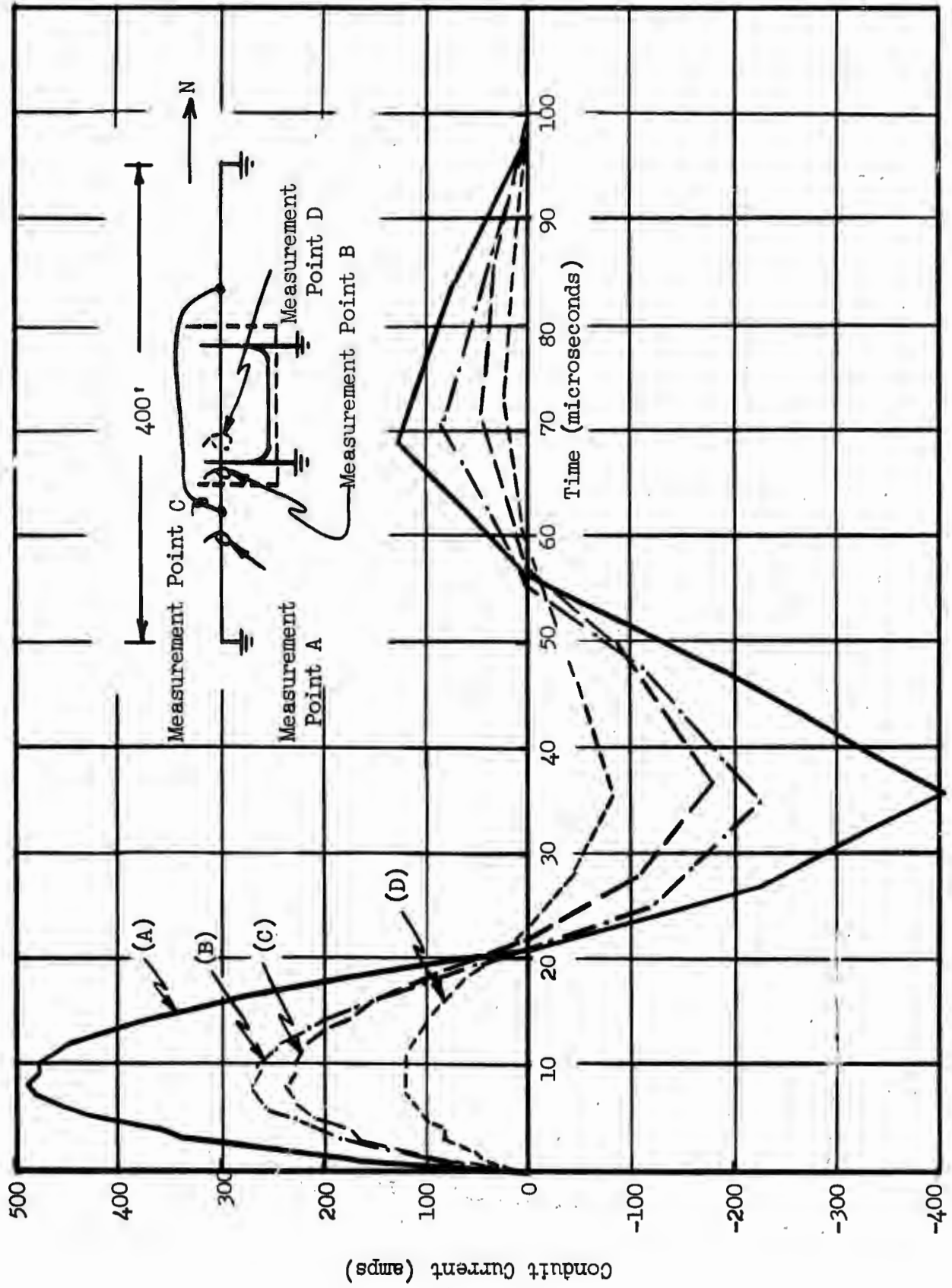


FIGURE 6.30 Conduit and Shunt Plate Currents, 400 Feet of Conduit

FIGURE 6.31 400' Conduit Grounded. Wire Mesh Added to Conduit Outside Box



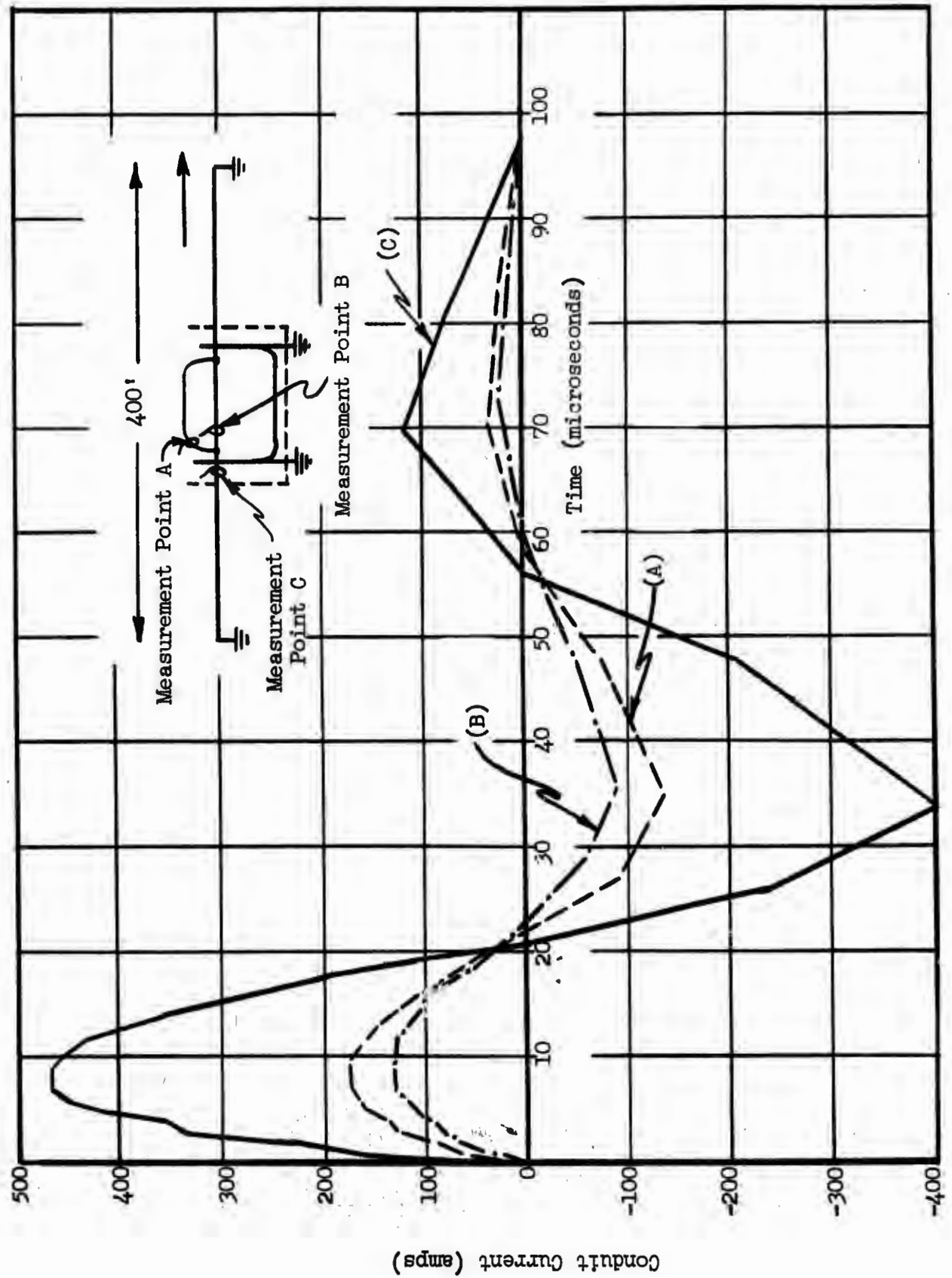


FIGURE 6.32 400' Conduit Grounded. Wire Mesh Added to Conduit Inside Box

The use of shunt plates provides an added benefit. Circulating induced current from the ambient H-field reduces the H-field between the conduit and the ground rod bed. Current from the external conduits divides fairly equally around this loop and, therefore, has little effect, Figure 6.33. Without the current shunt plates and counterpoise system, the H-field, at the same location, is the difference between the ambient H-field and the H-field generated by the conduit current, Figure 6.34, and can be derived as shown in Figure 6.35. As can be seen, the peak value of this H-field is 1.2:1 larger than the ambient field at the location of the measurement.

#### 6.4.5 Ambient H-field Distortion with 400 Foot Conduit

To investigate the loading effects of a buried 400 foot conduit on the ambient H-field, H-field measurements, Figure 6.36, were taken with the conduit carrying 465 amps and with zero amps. The measurement of the H-field was approximately twelve feet from the side of the center hole.

In the first test the conduit was disconnected from all ground beds and was opened at the center hole in line with the H-field probe. For the second test the conduit was connected at the center and to the ground beds. As can be seen in Figure 6.37, there was no noticeable change in the H-field.

#### 6.5 Conclusions

1. Calculation of the peak conduit current from the H-field by the lumped parameter model on buried conduit runs of 400 feet or longer will produce values considerably larger than the actual measured peak current, Figure 6.38.
2. Long buried conduit runs with counterpoise systems at each extremity will have the highest current flowing at the center, midway between the two counterpoises, Figure 6.38. This data clearly shows that the maximum effective (buried) length is approximately 400 feet for the soil conductivity (130 ohm-meters) of the test site for center current values. The magnetically induced current at the ends reaches a maximum value for lengths of 200 feet.

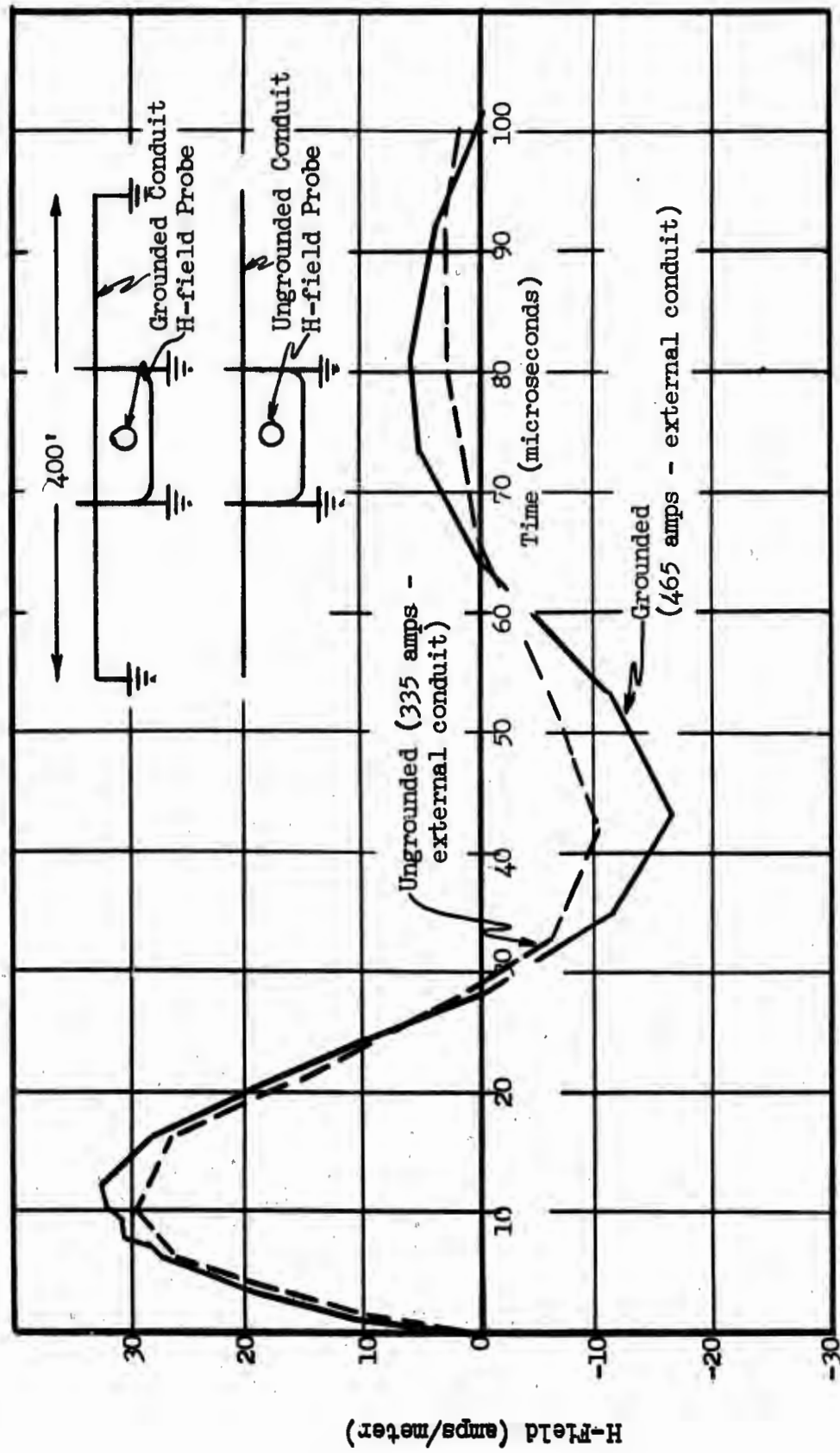
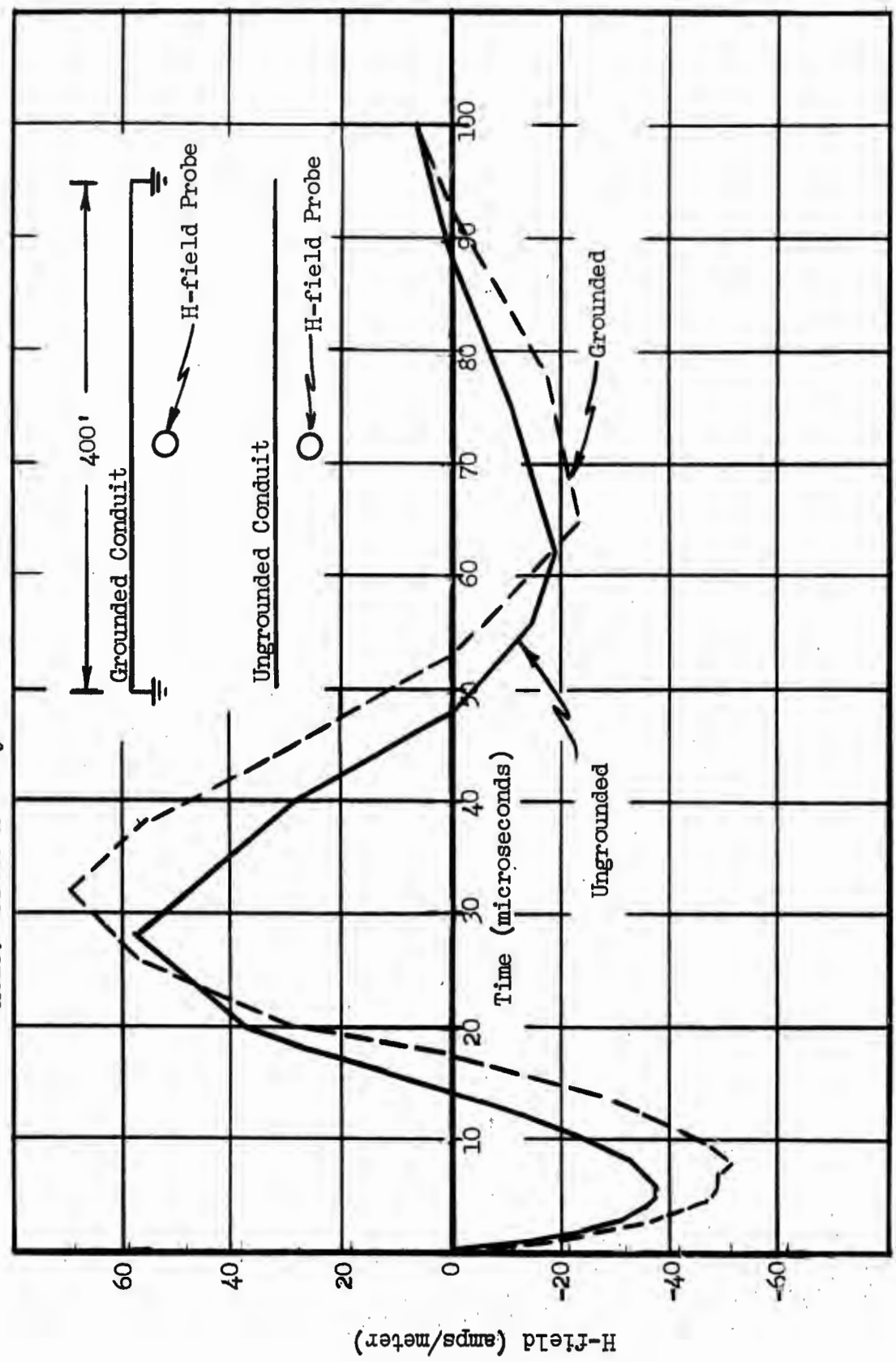


FIGURE 6.33 400 Foot Conduit Grounded and Ungrounded. H-field Measurement in 200' Hole. Probe Halfway between Conduit and Ground Plane.

FIGURE 6.34 400' Conduit Grounded and Ungrounded. H-field Measurement in 200' Hole. Probe Halfway between Conduit and Ground Plane.



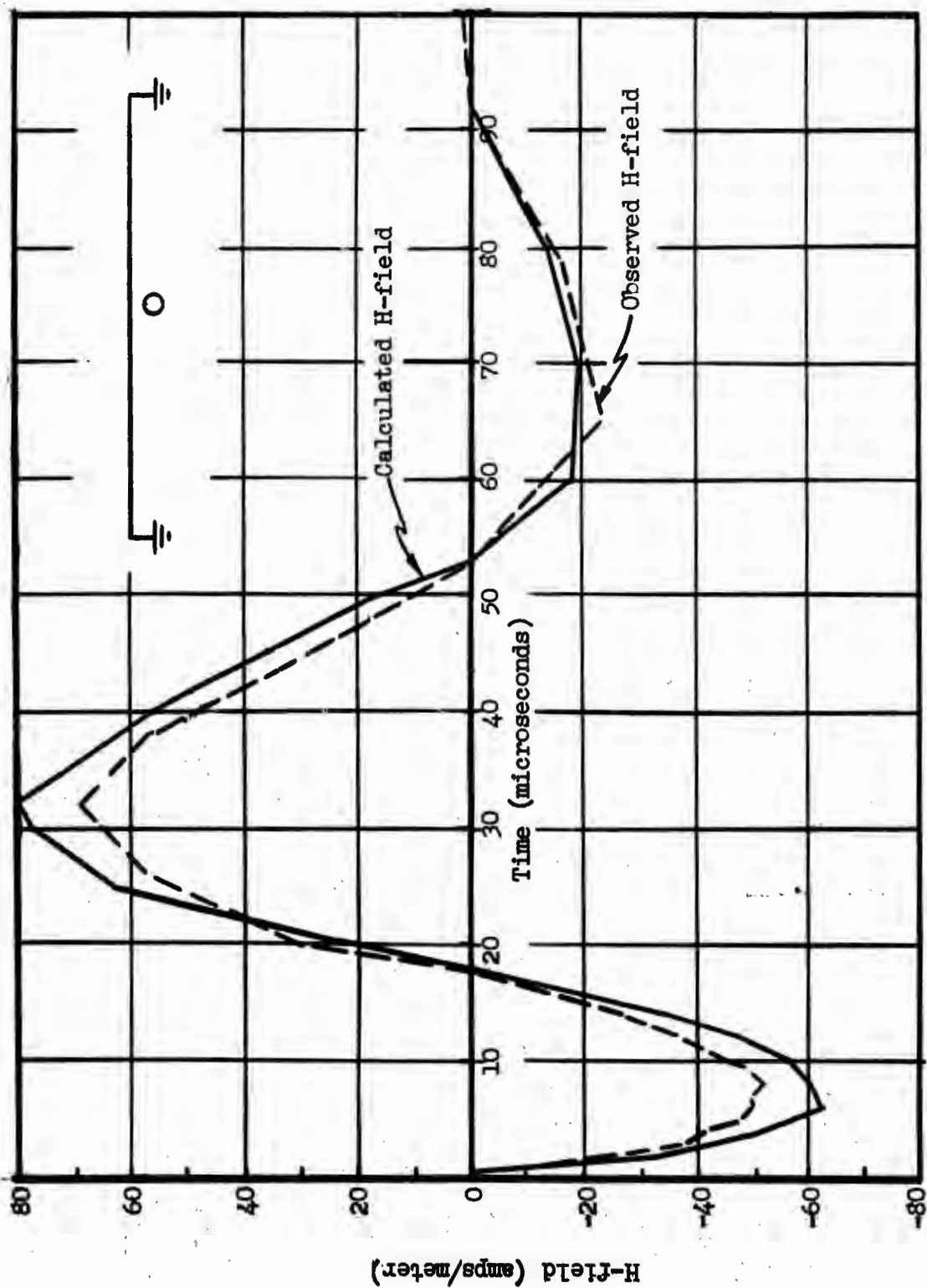


FIGURE 6.35 400' Conduit Grounded. H-field Measurement in 200' Hole. Probe Halfway between Conduit and Ground Plane.

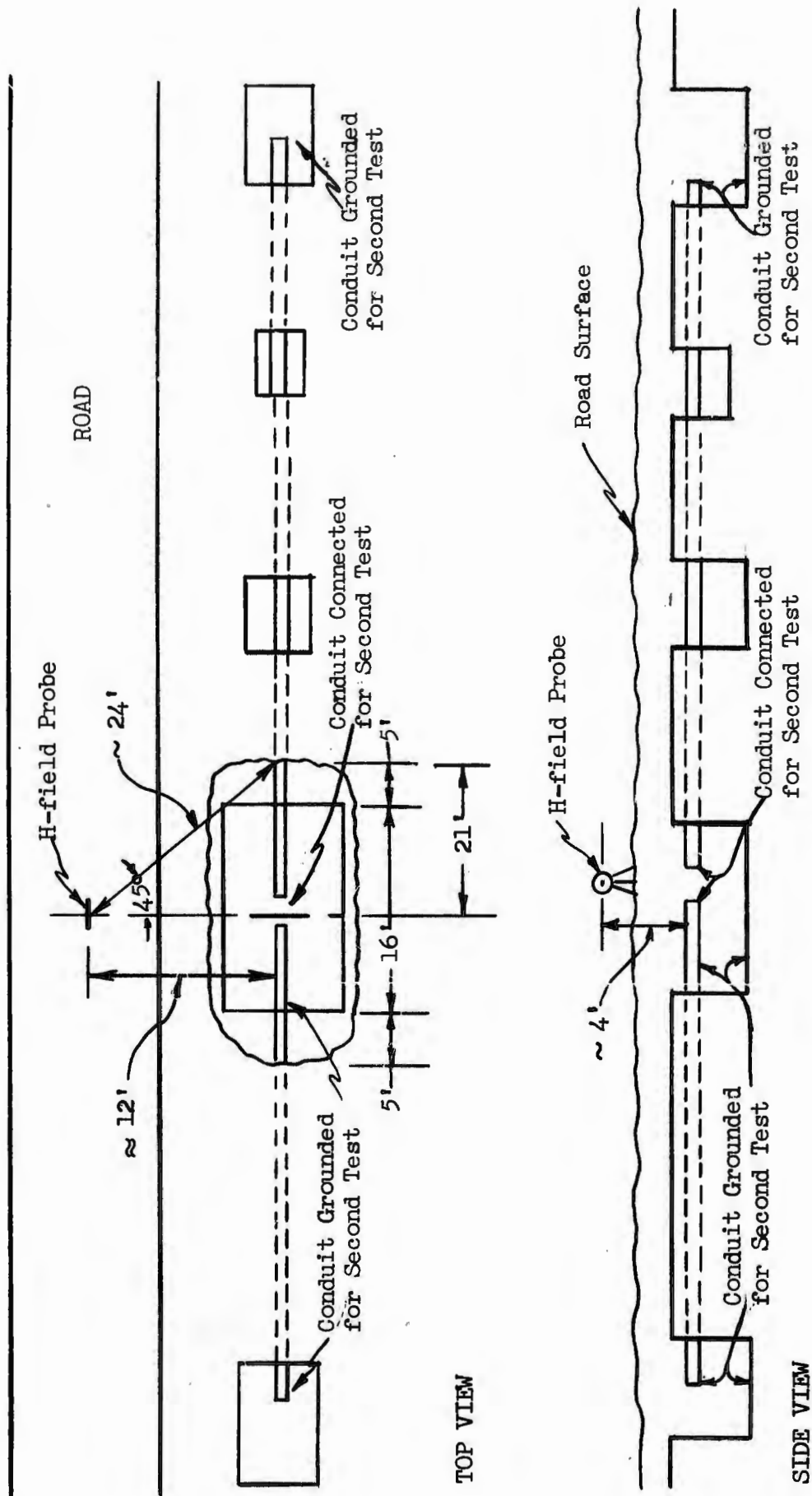


FIGURE 6.36 Measurement Setup of the Ambient H-field with and without Conduit Current

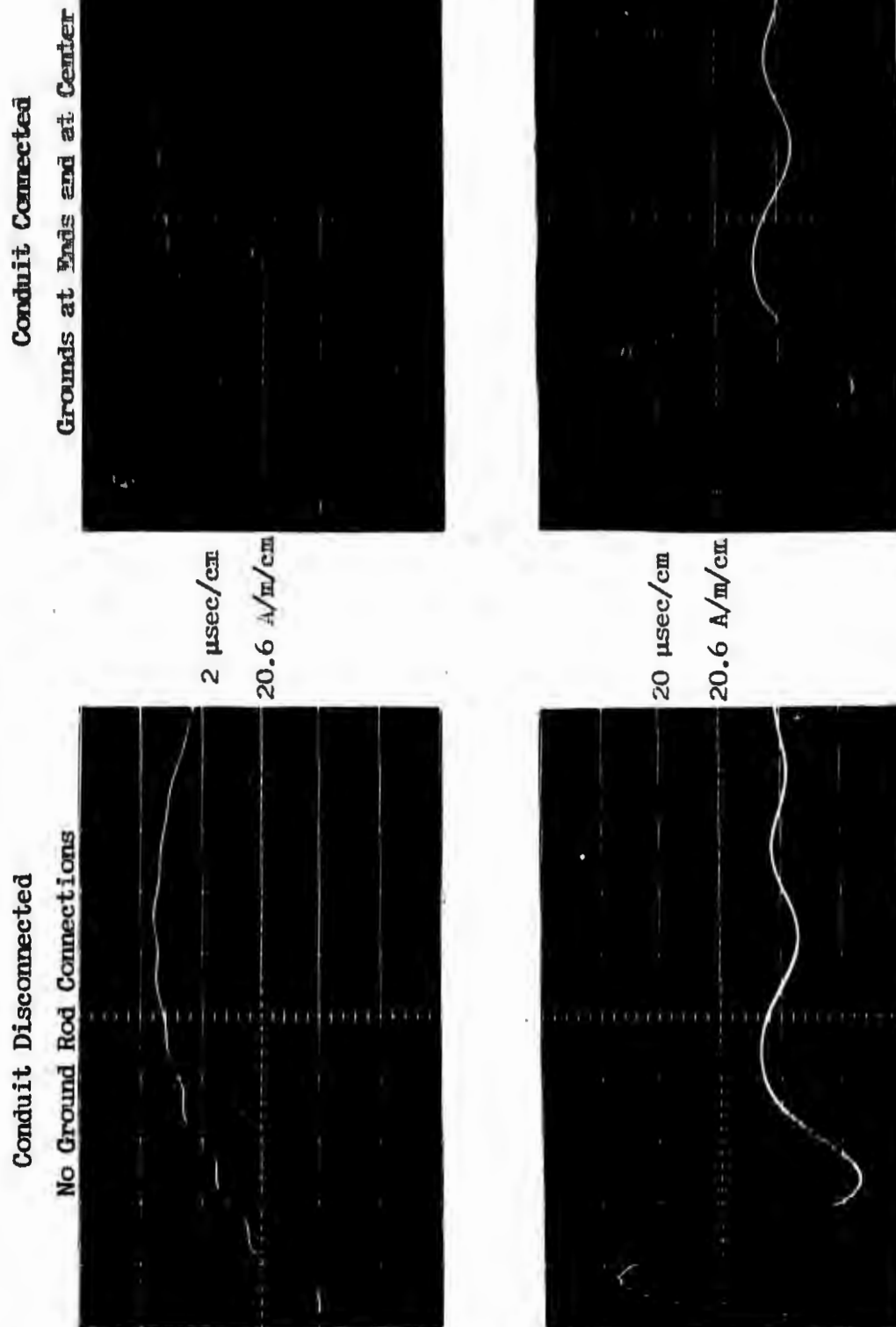


FIGURE 6.37 H-Field 12 Feet from Center Hole, 400 Foot Conduit,  
With and Without Conduit Connected and Grounded

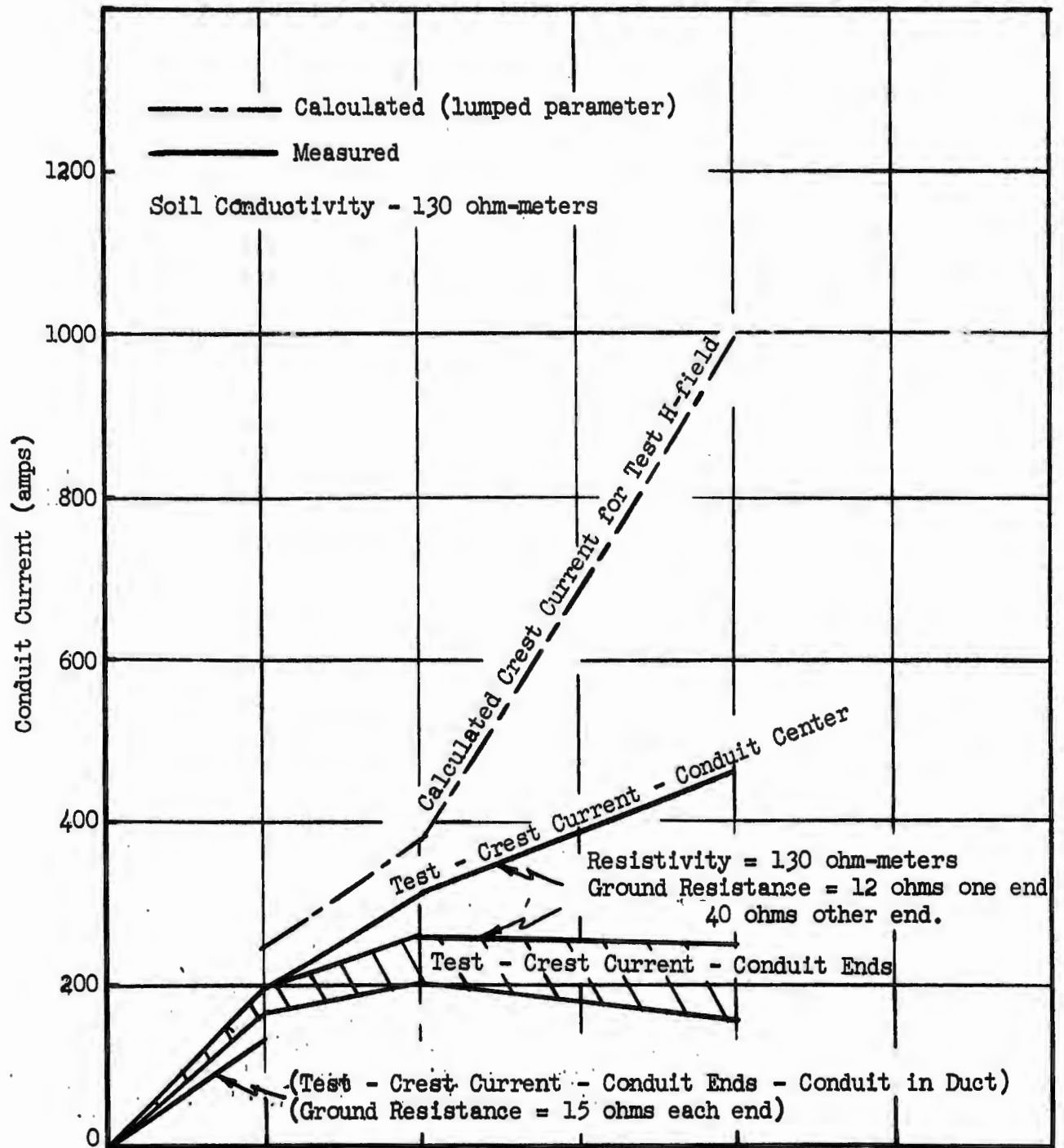


FIGURE 6.38 Conduit Current, Calculated and Test Results

3. Non-grounded, buried bare conduit center current approaches the grounded condition at lengths greater than 400 feet, Figure 6.39. This is also critical with respect to ground conductivity.
4. Placing the buried conduit within an isolated duct will reduce the center conduit current to values less than the buried bare conduit currents, Figure 6.38.
5. Conduit current can be reduced by using a low impedance screen located a few feet above the conduit and parallel to it, connected to the conduit at the counterpoise systems.
6. The calculated value of conduit current considers only one conduit. Other conduits contained within the same duct and connected to the same counterpoise systems will reduce this current.
7. Shunt plates and shunting paths around a building will reduce the conduit current within the building while the circulating current on metal structures and conduit from the H-field will reduce the ambient H-field within the building.

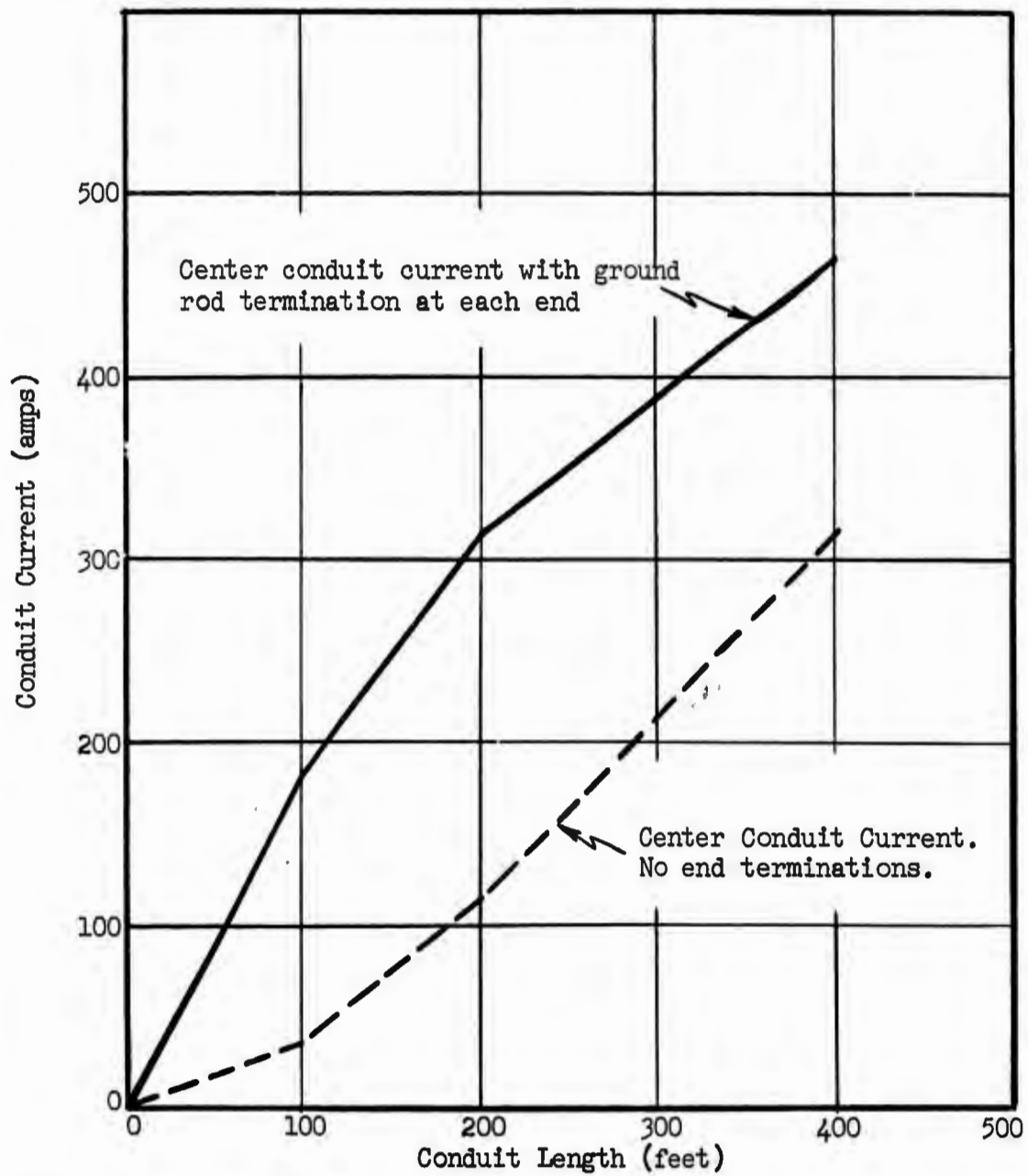


FIGURE 6.39 Conduit Current - Buried in Contact with Earth, with and without Ground Rods at the Ends

## SECTION 6.0 REFERENCES

1. Lyke, A. J., EXPERIMENTAL MEASUREMENT OF EARTH MAGNETIC FIELD ATTENUATION, 1 October 1966, General Electric Company, Pittsfield, Mass.
2. Fiegel, H. E., CONDUCTOR VOLTAGES CAUSED BY PULSE CURRENTS FLOWING IN A CONDUIT, 5 January 1966, General Electric Company, Pittsfield, Mass.
3. Caverly, D. W. and Lyke, A. J., EXPERIMENTAL MEASUREMENT OF CURRENT ON BURIED CONDUIT RESULTING FROM ELECTRIC AND MAGNETIC FIELDS, 30 January 1967, General Electric Company, Pittsfield, Mass.
4. Lyke, A. J., SOLID PANEL ENCLOSURE ATTENUATIONS AND ELECTRICAL SYSTEM RESPONSES TO MAGNETIC FIELD PULSES, 28 February 1967, General Electric Company, Pittsfield, Mass.
5. GROUND RESISTANCE TESTING, James G. Biddle Company, Philadelphia, 1935, pp. 59-60.

## **Section 7.0**

### **Abstracts**

7.0 ABSTRACTS

QUALITY ASSURANCE FOR NEMP SHIELDING PROTECTION

1 December 1967

Unclassified

by: G. W. Maihl

Provides the specifications and procedures for assuring the quality of NEMP shielding materials and equipment during the procurement, construction-installation-inspection, test evaluation, and maintenance phases of NIKE-X power plant and facilities.

MAGNETICALLY INDUCED VOLTAGES ON CONDUCTORS WITHIN CONDUIT AND CABLE

3 November 1967

Unclassified

by: H. H. Brustle and L. C. Walko

This report describes an investigation to determine the factors effective in inducing voltages on conductors within conduits. Investigated were such things as conduit wall thickness, openings in conduit, pulse current amplitude, aluminum armored power cable, conduit joints, flexible conduit, and the effect of conductor location within the conduit.

NIKE-X ELECTRICAL SYSTEMS NUCLEAR ELECTROMAGNETIC ENVIRONMENT (U)

5 December 1966

Classified SRD

Revised March 1967

Revised November 1967

Presents a summary of the present state of knowledge of the NEMP environment to which NIKE-X electrical systems may be exposed. Magnitudes and duration of above ground electric and magnetic fields constituting an NEMP environment are shown in graphical form. Separate considerations are given to field strengths of the horizontal and vertical E-field components and composite, semiempirical equations for predicting H-field intensities are presented.

ELECTROMAGNETIC SHIELDING

1 September 1967

Unclassified

by: D. W. Caverly

Contains analytical and experimental results for evaluating the shielding attenuation provided by various types of metal enclosures when encompassed in an EMP environment. Includes the effects of corners, openings, louvers, and wave guides.

EFFECTS OF FILTERS AND DC LOADS ON SURGE RESPONSE OF TYPICAL NIKE-X POWER SYSTEMS

30 November 1967

Unclassified

by: I. B. Johnson

Transient Network Analyzer results include the effects of RFI filters in the precision load power lines of a simulated MSCB NIKE-X power system; the variation in transient magnitude when precision loads are represented by a dc load instead of an ac load; and the difference in studying steep front pulse injection with an energized or unenergized TNA system.

AN INVESTIGATION OF DOCUMENTATION METHODS FOR NEMP-RELATED PHENOMENA

1 December 1967

Unclassified

by: Procedyne Corporation

In order to acquire some familiarization with the physical aspects of the documentation problem and to establish a physical basis for the comparison of a bibliographic record and a handbook, a partial annotated bibliography and table of contents for a handbook on NEMP shielding were developed.

MEASUREMENT SYSTEM FOR STEADY-STATE AND TRANSIENT PARAMETERS

1 December 1967

Unclassified

by: Procedyne Corporation

The material presented is an extension of previous efforts and contains the latest concepts on the specification and measurement of the power system parameters.

## **Appendix**

### **Shielding Attenuation - Buried Metallic Mat**

## APPENDIX

### SHIELDING ATTENUATION - BURIED METALLIC MAT

Analytical and experimental studies have shown the shielding properties of metallic structures (solid, welded wire fabric, and reinforcing bars) located above or below ground<sup>1</sup>. These shielding materials have been considered grounded but not in direct earth contact (such as contained in concrete, constructed on the inside of a building, or covered by an insulating organic material for corrosion protection). Recent investigations on buried conduit current have indicated the possible shielding properties of metallic mats, in direct contact with earth, placed above a buried structure, Figure A.1<sup>2</sup>. Buried conduit terminated by low resistance ground pads (15 ohms) have substantial currents from EMP environment. The largest portion of this current is induced from the ambient H-field which is encompassed by the conduit and the terminating ground rods. The effective area calculated for this loop has been determined from experiments. By knowing the ambient H-field, the effective area, the inductance and resistance of the conduit loop, values of current can be calculated for various conduit configurations and H-field wave forms.

Studies on shielding attenuation from rebar structures provide data for estimating the attenuation from loops of conduits (of similar configuration as studied in the conduit current experiments) grouped to form a shielding volume as shown in Figure A.2. Although the current as measured for the single conduit loop does not allow the direct computation of the attenuation for a group of conduit loops, a proportional relationship does exist based on the resistance, inductance, conduit size, and area of the individual loops.

From the test report, "Experimental Measurement of Current on Buried Conduit Resulting from Electric and Magnetic Fields", an above ground conduit loop 100 feet by 4 feet, Test #1, verified the calculations for the inductance, resistance, and the conduit current for a two-inch steel conduit (Figure A.3)<sup>2</sup>. The peak current measured was 41.8 amps.

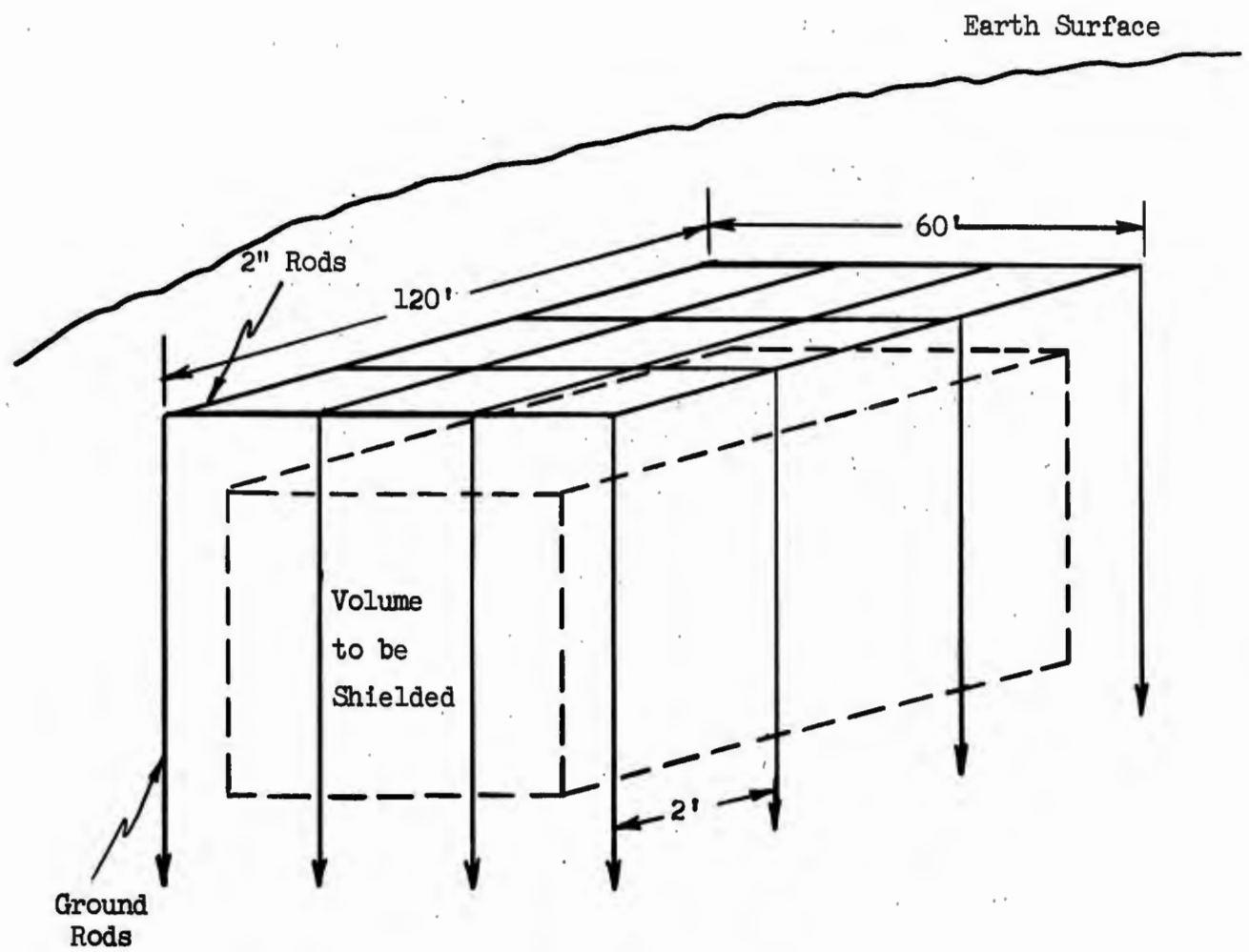


FIGURE A.1 Conduit-Ground Rod Shielding Mat Below Ground

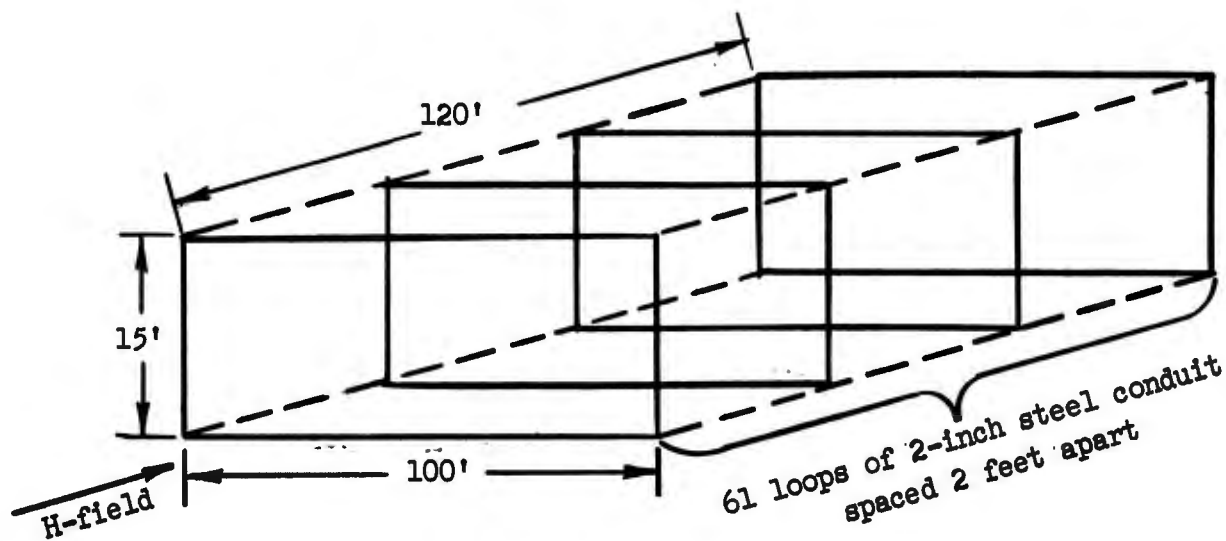


FIGURE A.2 100' x 15' x 120' Shielding Volume of 2-Inch Steel Conduit

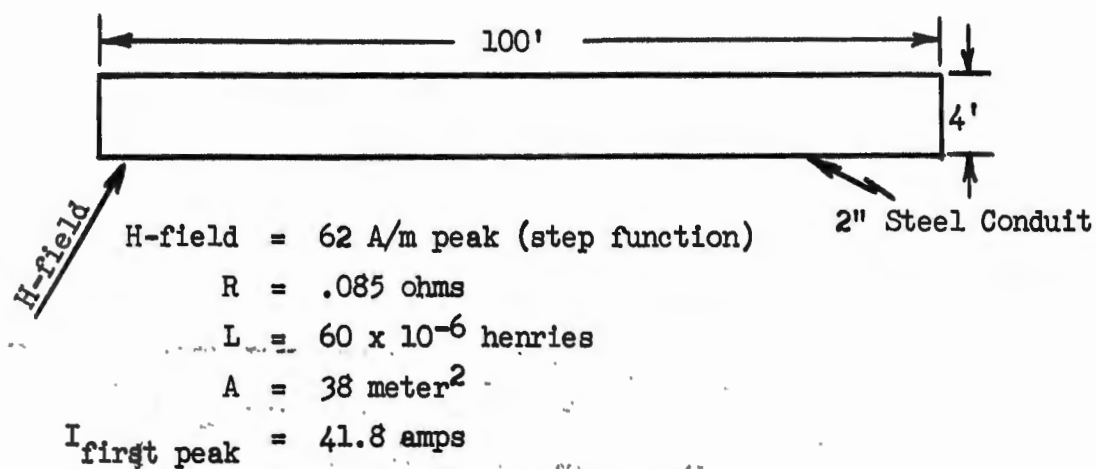


FIGURE A.3 Conduit Test Loop with Measured and Calculated Parameters

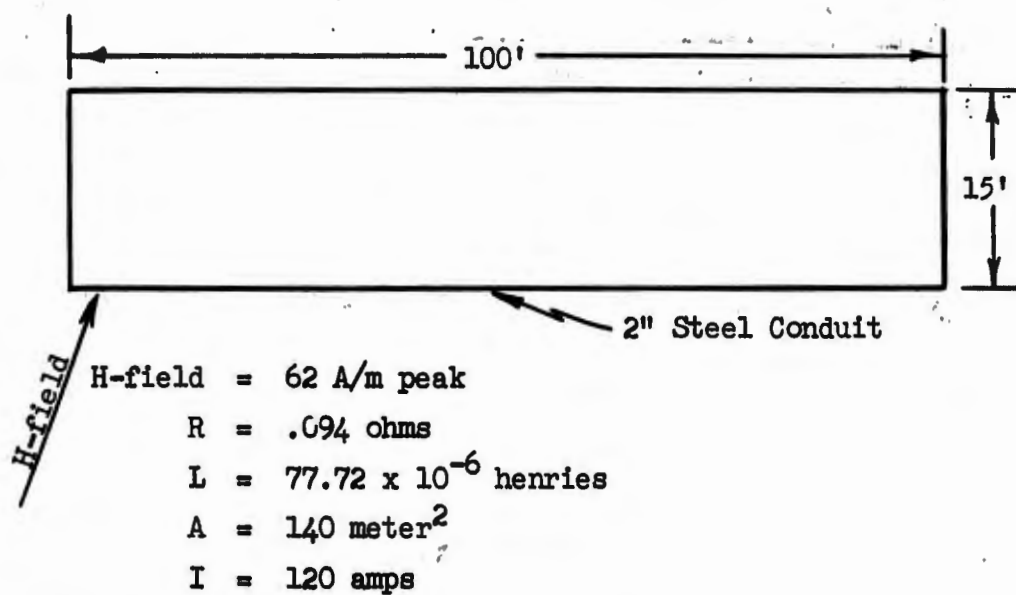


FIGURE A.4 Conduit Loop with Calculated Parameters

To determine the current in a conduit loop of a size that would be used in a shielded volume, the following change in parameters is applicable for a loop 100 feet by 15 feet, Figure A.4.

A. Resistance - proportional to the total length of conduit run (208 feet for a 100 foot by 4 foot loop and 230 feet for a 100 foot x 15 foot loop).  $\therefore R = \frac{230}{208} \times .085 = .094$  ohms

B. Area -  $a = 100 \times 15 \text{ feet}^2 = 140 \text{ meters}^2$

C. Inductance of the loop - calculated<sup>3</sup>

$$L = 0.004 \ell \left( 2.303 \log_{10} \frac{2D}{d} \right) - \frac{D}{\ell} + \mu \delta$$

$$L = 0.002 \ell \left( 2.303 \log_{10} \frac{4\ell}{d} \right) - 1 + \mu \delta$$

$$\text{where } \ell = 100 \text{ feet} = 3060 \text{ cm}$$

$$D = 15 \text{ feet}$$

$$d = 2 \text{ inches} = .166 \text{ feet}$$

$$\mu = 50$$

$$\delta = 0.0175$$

$$\therefore L = 77.72 \times 10^{-6} \text{ henries}$$

D. H-field - 62 A/m

E. Peak Current

$$I = \frac{\mu A H}{L} e^{-R/L t} \quad (\text{step function of H, reference 2})$$

By knowing the  $\Delta$  change in the various parameters the change in current can be found.

$$\Delta A = \frac{140}{38} = 3.7$$

$$\Delta L = \frac{77.72}{60} = 1.29$$

$$\Delta R = \frac{.094}{.085} = 1.1$$

$$\Delta H = 1.0$$

$$\Delta \mu = 1.0$$

$$\Delta e^{-R/Lt} \approx 1 \text{ for a given time since } \Delta R \text{ and } \Delta L \text{ change proportionally}$$

$$\therefore I = I_{(100' \times 4')} \times \frac{\Delta A}{\Delta L} = 41.8 \times \frac{3.7}{1.29} = 120 \text{ amps}$$

This is the peak current for a single conduit loop 100 x 15 feet of two-inch steel.

If 61 of these loops were spaced two feet apart (a volume of 100 x 15 x 120 feet), Figure A.2, the center volume attenuation can be obtained from the rebar calculations in the OCE NEMP PROGRAM, PROTECTIVE MEASURES<sup>4</sup>. The center volume attenuation obtained from Figure 5.36 (-6 dB) and Figure 5.34 (26 dB) of the Protective Measures<sup>4</sup> is 26 - 6 = 20 dB (10:1). This attenuation is assumed proportional to the current (120 amperes) calculated for the single loop (100 x 15 feet), since the conduit loop parameters are the same and the conduit spacing is constant.

To show the effects of ground rod earth resistance, resistors were added to the original conduit loop (Test #2). The insertion of 30 ohms in the loop reduced the peak conduit current from 41.8 to 14 amps (3:1), the other parameters being constant. For the previously calculated 100 x 15 foot loop, which has nearly the same inductance as the loop in Test #2, 30 ohms resistance would also reduce the current by a factor of approximately three to:  $\frac{120}{3} = 40$  amps. Extending this increase of resistance to the 61 conduit loops, considering that each loop contains 30 ohms, the center volume attenuation would be reduced by an amount proportional to the change in loop current. This results in an attenuation of:

$$\frac{10}{3} = 3.33 \text{ or } 10.5 \text{ dB}$$

Test #8 of the conduit tests was a buried conduit (100 feet long) terminated at each end by driven ground rods (9 to 10 feet total depth). The size of this conduit-ground rod buried loop was approximately the same as

the calculated 100 x 15 foot conduit loop with the added 30 ohms resistance. The values of resistance and inductance were similar (20 ohms vs. 30 ohms and  $75 \times 10^{-6}$  henries vs.  $77.7 \times 10^{-6}$  henries). The effective area of the conduit-ground rod loop increased to 607.5 meter<sup>2</sup> and the current to 165 amps. If a shielded volume (15' x 100' x 120', Figure A.1) was constructed with conduits under the surface of the earth and ground rods driven 15 feet deep, the effective area for each loop would be identical and the center volume attenuation would be:

$$\text{ATT} = \frac{I_{\text{underground}}}{I_{100' \times 15' \text{ with resistors}}} \times \text{ATT}_{100' \times 120' \times 15' \text{ with resistors}} = 165 \times 3.35$$

$$= 13.8 \text{ or } 22.8 \text{ dB}$$

The volume for which this attenuation applies would be within the conduit-ground rod area as shown in Figure A.5. Measurement of current along the buried conduit indicated very little current flow from the conduit to ground. The current flows along the conduit to the ground rod, dispersing through deeper ground to the other ground rod. The attenuation below the level of the ground rods has not been estimated.

Attenuation may also be provided by conduits buried in earth without ground rods. Test #9 shows that the loop resistance and inductance, as measured at one third the distance along the conduit, increased ( $R = 70$  ohms,  $L = 200 \times 10^{-6}$  henries). It appears that these values may vary for other points along the conduit. Therefore, the current will vary and be at a maximum at the center of the conduit. For a single two-inch steel conduit, 100 feet long, the current as measured thirty-three feet from each end was 30 amps. Assuming that this is the minimum current which flows between these two points (A and B, Figure A.6), the semicircle area shown could provide the following attenuation:

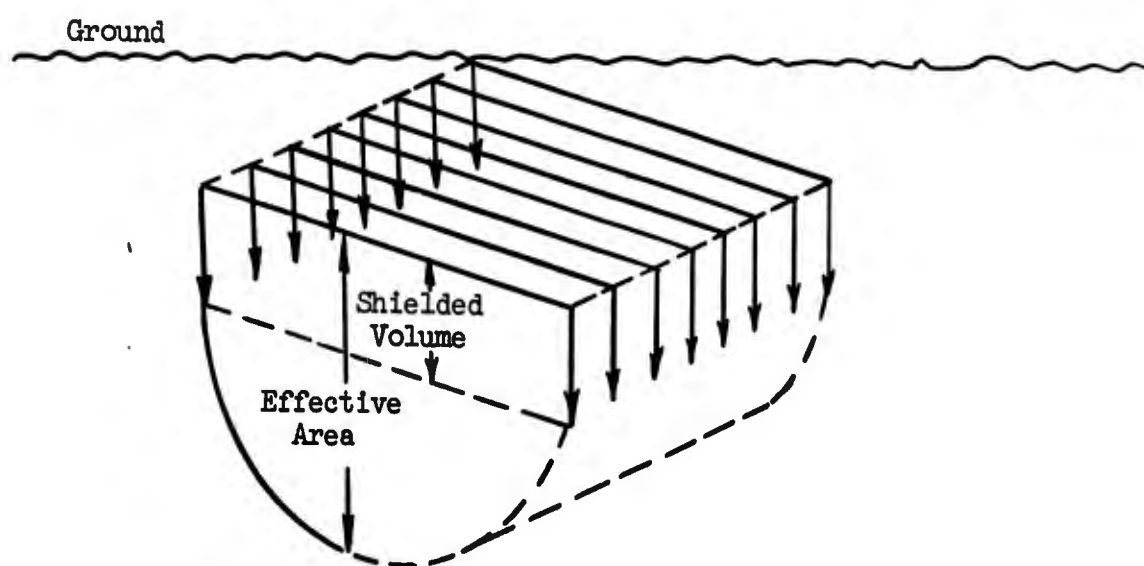
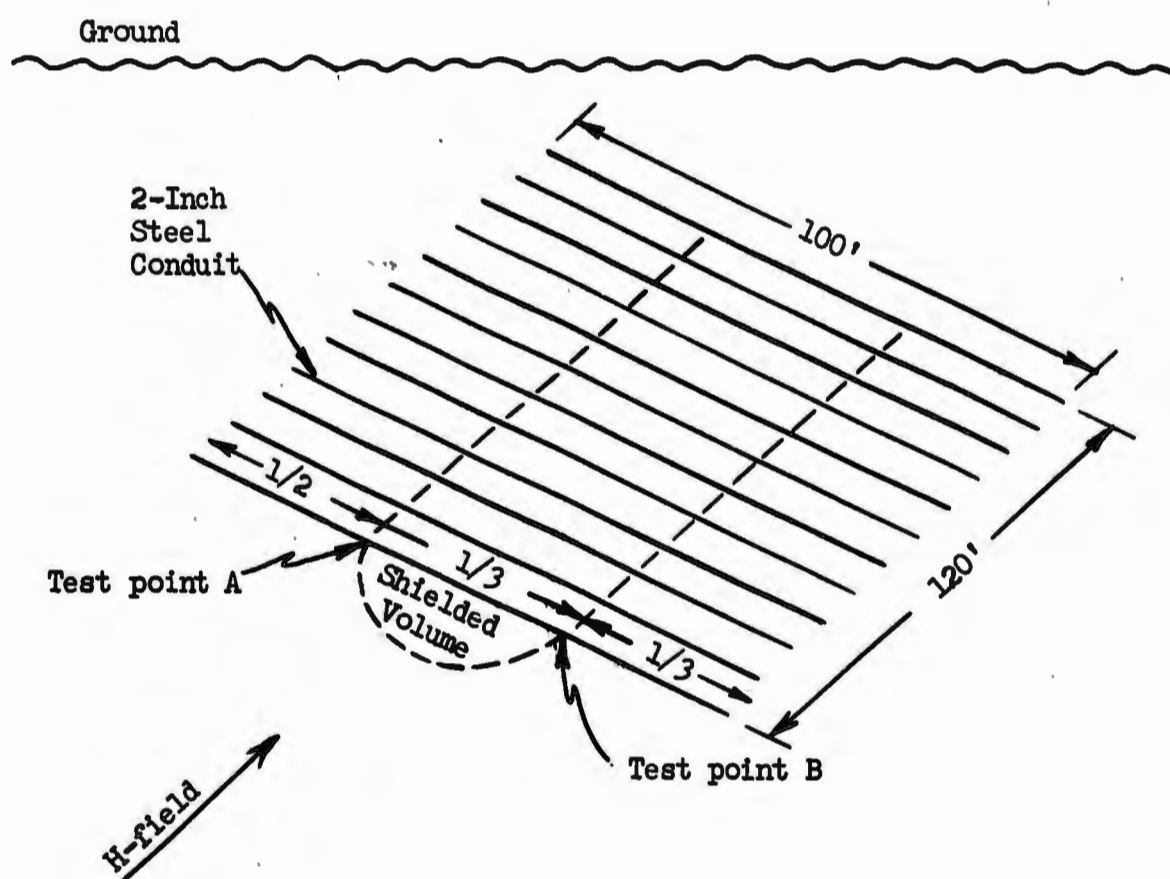


FIGURE A.5 Grounding Mat Showing Shielding Volume and Calculated Effective Area



**FIGURE A.6** Conduit Mat-Shielded Volume for a Value of Attenuation of 8 dB

$$\begin{aligned}
 \text{ATT} &= \frac{I_{1/3 \text{ points}}}{I_{100' \times 15' \text{ with resistors}}} \times \text{ATT}_{100' \times 120' \times 15' \text{ with resistors}} \\
 &= 30/40 \times 3.35 = 2.5 \text{ or } 8 \text{ dB.}
 \end{aligned}$$

The above calculation has only considered the current from the H-field environment. Current from the E-field in the ground will also provide attenuation since the flux from the E-field conduit current will tend to oppose the flux from E-field current deeper in the earth.

#### SUMMARY

The resultant calculated attenuation provided by a buried metallic mat with ground rods was approximately the same value as provided by a complete structure made of the same material and similar volume. This implies that for any mat of reinforcing bars or welded wire fabric with ground rods (providing low ground resistance) the probable attenuation can be estimated from the information in the "OCE NEMP PROGRAM, Development of Criteria for Protection of NIKE-X Power Plant and Facilities Electrical Systems Against Nuclear Electromagnetic Pulse Effects, Protective Measures". Experimental confirmation of this would be desirable.

#### APPENDIX REFERENCES

1. E. R. Uhlig, et al, TECHNICAL DATA FOR GENERAL NEMP DESIGN CRITERIA FOR NIKE-X POWER SYSTEM (U), General Electric Company, Classified Secret - Restricted Data, 5 August 1966.
2. D. W. Caverly, EXPERIMENTAL MEASUREMENT OF CURRENT ON BURIED CONDUIT RESULTING FROM ELECTRIC AND MAGNETIC FIELDS, General Electric Company, 30 January 1967.
3. U. S. Department of Commerce, National Bureau of Standards, RADIO INSTRUMENTS AND MEASUREMENTS, circular C74.
4. E. R. Uhlig, et al, OCE NEMP PROGRAM, DEVELOPMENT OF CRITERIA FOR PROTECTION OF NIKE-X POWER PLANT AND FACILITIES ELECTRICAL SYSTEMS AGAINST NUCLEAR ELECTROMAGNETIC PULSE EFFECTS, PROTECTIVE MEASURES, General Electric Company, 1 December 1967.